Laser control of quantum systems by ultrafast parallel adiabatic passage : application to high fidelity population transfer, state selectivity, and superposition of states

Vahe Hakobyan

Université de Bourgogne

THESIS

presented by

Vahe Hakobyan

to obtain the Degree of
DOCTOR of PHYSICS

Laser control of quantum systems by ultrafast parallel adiabatic passage: Application to high fidelity population transfer, state selectivity, and superposition of states

Directors of thesis
Stephane Guérin
Hans-Rudolf Jauslin

Defended the 8th of November 2011
Jury:

Arthur Ishkhanyan	Professor, Institute for Physical Research of Armenia	Referee
Leonid Yatsenko	Professor, Institute of Physics of Ukraine	Referee
Georges Jolicard	Professor, Université de Franche Comté	Examinator
Hans-Rudolf Jauslin	Professor, Université de Bourgogne	President

Institut Interdisciplinaire Carnot de Bourgogne (ICB), UMR 5209 CNRS
9 Av. A. Savary, BP 47 870 – 21078 Dijon Cedex – France

Abstract

In this work we establish and test the technique of parallel adiabatic passage (PLAP) that optimizes the adiabatic passage in the sense that it selects specific paths that allow a fast adiabatic dynamics while preserving the standard robustness of adiabatic techniques. The intuition of PLAP is based on the fact that the use of eigenvalues that are parallel for all times is expected to lead to a small nonadiabatic transition probability from Landau-Zener analysis for two-state approximations. In this work we test the robustness of this technique and show its superiority to the traditional linearly chirped dynamics with Gaussian pulses. We show its extension for two-photon and three-photon transitions on multilevel quantum systems, where the Stark shift plays an important role in a strong field regime. We have determined an optimal pulse shaping in which the static and dynamic energy level shifts are simultaneously compensated by a programmed phase of a laser field. Next the local parallel adiabatic passage technique is presented. This corresponds to a dynamics where the eigenvalue of the populated state is parallel to the closest one at all times.

We extend the idea of population transfer by adiabatic passage from the ground state to a superposition of states. The transfer is executed with spectrally shaped femtosecond laser pulses. The excited states are dynamically shifted in energy due to the presence of nonresonant components of different channels. We show that this Stark shift can be compensated by another field or by shaping appropriately the pulses.

Acknowledgements

I am thankful to my supervisors Stephane Guérin and Hans R. Jauslin whose guidance and support from initial to the final level enabled me to develop an understanding of the subject.

I offer my regards and blessing to all who supported me in any respect during the completion of the project. Specially I thank my wife Yulia Kalugina for her help and support.

I would like to thank Frédérique Bernard for her great support during the three years.

This thesis I dedicate to my parents.

Contents

List of figures

List of tables

Introduction

Programming the spectral phase and amplitude of ultrafast laser fields from simple transform-limited pulses [1] has enabled the development of many nonlinear light-matter interactions. By changing appropriately the pulse parameters, one can in principle coherently control an atomic or molecular process by steering it through a desirable quantum path or through multiple quantum paths without additional control of their interferences [2,3]. Ultrafast coherent control has been applied for example to the optimization of nonlinear processes, such as multi-photon absorption, second- and third-harmonic generation, etc [4–9]. In particular, ultrafast coherent control in multi-photon absorption has been studied widely in the weak-field regime where the energy level structure of the matter can be considered as unchanged and population transfers are small [10–13]. There, the main goal is the laser spectral shaping to induce quantum interference among many near-degenerate quantum pathways for the given absorption process. However, although a short laser pulse of high peak intensity enhances nonlinear process in general, it can sometimes fail to optimize such absorption process. This is due to light-induced energy level modifications, such as the power broadening and the dynamical Stark shift.

Even before the advent of ultrafast lasers, there were experiments performed with a two-photon absorption in atomic vapors in a strong-field regime, such as the coherent pulse breakup into subpulses [14]. In recent years, there have been many studies towards strong-field coherent control [15–21]. It is now well known that, in general, a control scheme devised in weak-field regime cannot be directly applied to strong field coherent control, although the partial information of the weak-field solution can be still useful [15]. More generally, intuitive interpretations taken from the frequency domain, generally valid in perturbative regime fail in strong field. Only the interpretation of the Schrödinger equation in the time domain allows one to take into account the strong field effects (such as Stark shifts). There have been many approaches developed for strong-field coherent controls: the selective population of dressed states [16], the strong-field atomic phase matching [17], the phenomenological study of the symmetry breaking in spectro-temporal two-dimensional maps [18], the piecewise adiabatic passage [19] and the adiabatic Floquet theory [20]. Also, an analytical control approach has been developed in which the strong-field interaction is probed by laser pulses prepared in a polynomial sum of spectral phase terms [21]. Manipulating the state of a quantum system by external fields is an important issue in a wide variety of problems [22–25]. Modern applications, such as quantum information processing, necessitate a fine control corresponding typically to an admissible error of at most 10^{-4} [25]. Such control should also feature robustness with respect to variations or a non-perfect knowledge of the experimental parameters. Finally, fast processes that are not subject to dissipation, nor to decoherence, are desirable. Tools for designing the time dependent laser parameters are required in order to drive the dynamics from an initial state to a given target state. The technique of optimal control theory has been developped for this purpose. However, due to the requirement of reaching strictly the target state, combined with conditions of optimality (shortest time or pulse area), the resulting laser parameters are of very complicated forms that are difficult to implement in practice, in particular in ultrafast regimes.

The purpose of this thesis is to develop alternative tools in the adiabatic regime aiming at designing the pulse parameters to reach a certain state or superposition of states. Usually adiabatic techniques are applied in simple effective systems (with a few states), where the path to reach the target is easily identified, with an energy (or pulse area) sufficiently large to reach the target according to the adiabatic theorem.
In this work, we establish and test the technique of parallel adiabatic passage (PLAP) that optimizes the adiabatic passage in the sense that it selects specific paths that allow a fast adiabatic dynamics while preserving the standard robustness of adiabatic techniques. The intuition of PLAP is based on the fact that the use of eigenvalues that are parallel for all times is expected to lead to small nonadiabatic transition probability from Landau-Zener analysis. This has been shown rigorously using the Davis-Dykhne-Pechukas (DDP) formula in a two-state model [26]. In this work we test the robustness of this technique and show its superiority to the traditional linearly chirped dynamics with Gaussian pulses.

We show its extension for a two-photon transition, where the Stark shift plays an important role in a strong field regime. The PAP technique allows a dynamics where the Stark shift is perfectly compensated in an effective two-state system for a multilevel system (i.e. with more then two states). When more then two states are involved in the dynamics (through resonances), it is in practice difficult to force all the states to evolve in a parallel way (see however an extension of the STIRAP for a three-state system [27]).
We have tested in this thesis the alternative technique of local parallel adiabatic passage. This corresponds to a dynamics where the eigenvalue, corresponding to the eigenvector carrying the dynamics in the adiabatic limit, is parallel to the closest one at all times. This technique is numerically shown to be efficient as it allows a selective population transfer in a multilevel system in a ultrafast way.
We have finally considered the production of a superposition of states in a three state system with two excited states, forming two channels from the ground state. Population transfer from one energy state to a coherent superposition of states is an important tool in atomic and molecular physics and chemistry. Preparation of such superpositions with well defined amplitudes and phases of the constituent eigenstates is the starting point for many techniques. In many situations it is desirable to make the population transfer complete, that is to move the entire ensemble of atoms or molecules to the target superposition state. We have shown that the combination of two fields, each resonant for each channel, with an additional field that compensates the Stark shift resulting from the crosstalk of the channels allows the generation of any superposition of the two excited states with. We can indeed ultimately use the PLAP technique in this system since we can recover an effective two state system when the Stark shift is compensated.
In chapter I we discuss two-state two-photon transitions, some approximation methods to solve the time dependent Schrödinger equation and the general idea of the pulse shaping technique. Chapter II is dedicated to the theoretical analysis of a two state transition in Cs atoms. The

goal is here to find an optimal pulse shaping in which the static and dynamic energy level shifts are simultaneously compensated by a programmed phase of a laser field.
In chapter III we investigate the technique of optimization which is based on the DDP formula: The population transfer by adiabatic passage is here defined as optimal when it occurs for the smallest coupling area for which the DDP formula gives a complete population transfer. Despite the mathematical need of an adiabatic limit $T \to \infty$, where T corresponds to the duration of the interaction with the field, which corresponds to an infinite pulse area, the DDP formula is known to be already very accurate for a finite and relatively small area (see for instance [28]). In practice, it is an important issue to determine the needed value of this area to get an efficient population transfer (that has to be quantitatively defined depending on the problem that is studied), while preserving the robustness of the process. We remark that the DDP formula does not give any direct information about robustness of the process, which is expected to be better for a more adiabatic process. We analyze it through numerical simulations for a concrete model.
In this work we focus more specifically on dynamics where the Stark shift plays an important role. In the strong-field regime where the structure of the energy levels is strongly altered by Stark shifts during the pulse interaction, a more complicated ultrafast pulse design is required. One obvious strategy is to shape the laser pulse both in time and frequency, in such a way that the absorption condition is maintained during the interaction, i.e. the laser frequency has to follow the energy difference of the concerned dressed states. It is the case for two-photon transitions or when two resonant channels, acting on close transitions, can not be taken independently. We show in these two cases how one can design an ultrafast field to compensate it. We first consider a moderate field intensity regime where an experiment has been set up by J. Ahn group in Korea with who we have ongoing collaboration, that confirm our predictions (chapter II). We next consider a high field intensity regime and in particular adiabatic passage technique.
In chapter IV and chapter V we extend the technique of PAP for Cs and Na atoms in the gas phase to two-photon and three-photon transitions respectively. We show that following the energy differences gives efficient solutions and allows one to get selective population transfer between different atomic levels. We also present a linear chirp technique combined with a static detuning from the resonance (refered to as a shift linear chirp technique) which is also an efficient way to get complete transfer of population. We numerivally determine for these two techniques the programmable field shapings.
In chapter VI we present population transfer by adiabatic passage from the ground state to the superposition of states in K atom. The transfer is executed with spectrally shaped femtosecond laser pulses. The excited states are dynamically shifted in energy due to the presence of nonresonant components of the two different channels of the K atom. We show that a third field or an appropriate shaping of the initial fields can compensate this Stark shift.

The present thesis is organized as follows:

- Chapter I Two-state system and multiphoton processes.
- Chapter II Optimization of two-photon transition by phase shaping: Application to Cesium.
- Chapter III Adiabatic evolution of a quantum system. Optimal adiabatic passage by shaped pulses: Efficiency and robustness.
- Chapter IV Multiphoton parallel adiabatic passage by shaped pulses: Application to Cesium.
- Chapter V Selective transfer of population in multi-level system by parallel adiabatic passage: Application to Sodium.
- Chapter VI Superposition of states by controlled Stark shift adiabatic passage: Application to Potassium.

First part

Two-state systems, approximations to solve the time-dependent Schrödinger equation, and optimization of two-photon transitions

Chapter 1

Two-state approximations and two-photon processes

In this chapter some basic concepts of the description of a two level atom interacting with a monochromatic laser field are presented.

1.1 Two-state system

We shall consider two-level atom, with a ground state $|g\rangle$ and excited state $|e\rangle$, which are the eigenstates of the two-level Hamiltonian H_0

$$H_0|g\rangle = E_g|g\rangle, \quad H_0|e\rangle = E_e|e\rangle, \tag{1.1}$$

where E_g and E_e are the eigenvalues of H_0. The eigenvectors $|g\rangle$ and $|e\rangle$ serve as a basis of the Hilbert space where the state vector $\Psi(t)$ can be expressed as

$$|\psi(t)\rangle = C_g(t)|g\rangle + C_e(t)|e\rangle, \tag{1.2}$$

where $C_n(t)(n = g, e)$ is a probability amplitude, whose absolute square is the probability $P_n(t)$ that the atom will be found in the state $|n\rangle$ at time t

$$P_n(t) = |C_n(t)|^2 \quad n = g, e. \tag{1.3}$$

We shall consider the interaction between a two level atom with a monochromatic laser field (Fig. 1.1)

$$\mathbf{E}(t) = \mathcal{E}_0(t)\mathbf{e}\cos(\omega_L t + \phi). \tag{1.4}$$

Here $\mathcal{E}_0(t)$ is a slowly varying envelope, $\mathbf{e}$ is a unit vector, defining the direction of the laser field (polarization direction), ω_L is a laser frequency, and $\omega_L t + \phi$ is the laser phase. In the dipole approximation the interaction energy is given

$$V(t) = -\boldsymbol{\mu}\mathbf{E}(t), \tag{1.5}$$

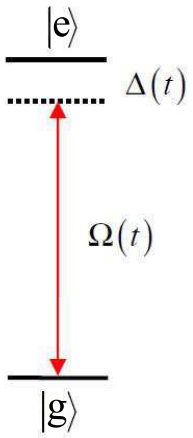

FIG. 1.1 - *A two-level atom with ground state $|g\rangle$ and excited state $|e\rangle$. $\Omega(t)$ is the Rabi frequency, which parameterizes the strength of the atom-laser interaction and $\Delta(t)$ is a laser detuning.*

where $\boldsymbol{\mu}$ is an electric dipole of an atom.

A state vector $|\psi(t)\rangle$ evolution is governed by the time-dependent Schrödinger equation

$$i\hbar\frac{d}{dt}|\psi(t)\rangle = (H_0 + V(t))|\psi(t)\rangle. \tag{1.6}$$

Substituting $|\psi(t)\rangle$ in the Schrödinger equation (1.6) by Eq. (1.2), one obtains a set of two coupled ordinary differential equations for the probability amplitudes

$$i\hbar\frac{d}{dt}C_g(t) = V_{ge}(t)C_e(t), \tag{1.7}$$

$$i\hbar\frac{d}{dt}C_e(t) = \hbar\omega_0 C_e(t) + V_{eg}C_g(t), \tag{1.8}$$

where we take $E_g = 0$, $\omega_0 = E_e/\hbar$ (transition frequency), and $V_{ge}(t) = \langle g|V(t)|e\rangle = V^*_{eg}(t)$. By the transformation $\tilde{C}_e(t) = C_e(t)e^{i\omega_L t}$, Eqs. (1.7) and (1.8) become

$$i\hbar\frac{d}{dt}C_g(t) = V_{ge}(t)\tilde{C}_e(t)e^{-i\omega_L t}, \tag{1.9}$$

$$i\hbar\frac{d}{dt}\tilde{C}_e(t) = V_{eg}(t)C_g(t)e^{i\omega_L t} + \hbar(\omega_0 - \omega_L)C_e(t). \tag{1.10}$$

This transformation corresponds to a field dressing by minus one photon of the excited state. It can be rewritten as

$$R = \begin{bmatrix} 1 & 0 \\ 0 & e^{-i\omega_L t} \end{bmatrix}, \quad \begin{bmatrix} \tilde{C}_g \\ \tilde{C}_e \end{bmatrix} = R^{-1}\begin{bmatrix} C_g \\ C_e \end{bmatrix} \tag{1.11}$$

with the corresponding Hamiltonian

$$R^\dagger H R - iR^\dagger\frac{\partial R}{\partial t} = \begin{bmatrix} 0 & V_{ge}(t)e^{-i\omega_L t} \\ V_{eg}(t)e^{i\omega_L t} & \hbar(\omega_0 - \omega_L) \end{bmatrix}. \tag{1.12}$$

The matrix elements of the coupling (1.5) can be written as

$$V_{eg}(t) = \hbar\Omega(t)\cos(\omega_L t + \phi), \tag{1.13}$$

$$V_{ge}(t) = \hbar\Omega^*(t)\cos(\omega_L t + \phi), \tag{1.14}$$

where

$$\Omega(t) = -\frac{\mathcal{E}_0(t)\langle e|\mathbf{e}\boldsymbol{\mu}|g\rangle}{\hbar} \tag{1.15}$$

is the *Rabi frequency* characterizing the strength of the laser-atom interaction. We assume that the laser frequency ω_L is equal or very close to the transition frequency ω_0, then the term with frequency $\omega_L + \omega_0$ oscillates rapidly at nearly twice the transition frequency, while the term with atom-laser detuning $\Delta = \omega_0 - \omega_L$ oscillates slowly. Unless the laser pulse is very short (e.g. a femtosecond pulse) or very intense, the rapidly oscillating term can be neglected. This is called rotating wave approximation (RWA). Under this approximation Eqs. (1.9) and (1.10) become

$$i\hbar\frac{d}{dt}C_g(t) = \tilde{C}_e(t)\frac{\hbar\Omega^*(t)}{2}e^{i\phi}, \tag{1.16}$$

$$i\hbar\frac{d}{dt}\tilde{C}_e(t) = C_g(t)\frac{\hbar\Omega(t)}{2}e^{-i\phi} + C_e(t)\hbar\Delta. \tag{1.17}$$

The transformation $R(t)$ (1.11) can be incorporated in this basis that then writes as $\{|g;0\rangle, |e;-1\rangle\}$ with the second label standing for the relative number of photons.

1.2 Approximations to solve the time-dependent Schrödinger equation

In order to solve approximately the time dependent Schrödinger equation

$$i\frac{d}{dt}\psi(t) = H(t)\psi(t), \tag{1.18}$$

where we use units such that $\hbar = 1$, one can rewrite it as

$$\psi(t) = \psi(t_i) - i\int_{t_i}^{t} dsH(s)\psi(s), \tag{1.19}$$

where t_i is the starting time of the process.

Time-dependent perturbation theory. One can replace the solution $\psi(s)$ in the integral by the right hand side of Eq. (1.19):

$$\psi(t) = \Big[1 - i\int_{t_i}^{t} dt' H(t')\Big]\psi(t_i) - \int_{t_i}^{t} dt' H(t')\int_{t_i}^{t'} dt'' H(t'')\psi(t''), \tag{1.20}$$

and iterate

$$\psi(t) = \Big[1 - i\int_{t_i}^{t} dt' H(t')\Big]\psi(t_i) - \int_{t_i}^{t} dt' H(t') \int_{t_i}^{t'} dt'' H(t'')\Big[1 - i\int_{t_i}^{t'} dt''' H(t''')\Big]\psi(t_i)$$
$$+ \int_{t_i}^{t} dt' H(t') \int_{t_i}^{t'} dt^{(2)} H(t^{(2)}) \int_{t_i}^{t^{(2)}} dt^{(3)} H(t^{(3)}) \int_{t_i}^{t^{(3)}} dt^{(4)} H(t^{(4)})\psi(t^{(4)})$$
$$\vdots \quad (1.21)$$

In a representation (for instance in the interaction representation), where the Hamiltonian has only off-diagonal elements $H_{i\neq j}$. If the partial area of these off-diagonal components are of order ϵ: $\int_{t_i}^{t} dt H_{i\neq j}(t) \equiv \epsilon A_{i\neq j}$ with $A_{i\neq j}$ of order 1, then one can approximate the solution by the first order

$$\psi(t) = \Big[1 - i\int_{t_i}^{t} dt' H(t')\Big]\psi(t_i) + O(\epsilon^2), \quad (1.22)$$

or from Eq. (1.21) by the second order

$$\psi(t) = \Big[1 - i\int_{t_i}^{t} dt' H(t')\Big]\psi(t_i) - \int_{t_i}^{t} dt' H(t') \int_{t_i}^{t'} dt'' H(t'')\psi(t_i) + O(\epsilon^3), \quad (1.23)$$

where

$$f(\epsilon) = O(g(\epsilon)) \quad \text{means} \quad \left|\frac{f(\epsilon)}{g(\epsilon)}\right| \leq const. \quad \text{for } \epsilon \to 0. \quad (1.24)$$

1.2.1 Application to a two-state problem

For a two-state problem, the general Hamiltonian in the two-state basis $\{|g\rangle, |e\rangle\}$ can be written as:

$$\hat{H}(t) = \begin{bmatrix} 0 & \frac{1}{2}\Omega^*(t)e^{i\varphi(t)} \\ \frac{1}{2}\Omega(t)e^{-i\varphi(t)} & \Delta + S(t) \end{bmatrix}. \quad (1.25)$$

This Hamiltonian (1.25) results, in particular for a two-photon transition, from Eqs. (1.16) and (1.17) to which a stark shift $S(t)$ has been added (see section 1.4 for details). But this Hamiltonian describes more general processes as long as only two states are significantly populated during the dynamics. We consider the initial condition $\psi(t_i) = \begin{bmatrix} 1 \\ 0 \end{bmatrix}$. In the interaction representation, corresponding to a transformation $\psi(t) = T^\dagger \Psi(t)$ with

$$T(t) = \begin{bmatrix} 1 & 0 \\ 0 & e^{-i[\Delta t + \int_{t_i}^{t} S(u)du]} \end{bmatrix}, \quad (1.26)$$

leading to

$$i\hbar \frac{d}{dt}\Psi(t) = \hat{H}(t)\Psi(t) \quad (1.27)$$

with

$$H(t) = T^\dagger(t)\hat{H}(t)T(t) - iT^\dagger(t)\frac{\partial T}{\partial t}(t) = \hbar \begin{bmatrix} 0 & \frac{1}{2}\Omega^*(t)e^{i[\varphi(t) - \Delta t - \int_{t_i}^{t} S(u)du]} \\ * & 0 \end{bmatrix}, \quad (1.28)$$

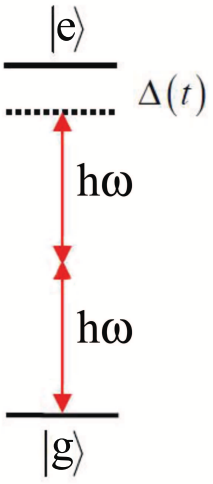

FIG. 1.2 - *Two-photon transition between ground $|g\rangle$ and excited $|e\rangle$ states in a two-level atom. $\hbar\omega$ is the energy of the photon and $\Delta(t)$ is the laser detuning. Intermediate states that allow the two-photon transition in the dipole approximation have not been displayed.*

we get at the first order [Eq. (1.22)] for the excited state:

$$\langle e|\psi\rangle(t) = -i\frac{1}{2}\int_{t_i}^{t} dt'\Omega(t')e^{-i[\varphi(t')-\Delta t'-\int_{t_i}^{t'} S(u)du]} + O(\epsilon^2). \tag{1.29}$$

The error of order $O(\epsilon^2)$ is here with respect to the area of the Rabi frequency: $\epsilon(t) \equiv \int_{t_i}^{t} dt'\Omega(t')$ (this definition of ϵ is just to follow the order of the expansion and the errors that are made.)

Inspecting the second order [Eq. (1.23)], we obtain

$$\langle e|\int_{t_i}^{t} dt'H(t')\int_{t_i}^{t'} dt''H(t'')|\psi(t_i)\rangle = 0, \tag{1.30}$$

which means that Eq.(1.29) is in fact valid until the second order:

$$\langle e|\psi\rangle(t) = -i\frac{1}{2}\int_{t_i}^{t} dt'\Omega(t')e^{-i[\varphi(t')-\Delta t'-\int_{t_i}^{t'} S(u)du]} + O(\epsilon^3). \tag{1.31}$$

1.2.2 Application to a two-photon transition

In a two-photon transition the atom is excited from the ground state to an excited state by absorbing two photons (Fig. 1.2). In a problem corresponding to a two-photon transition between the states $|g\rangle$ and $|e\rangle$ (of respective energy $\hbar\omega_g$ and $\hbar\omega_e$),

$$\Delta = \omega_e - \omega_g - 2\omega_0 \tag{1.32}$$

is a (static) two-photon detuning (with respect to the mean frequency ω_0 of the laser), $S(t)$ is a relative (dynamical) Stark shift, and the total field $E(t)$ of amplitude $\mathcal{E}(t) > 0$ is defined as

(in the complex representation):

$$E(t) = \mathcal{E}(t)e^{-i(\omega_0 t+\phi(t))}, \quad \phi(t) = 2\varphi(t). \tag{1.33}$$

The Rabi frequency and the Stark shift are respectively connected to the field through

$$\Omega(t) = \alpha_{ge}\mathcal{E}^2(t), \quad S(t) = (\alpha_{ee} - \alpha_{gg})\mathcal{E}^2(t) \tag{1.34}$$

where α_{ij} is a component i, j of the polarizability tensor. This model results from stationary perturbation theory applied on an initially more complicated system including many other intermediate states $\{|m\rangle\}$ that are assumed to be coupled by one-photon processes from the ground and excited states through the Rabi frequencies Ω_{jm}, $j = g, e$ (see section 1.4 for a more precise statement).

Effect of Stark shifts

Below we show, that in such a two-photon transition problem, Stark shift plays a significant role for a sufficiently large pulse area. Writing the Stark shift in the form $S(t) = r\Omega(t)$, one can make the expansion:

$$e^{i[\int_{t_i}^{t'} S(u)du]} = e^{ir\epsilon(t')} = 1 + ir\epsilon(t') + O(\epsilon^2). \tag{1.35}$$

Solution at the first order. If one firstly considers the lowest (i.e. first) order of the perturbation theory Eq. (1.29) and inserting the latter result in Eq. (1.29), one obtains

$$\langle e|\psi\rangle(t) = -i\frac{1}{2}\int_{t_i}^{t} dt'\Omega(t')e^{-i[\varphi(t')-\Delta t']} + O(\epsilon^2), \tag{1.36}$$

i.e. the Stark shift is of the order of the error if one considers the lowest order of the perturbation expansion, and, thus, can be neglected at this order.

This expression can be rewritten as a function of the Fourier transform of the field including its time-dependent phase (here we used a convention opposite to the standard one):

$$\tilde{\mathcal{A}}(\omega) = \mathcal{F}_\omega[\mathcal{A}(t)] = \frac{1}{\sqrt{2\pi}}\int_{-\infty}^{+\infty} \mathcal{A}(t)e^{i\omega t}dt \tag{1.37}$$

with

$$\mathcal{A}(t) = \mathcal{E}(t)e^{-i\phi(t)}. \tag{1.38}$$

We can decompose $\tilde{\mathcal{A}}(\omega)$ into an amplitude and an angle:

$$\tilde{\mathcal{A}}(\omega) = |\tilde{\mathcal{A}}(\omega)|e^{-i\alpha(\omega)}. \tag{1.39}$$

We obtain (for $t_i = -\infty$, at time $t = +\infty$, and up to the correction of third order)

$$\langle e|\psi\rangle = -i\frac{1}{2}\alpha_{ge}\int_{-\infty}^{+\infty} dt'[\mathcal{E}(t')e^{-i\phi(t)}]^2 e^{i\Delta t} \tag{1.40a}$$

$$= -i\sqrt{\frac{\pi}{2}}\alpha_{ge}\mathcal{F}_{\Delta}[\mathcal{A}^2(t)] \tag{1.40b}$$

$$= -i\sqrt{\frac{\pi}{2}}\alpha_{ge}\tilde{\mathcal{A}}(\Delta) * \tilde{\mathcal{A}}(\Delta) \tag{1.40c}$$

$$= -i\sqrt{\frac{\pi}{2}}\alpha_{ge}\int_{-\infty}^{+\infty} \tilde{\mathcal{A}}(u)\tilde{\mathcal{A}}(\Delta - u)du, \tag{1.40d}$$

which finally gives (defining $\omega = u - \Delta/2$)

$$\langle e|\psi\rangle = -i\sqrt{\frac{\pi}{2}}\alpha_{ge}\int_{-\infty}^{+\infty} \tilde{\mathcal{A}}(\Delta/2 + \omega)\tilde{\mathcal{A}}(\Delta/2 - \omega)d\omega. \tag{1.41}$$

If one assumes that the mean laser frequency matches the transition:$\Delta = 0$, the two-photon transition amplitude can be rewritten as

$$\langle e|\psi\rangle = -i\sqrt{\frac{\pi}{2}}\alpha_{ge}\int_{-\infty}^{+\infty} \tilde{E}(\omega_0 + \omega)\tilde{E}(\omega_0 - \omega)d\omega. \tag{1.42}$$

This result can be interpreted as follows: in the perturbative regime, the two-photon process is a combination of two single photons of respective frequencies $\omega_0 - \omega$ and $\omega_0 + \omega$. It is in fact a sum of these combinations for all possible ω. The frequencies $\omega_0 - \omega$ and $\omega_0 + \omega$ should correspond to non-negligible components of the Fourier transform of the field, as shown schematically in the Fig. 1.3. Hence, all frequency components of a single pulse contribute to the two-photon transition probability, which can be controlled by tailoring the spectral phases of the pulse. This is studied in detail and experimentally tested as described in the next chapter.

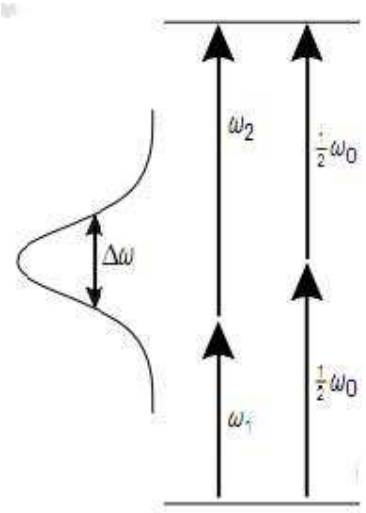

FIG. 1.3 - *Schematic diagram of the energy levels of the two-photon transitions.*

Solution at the second order. One can use the fact that, in fact, our expansion (1.31) is valid until the second order: the Stark shift is then expected to play a role at this second order, i.e. for a large enough pulse area. This can be seen considering the further expansion

$$e^{i[\int_{t_i}^{t'} S(u)du]} = e^{ir\epsilon(t')} = 1 + ir\epsilon(t') - \frac{r^2}{2}\epsilon^2(t') + O(\epsilon^3) \tag{1.43}$$

to finally obtain

$$\langle e|\psi\rangle(t) \;=\; -i\frac{1}{2}\int_{t_i}^{t} dt'\Omega(t')e^{-i[\varphi(t')-\Delta t']}\left[1 + i\int_{t_i}^{t'} duS(u)\right] + O(\epsilon^3).$$

Compensation of the Stark shifts

To maximize the resonance effects, one can compensate the Stark shift from (1.31) by imposing at each time

$$\dot{\varphi}(t) = S(t). \tag{1.44}$$

For a Stark shift of the form $S(t) = S_0 e^{-t^2/\tau^2}$, it can be a good strategy to compensate it near its maximum, i.e. around $t = 0$.

The compensation of the Stark shift based on this expansion is the subject of the next chapter for a concrete system (Cs) at moderate field intensities.

1.3 Approximations for numerical calculations

For strong field regimes, where the population of the initial state is signifanctly transfered to excited state, the preceding approximations are not valid and one has to solve numerically the Schrödinger equation. Below we show the numerical algorithm to be used specifically when the transformation is time-dependent. We assume that only a few states are essential, i.e. are non-negligibly populated during the dynamics, such that they can form the complete basis on which we expand the solution.

One divides the total time T of integration in N intervals of constant duration $\Delta t = T/N$: $t \in [t_i = t_0, t_f = t_N = t_i + T]$ such that $t_n = t_0 + n\Delta t$, $n = 0, \cdots, N$. Various approximations can be obtained depending on how one approximates the integral in Eq. (1.19). In the following, we denote $\psi_n \equiv \psi(t_n)$, $H_n \equiv H(t_n)$, and $\epsilon \equiv \Delta t$ (Note here that ϵ is different from the one used in the preceding section).

Explicit first order scheme. Using the simplest approximation with rectangles, of error $O(\epsilon^2)$:

$$\int_{t_n}^{t_{n+1}} dsH(s)\psi(s) = \epsilon H_n\psi_n + O(\epsilon^2), \tag{1.45}$$

leads to

$$\psi_{n+1} = [1 - i\epsilon H_n]\psi_n + O(\epsilon^2). \tag{1.46}$$

Iterating, we obtain:

$$\psi_1 = [1 - i\epsilon H_0]\psi_0 + O(\epsilon^2) \tag{1.47a}$$

$$\psi_2 = \Big[1 - i\epsilon \sum_{n=0}^{1} H_n\Big]\psi(t_0) + 2 \times O(\epsilon^2) \tag{1.47b}$$

$$\dots$$

$$\psi_N = \Big[1 - i\epsilon \sum_{n=0}^{N-1} H_n\Big]\psi_0 + N \times O(\epsilon^2) \tag{1.47c}$$

The notation "$2 \times O(\epsilon^2)$" means that a same type of error of order $O(\epsilon^2)$ has been committed twice. Since $N = T/\epsilon$, we finally get an approximation with error $O(\epsilon)$, known as the first order explicit scheme:

$$\psi_N = \Big[1 - i\epsilon \sum_{n=0}^{N-1} H_n\Big]\psi_0 + O(\epsilon). \tag{1.48}$$

Using $\epsilon \sum_{n=0}^{N-1} H_n = \int_{t_i}^{t_f} H(s)ds + O(\epsilon)$ implies

$$\psi(t_f) = \Big[1 - i \int_{t_i}^{t_f} H(s)ds\Big]\psi(t_i) + O(\epsilon), \tag{1.49}$$

which would give an accurate approximation for a small enough ϵ. However the explicit scheme (1.47) is known to be *unstable* for large time. This means that the multiplicative coefficient of the error $O(\epsilon)$ diverges for large time. This can be easily seen if one takes, for instance, a Hamiltonian with terms proportional to time t (known as secular or resonant terms). In that case, the solution (1.49) grows linearly with time. This scheme is thus not unitary since it does not preserve the norm of the state-solution. One can, however, interpret this result (1.49) as an approximation for small enough times. This is indeed what we get for the first order time dependent perturbation theory (1.22).

Explicit exponential scheme. One can improve the error approximating the integral in Eq. (1.19) by trapezoids:

$$\int_{t_n}^{t_{n+1}} dsH(s)\psi(s) = \epsilon H(t_{n+\frac{1}{2}})\psi(t_{n+\frac{1}{2}}) + O(\epsilon^3). \tag{1.50}$$

We next make the following expansion and use the Schrödinger equation (1.18):

$$\psi_{n+\frac{1}{2}} = \psi_n + \frac{\epsilon}{2}\frac{d\psi}{dt}(t_n) + O(\epsilon^2) \tag{1.51a}$$

$$= \psi_n - i\frac{\epsilon}{2}H_n\psi_n + O(\epsilon^2) \tag{1.51b}$$

We obtain, also using $H_n = H_{n+\frac{1}{2}} + O(\epsilon)$:

$$\int_{t_n}^{t_{n+1}} dsH(s)\psi(s) = \epsilon\psi_n\Big[H_{n+\frac{1}{2}} - i\frac{\epsilon}{2}H_{n+\frac{1}{2}}^2\Big] + O\left(\epsilon^3\right). \tag{1.52}$$

This implies for Eq. (1.19):

$$\psi_{n+1} = \psi_n - i\int_{t_n}^{t_{n+1}} ds H(s)\psi(s) \tag{1.53a}$$

$$= \left\{1 - i\epsilon H_{n+\frac{1}{2}} + \frac{1}{2}\left[i\epsilon H_{n+\frac{1}{2}}\right]^2\right\}\psi(t_n) + O\left(\epsilon^3\right) \tag{1.53b}$$

$$= e^{-i\epsilon H_{n+\frac{1}{2}}}\psi_n + O\left(\epsilon^3\right) \tag{1.53c}$$

leading to an error of $N \times O(\epsilon^3) = O(\epsilon^2)$ for the full integration. This scheme is stable and unitary (due to the exponential form) and is thus often used for numerical integration of the Schrödinger equation with a time-dependent Hamiltonian.

1.4 The two-state approximation for a two-photon transition

Definition Consider the two-photon interaction of an ultrashort pulse with a field $E(t)$ with a two-level atom. The effective Hamiltonian for a two-photon transition between two states of respective energies ω_g and ω_e by a laser of phase $\phi(t)$, corresponding to the instantaneous laser frequency $\omega_L(t) \equiv \dot{\phi}(t)$, reads in the resonant approximation

$$H_2(t) = \hbar \begin{bmatrix} \omega_g + S_g(t) & \frac{1}{2}\Omega^*(t)e^{2i\phi(t)} \\ \frac{1}{2}\Omega(t)e^{-2i\phi(t)} & \omega_e + S_e(t) - i\frac{1}{2}\Gamma_e(t) \end{bmatrix}. \tag{1.54}$$

The Stark shifts $S_g(t)$ and $S_e(t)$, respectively of the ground and excited states, are due to their coupling to the intermediate states m and the continuum channels ℓ (corresponding for instance to $s, p, d, \cdots$ continua for atoms):

$$S_j(t) = -\frac{\mathcal{E}^2(t)}{2\hbar^2}\left[\sum_{m\neq j}|\mu_{jm}|^2\frac{\omega_{mj}}{\omega_{mj}^2 - \omega_L^2(t)} + \mathcal{P}\int\frac{dE}{\hbar}\sum_\ell |\mu_{j;E,\ell}|^2\frac{\omega_{Ej}}{\omega_{Ej}^2 - \omega_L^2(t)}\right], \quad j = e, g \tag{1.55}$$

with μ_{jm} (resp. $\mu_{j;E,\ell}$) the transition dipole moments between the state j, of energy $\hbar\omega_j$, and the intermediate state (resp. the continuum state of the channel ℓ and of energy E), and $\omega_{mj} = \omega_m - \omega_j$, $\omega_{Ej} = E/\hbar - \omega_j$. $\mathcal{P}$ indicates the principal part of the integral when it is indefinite (if $\omega_j + \omega_L$ reaches the continuum). The two-photon Rabi frequency between the ground and the excited state is

$$\Omega(t) = -\frac{\mathcal{E}^2(t)}{2\hbar^2}\left[\sum_{m\neq e,g}\frac{\mu_{gm}\mu_{me}}{\omega_m - \omega_g - \omega_L(t)} + \int\frac{dE}{\hbar}\sum_\ell\frac{\mu_{g;E,\ell}\mu_{E,\ell;e}}{E/\hbar - \omega_g - \omega_L(t)}\right]. \tag{1.56}$$

The field intensity $I(t)$ is related to the field amplitude $\mathcal{E}(t)$ through the relation

$$I(t) = \frac{1}{2}\epsilon_0 c\mathcal{E}^2(t), \quad I[\mathrm{W/cm^2}] \approx 3.50945 \times 10^{16}\left(\mathcal{E}[\mathrm{u.a.}]\right)^2. \tag{1.57}$$

It is usually a good approximation to consider the mean (or central) frequency of the laser ω_0 instead of the instantaneous one $\omega_L(t)$ to calculate the Stark shifts and the Rabi frequency. This is generally the case when the frequency of the laser is chirped on an interval $\Delta\omega_L \ll \omega_0$. In that case, one has a fixed ratio

$$r = (S_e(t) - S_g(t))/\Omega(t). \tag{1.58}$$

In Eq.(1.54) we considered that the excited state is lossy through ionization by the laser. This is taken into account by summing the partial rates to the continuum channel ℓ:

$$\Gamma_e(t) = \sum_\ell \Gamma_e^{(\ell)}, \quad \Gamma_e^{(\ell)} = \frac{\pi}{2\hbar}\mathcal{E}^2(t)|\mu_{e;E=\hbar\omega_e+\hbar\omega_L,\ell}|^2. \tag{1.59}$$

The partial rates have been written here for the case of a one photon resonance in the continuum from the excited state.

Condition of validity. This resonant two-state approximation is valid when, for all $m \neq g, e$ and $j = g, e$,

$$|\Omega_{jm}| \ll |\Delta_{jm}|, \tag{1.60a}$$

$$|\Omega_{jm}|, |\omega_e - \omega_g - 2\omega_L| \ll \omega_L \quad \text{(resonant approximation)} \tag{1.60b}$$

with the one-photon detunings

$$\Delta_{gm} = \omega_m - \omega_g - \omega_L, \quad \Delta_{em} = -\omega_m + \omega_e - \omega_L \tag{1.61}$$

corresponding to the one-photon Rabi frequencies

$$\Omega_{jm} = \frac{\mathcal{E}}{\hbar}\mu_{jm}. \tag{1.62}$$

Dynamics and dressed effective Hamiltonian. The dynamics is given by the Schrödinger equation

$$i\hbar\frac{\partial}{\partial t}\psi(t) = H_2(t)\psi(t). \tag{1.63}$$

One can alternatively consider a transformed state $\widetilde{\psi}(t) = T^\dagger(t)\psi(t)$ which leads to the Schrödinger equation

$$i\frac{\partial}{\partial t}\widetilde{\psi}(t) = \widetilde{H}_2(t)\widetilde{\psi}(t) \tag{1.64}$$

with the Hamiltonian

$$\widetilde{H}_2(t) = T^\dagger(t)H_2(t)T(t) - iT^\dagger(t)\frac{\partial T}{\partial t}(t). \tag{1.65}$$

We consider the phase transformation

$$T(t) = \begin{bmatrix} 1 & 0 \\ 0 & e^{-2i\phi(t)} \end{bmatrix}, \tag{1.66}$$

which has as physical interpretation the dressing of the upper state by minus two photons of frequency $\dot{\phi}$. We remark that this transformation leaves the population of the states unchanged. This leads to

$$\begin{aligned}\widetilde{H}_2(t) &= \hbar \begin{bmatrix} \omega_g + S_g(t) & \frac{1}{2}\Omega^*(t) \\ \frac{1}{2}\Omega(t) & \omega_e + S_e(t) - i\frac{1}{2}\Gamma_e(t) - 2\dot{\phi}(t) \end{bmatrix} \\ &= \hbar[\omega_g + S_g(t)] \begin{bmatrix} 1 & 0 \\ 0 & 1 \end{bmatrix} + \frac{\hbar}{2} \begin{bmatrix} 0 & \Omega^*(t) \\ \Omega(t) & 2\Delta(t) - i\Gamma_e(t) \end{bmatrix} \end{aligned} \tag{1.67}$$

with

$$\Delta(t) = S(t) + \delta(t), \quad S(t) = S_e(t) - S_g(t), \tag{1.68}$$

and the time dependent two-photon detuning

$$\delta(t) = \omega_e - \omega_g - 2\omega_L(t). \tag{1.69}$$

This gives the relation between the instantaneous phase of the laser and the two-photon detuning:

$$\phi(t) = \frac{\omega_e - \omega_g}{2} t - \frac{1}{2} \int^t ds\ \delta(s). \tag{1.70}$$

We often omit from Eq. (1.67) the diagonal matrix proportional to the identity since it leads to a global phase of the state, and we can thus consider the generic Hamiltonian

$$H(t) = \frac{\hbar}{2} \begin{bmatrix} 0 & \Omega(t) \\ \Omega(t) & 2\Delta(t) - i\Gamma_e(t) \end{bmatrix}, \tag{1.71}$$

where we have assumed for simplicity that Ω is real.

1.5 Beyond the two-state approximation

If one intermediate state n is such that $|\Omega_{jn}| \sim |\Delta_{jn}|$ ($j = g$ or $j = e$), it induces in the system one-photon processes. This should be included explicitly in the Hamiltonian leading to a resonant three-state approximation:

$$H_3(t) = \hbar \begin{bmatrix} \omega_g + S_g(t) & \frac{1}{2}\Omega_{gn}(t)e^{i\phi(t)} & \frac{1}{2}\Omega_{ge}(t)e^{2i\phi(t)} \\ \frac{1}{2}\Omega^*_{gn}(t)e^{-i\phi(t)} & \omega_n + S_n(t) & \frac{1}{2}\Omega^*_{en}(t)e^{i\phi(t)} \\ \Omega^*_{ge}(t)e^{-2i\phi(t)} & \frac{1}{2}\Omega_{en}(t)e^{-i\phi(t)} & \omega_e + S_e(t) - i\frac{1}{2}\Gamma_e(t) \end{bmatrix} \tag{1.72}$$

with

$$S_j(t) = -\frac{\mathcal{E}^2(t)}{4\hbar^2} \left[\sum_{m \neq j,n} \frac{|\mu_{jm}|^2}{\hbar^2} \frac{\omega_{mj}}{\omega_{mj}^2 - \omega_L^2(t)} + \mathcal{P} \int \frac{dE}{\hbar} \sum_\ell \frac{|\mu_{j;E,\ell}|^2}{\hbar^2} \frac{\omega_{Ej}}{\omega_{Ej}^2 - \omega_L^2(t)} \right], \tag{1.73a}$$

$$S_n(t) = -\frac{\mathcal{E}^2(t)}{4\hbar^2} \left[\sum_{m \neq g,e,n} \frac{|\mu_{nm}|^2}{\hbar^2} \frac{\omega_{mn}}{\omega_{mn}^2 - \omega_L^2(t)} + \mathcal{P} \int \frac{dE}{\hbar} \sum_\ell \frac{|\mu_{n;E,\ell}|^2}{\hbar^2} \frac{\omega_{En}}{\omega_{En}^2 - \omega_L^2(t)} \right] \tag{1.73b}$$

$$\Omega_{ge}(t) = -\frac{\mathcal{E}^2(t)}{2\hbar^2} \left[\sum_{m \neq e,g,n} \frac{\mu_{gm}\mu_{me}}{\omega_m - \omega_g - \omega_L(t)} + \int \frac{dE}{\hbar} \sum_\ell \frac{\mu_{g;E,\ell}\mu_{E,\ell;e}}{E/\hbar - \omega_g - \omega_L(t)} \right]. \tag{1.73c}$$

Using the phase transformation (corresponding to a dressing of the intermediate state n with minus one photon and of the excited state e with minus two photons)

$$T(t) = \begin{bmatrix} 1 & 0 & 0 \\ 0 & e^{-i\phi(t)} & 0 \\ 0 & 0 & e^{-2i\phi(t)} \end{bmatrix}, \tag{1.74}$$

we get (omitting the global phase)

$$\widetilde{H}_3(t) = \hbar \begin{bmatrix} S_g(t) & \frac{1}{2}\Omega_{gn}(t) & \frac{1}{2}\Omega_{ge}(t) \\ \frac{1}{2}\Omega^*_{gn}(t) & \Delta_{gn}(t) + S_n(t) & \frac{1}{2}\Omega^*_{en}(t) \\ \Omega^*_{ge}(t) & \frac{1}{2}\Omega_{en}(t) & \delta(t) + S_e(t) - i\frac{1}{2}\Gamma_e(t) \end{bmatrix} \tag{1.75}$$

with the one photon detuning

$$\Delta_{gn}(t) = \omega_n - \omega_g - \dot{\phi}(t) = \omega_n - \frac{\omega_g + \omega_e}{2} + \frac{1}{2}\delta(t). \tag{1.76}$$

Keeping the leading order in the field amplitude, this can be approximated by

$$\widetilde{H}_3(t) \approx \frac{\hbar}{2} \begin{bmatrix} 0 & \Omega_{gn}(t) & 0 \\ \Omega^*_{gn}(t) & 2\Delta_{gn}(t) & \Omega^*_{en}(t) \\ 0 & \Omega_{en}(t) & 2\delta(t) - i\Gamma_e(t) \end{bmatrix}. \tag{1.77}$$

This can be directly generalized for more than one resonant intermediate state. It is however better to use the effective Hamiltonian (1.75) in a strong field regime, especially when $\delta \ll \Delta_{gm}$. It is in practice useful to decompose the phase of the laser as $\omega_0 t + \phi(t)$ with ω_0 the mean frequency of the laser (before its shaping, see next section) and $\phi(t)$ a relative phase.

1.6 Pulse-Shaping Techniques for Femtosecond Pulses

Femtosecond pulses are used in many fields due to their specificities of extreme short duration, ultra-high peak power or large spectral bandwidth. Reliable generation of pulses below 100fs occurred the first time in 1981 with the invention of the colliding pulse modelocked (CPM) ring dye laser [29]. Despite relative low energy per pulses, the ultrashort pulse duration leads to peak power large enough for non-linear pulse compression culminating in pulses as short as 6 fs in the visible. Recent advances in laser technology as the use of solid-state gain media, laser diode pumping, fiber laser, have led to simple, reliable, turn key ultrashort laser oscillators with pulse duration ranging from few ps down to 5 fs.

Application of these ultrashort pulses requires to control their temporal shape. The dispersion of materials and optical devices has been used to compress, stretch or replicate the pulses. Limitations on the ability to control the temporal shape of the pulse by classical optical devices have lead to the development of pulse shapers. These devices are linear filters enabling the

independent control of the spectral amplitude and phase giving a complete control of the temporal shape and phase of the pulse. Due to the extreme short duration of the pulses, the control cannot be achieved directly by temporal modulators. The control has to be done in the spectral domain. Two technologies of pulse shapers are widely used: spatial amplitude and phase modulators implemented in a zero-dispersion line or 4-f line, and acousto-optic programmable dispersive filters. Experimental implementations of these pulse shaping examples will then be presented.

1.6.1 Definitions

Ultrashort pulses characteristics

The field can be determined either by the temporal phase and amplitude or by the spectral phase and amplitude. The extreme shortness of ultrashort pulses implies a large spectral bandwidth. This field can be expressed in an experimental representation as:

$$\mathbf{E}(t) = \mathcal{E}_0 \Lambda(t) e^{i(\omega_0 t + \phi(t))}, \tag{1.78}$$

where ω_0 is the central angular frequency, $\Lambda(t)$ is the envelope with $0 \leq \Lambda(t) \leq 1$ and $\mathcal{E}_0$ is the peak amplitude, and $\omega_0 t + \phi(t)$ its temporal phase. The spectrum $\tilde{I}(\omega)$, or spectral power density, is the square modulus of the spectral amplitude: $\tilde{I} = A(\omega)^2$. Its temporal counterpart $I(t)$ equals the square modulus of the temporal amplitude $A(t)$: $I(t) = (\mathcal{E}_0 \Lambda(t))^2$. We define the normalization of the field as

$$\frac{1}{N} \int_{-\infty}^{+\infty} |\tilde{\mathbf{E}}(\omega)|^2 \frac{d\omega}{2\pi} = \frac{1}{N} \int_{-\infty}^{+\infty} |\mathbf{E}(t)|^2 dt = 1. \tag{1.79}$$

The pulse center is then defined by

$$t_0 = \frac{1}{N} \int_{-\infty}^{+\infty} t |\mathbf{E}(t)|^2 dt, \tag{1.80}$$

and the central frequency by

$$\omega_0 = \frac{1}{N} \int_{-\infty}^{+\infty} \omega |\tilde{\mathbf{E}}(\omega)|^2 \frac{d\omega}{2\pi}. \tag{1.81}$$

To analyse the different effects of the spectral phase, it is useful to expand the spectral phase into a Taylor series:

$$\tilde{\phi}(\omega) = \tilde{\phi}(\omega_0) + \tilde{\phi}^{(1)}(\omega_0)(\omega - \omega_0) + \frac{\tilde{\phi}^{(2)}(\omega_0)}{2!}(\omega - \omega_0)^2 + \frac{\tilde{\phi}^{(3)}(\omega_0)}{3!}(\omega - \omega_0)^3 ... \tag{1.82}$$

The first order spectral phase term corresponds to a time delay, the second order spreads linearly in time the frequency and so stretches the pulse. The third order introduces pre-pulses or post-pulses around the main pulse. The temporal intensity can be modified by changing the spectral phase only, but its complete control requires shaping both the spectral phase and amplitude.

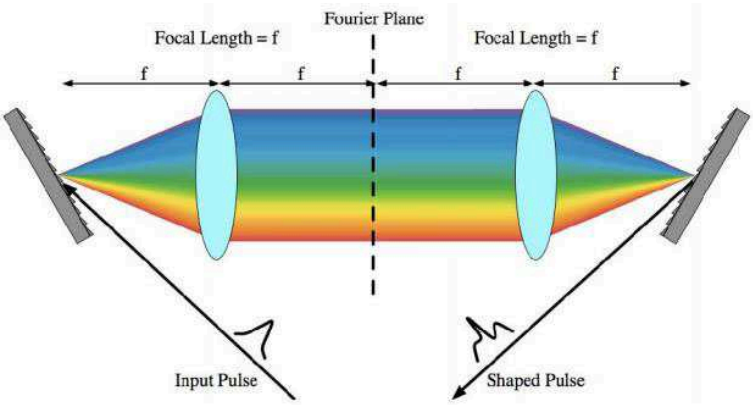

FIG. 1.4 - *Basic layout for Fourier transform femtosecond pulse shaping.*

Femtosecond pulse shaping using spatial light modulators

The dispersion-free apparatus in Fig. 1.4 is subsequently adopted for manipulating pulses on the 100 fs time scale, with the use of fixed masks initially, and later with programmable Spatial Light Modulators (SLM). The apparatus of Fig. 1.4 (without the mask) can also be used to introduce dispersion for pulse stretching or compression by changing the grating-lens spacing. This idea is extensively used for high-power femtosecond chirped pulse amplifier. The waveform synthesis is achieved by spatial masking of the spatially dispersed optical frequency spectrum. Figure 1.4 shows the basic pulse shaping apparatus, which consists of a pair of diffraction gratings and lenses, arranged in a configuration known as a "zero dispersion pulse compressor", and a pulse shaping mask. The individual frequency components contained within the incident ultrashort pulse are angularly dispersed by the first diffraction grating, and then focused to small diffraction limited spots at the back focal plane of the first lens, where the frequency components are spatially separated along one dimension. Essentially the first lens performs a Fourier transform which converts the angular dispersion from the grating to a spatial separation at the back focal plane. Spatially patterned amplitude and phase masks (or a SLM) are placed in this plane in order to manipulate the spatially dispersed optical Fourier components. After, a second lens and grating recombine all the frequencies into a single collimated beam, a shaped output pulse is obtained, with the output pulse shape given by the Fourier transform of the pattern transferred by the masks onto the spectrum.

1.6.2 Example for an input Gaussian pulse and linear chirping

We assume an input field of Gaussian shape with the mean frequency ω_0 and the full width at half maximum (for the corresponding intensity) $T_{\mathrm{in,FWHM}} = T_{\mathrm{in}}\sqrt{2\ln 2}$:

$$E_{\mathrm{in}}(t) = \mathcal{E}_{0\mathrm{in}}\Lambda_{T_{\mathrm{in}}}(t)e^{i\omega_0 t}, \quad \Lambda_{T_{\mathrm{in}}}(t) = e^{-(t/T_{\mathrm{in}})^2} \tag{1.83}$$

We define the transparency coefficients $0 \leq \mathcal{T}(\omega) \leq 1$ and phase $\varphi(\omega)$ as follows:

$$\widetilde{E}(\omega) = \mathcal{T}(\omega) e^{i\varphi(\omega)} \widetilde{E}_{\text{in}}(\omega). \tag{1.84}$$

When the frequency of the input field matches the transition frequency: $\omega_0 = \omega_e - \omega_g$, a linear chirping results from a single modulator with a quadratic spectral phase:

$$\mathcal{T}(\omega) = 1, \quad \varphi(\omega) = \gamma(\omega - \omega_0)^2. \tag{1.85}$$

This leads to the output field which is of maximum amplitude when it is exactly resonant:

$$E(t) = \mathcal{E}_{0\text{in}} \sqrt{\frac{T_{\text{in}}}{T}} e^{-(t/T)^2} e^{i(\omega_0 t + \phi(t) - \theta)} \tag{1.86}$$

with the instantaneous frequency

$$\begin{aligned} \omega(t) \equiv \omega_0 + \dot{\phi}(t) &= \omega_0 - \frac{8\gamma}{T_{\text{in}}^4 + 16\gamma^2} t & (1.87a) \\ &\simeq \omega_0 - \frac{1}{2\gamma} t, \text{ for } \gamma \gtrsim T_{\text{in}}^2, & (1.87b) \end{aligned}$$

the phase

$$\theta = \arg \sqrt{T_{\text{in}}^2 - 4i\gamma}, \tag{1.88}$$

and the duration

$$\begin{aligned} T &= \frac{4\gamma}{T_{\text{in}}} \sqrt{1 + \left(\frac{T_{\text{in}}^2}{4\gamma}\right)^2} & (1.89a) \\ &\simeq \frac{4\gamma}{T_{\text{in}}^2} T_{\text{in}}, \text{ for } \gamma \gtrsim T_{\text{in}}^2. & (1.89b) \end{aligned}$$

The width of the chirp that can be characterized by $|\dot{\phi}(T/2) - \dot{\phi}(-T/2)| = |\dot{\phi}(T)|$ is thus in practice limited by the spectrum of the laser:

$$\dot{\phi}(T) \lesssim \frac{2}{T_{\text{in}}}, \tag{1.90}$$

reaching its asymptotic value $4/T_{\text{in}}$ for $\gamma \gtrsim T_{\text{in}}^2$, corresponding to the duration $T \gtrsim 4T_{\text{in}}$.

If there is a mismatch between the mean laser frequency ω_0 and the transition frequency $\omega_1 := \omega_e - \omega_g$, and if one wants an effective frequency that is resonant (i.e. $\Delta = 0$) when the output field is maximum in the time domain, we have to shape the spectral amplitude as

$$\mathcal{T}(\omega) = e^{\frac{1}{4}[(\omega-\omega_0)^2 T_{\text{in}}^2 - (\omega-\omega_1)^2 T_a^2]}, \quad \varphi(\omega) = \gamma(\omega - \omega_1)^2 \tag{1.91}$$

with the requirement that the shaping operates well within the bandwidth:

$$|\omega_0 - \omega_1| \lesssim \left(\frac{1}{T_{\text{in}}} - \frac{1}{T_a}\right) \sqrt{2 \ln 2}, \quad T_a > T_{\text{in}}. \tag{1.92}$$

This leads to the output field which is of maximum amplitude when it is exactly resonant:

$$E(t) = \mathcal{E}_{0\text{in}}\sqrt{\frac{T_a}{T}}e^{-(t/T)^2}e^{i[\omega_1 t+\phi(t)-\theta]} \tag{1.93}$$

with the instantaneous frequency

$$\omega(t) \equiv \omega_1 + \dot{\phi}(t) = \omega_1 - \frac{8\gamma}{T_a^4+16\gamma^2}t \tag{1.94a}$$

$$\simeq \omega_0 - \frac{1}{2\gamma}t, \text{ for } \gamma \gtrsim T_a^2, \tag{1.94b}$$

the phase

$$\theta = \arg\sqrt{T_a^2 - 4i\gamma}, \tag{1.95}$$

and the duration

$$T = \frac{4\gamma}{T_a}\sqrt{1+\left(\frac{T_a^2}{4\gamma}\right)^2} \tag{1.96a}$$

$$\simeq \frac{4\gamma}{T_a}, \text{ for } \gamma \gtrsim T_a^2. \tag{1.96b}$$

1.6.3 Spectrogram for two-photon processes

To provide an intuitive picture of the time evolution of the spectrum of the laser, time-frequency spectrograms such as the Wigner function have been proposed (see for instance [30,31]). The Wigner function of an electric field $E(t)$ can be written as [30]

$$W(\omega,t) = \int E^*(\omega+\omega'/2)E(\omega-\omega'/2)e^{i\omega' t}d\omega'. \tag{1.97}$$

For a two-photon process, we prefer to use a second harmonic Wigner function defined as

$$W_2(\omega,t) = \int W(\omega',t)W(\omega-\omega',t)d\omega'. \tag{1.98}$$

The absolute value of this second harmonic Wigner function defines the two-photon spectrogram used in Figs. 2.3 and 2.4 of the next chapter.

Chapter 2

Optimization of two-photon transition by phase shaping

In this chapter we show that for moderate intensities, in order to optimize the two-photon absorption in atomic Cesium in the ground states, the frequency of the laser pulse can be swept following the temporal change of the absorption energy gap. By moderate intensities we mean that we consider the perturbation expansion up to the second order (1.31) for which the Stark shifts are non negligible and the population transfer is of order $10-15\%$ (i.e. small but non negligible) (see section 2.3.2 for a more precise statement) In the case of a Gaussian pulse, it is shown that a temporal cubic phase is sufficient to retain the resonance condition during the interaction since it allows one to recover very accurately the population transfer that would occur without Stark shifts. This result has been demonstrated in the group of J. Ahn (Korea) as described below [71]. We also extend theoretically this study for strong fields for which the population transfer is large.

In the next Section, we describe the model and the pulse shaping scheme. Section 2.2 is devoted to the description of the experiments performed by our collaborators S. Lee *et al.* In Section 2.3, we present the results and their interpretation before concluding in Section 2.4.

2.1 Theoretical consideration

The model and the general phase matching condition. From the preceding chapter [see Eq. (1.54) from which a global phase has been omitted], a two-photon transition in a two-state system, the effective Hamiltonian in the resonant approximation can be written in the dressed state basis $|g;0\rangle, |e;-2\rangle$ as

$$H(t) = \hbar \begin{bmatrix} 0 & \frac{1}{2}\Omega(t)e^{2i\phi(t)} \\ \frac{1}{2}\Omega(t)e^{-2i\phi(t)} & \Delta + S(t) \end{bmatrix}, \tag{2.1}$$

where $\Omega(t)$ (chosen real) is the two-photon Rabi frequency and $\phi(t)$ is the phase of the laser field, relative to central frequency ω_0. We have decomposed the detuning as the static two-photon detuning $\Delta = \omega_e - \omega_g - 2\omega_0$, and $S(t)$ the relative dynamical Stark shift. We have

omitted irrelevant global phases. For a field amplitude of shape $\sqrt{\Lambda(t)}$, the Rabi frequency is of the form $\Omega(t) = \Omega_0\Lambda(t)$ with Ω_0 proportional to the peak field intensity I_{peak}, and the Stark shift has the same time dependence: $S(t) = S_0\Lambda(t)$ with S_0 also proportional to I_{peak}: $S_0 = r\Omega_0$. We consider Gaussian pulse shape $\Lambda(t) = \exp[-(t/\tau)^2]$.

The Hamiltonian can be rewritten as $\hat{H} = \hat{T}^\dagger H\hat{T} - i\hbar\hat{T}^\dagger d\hat{T}/dt$:

$$\hat{H}(t) = \hbar \begin{bmatrix} 0 & \frac{1}{2}\Omega(t) \\ \frac{1}{2}\Omega(t) & \Delta + S(t) - 2\dot{\phi}(t) \end{bmatrix} \tag{2.2}$$

in a representation $\Psi(t) = \hat{T}^\dagger\psi(t)$ of the original state $\psi(t)$ associated to the diagonal transformation (which leaves the population unchanged)

$$\hat{T}(t) = \begin{bmatrix} 1 & 0 \\ 0 & e^{-i2\phi(t)} \end{bmatrix}. \tag{2.3}$$

It is known (see for instance [32] for a proof using the geometric control theory and [17] for an experimental demonstration through a learning algorithm) that, for such two-state Hamiltonians (2.2), the minimum pulse area of the Rabi frequency to achieve the complete transfer is $\int dt\Omega(t) = \pi$ and that it is achieved when the exact resonance is satisfied at each time:

$$2\dot{\phi}(t) = \Delta + S(t). \tag{2.4}$$

This phase matching condition can be interpreted as a compensation of the dynamical Stark shifts by the shaping of the pulse to maximize the resonance effects. Additional chirping of the field can not decrease the π-pulse area. This result (2.4) can be also derived within the second order of the perturbation theory [33] [see Eq. (1.31)] which yields for the probability of population transfer to the excited state:

$$P_e(t) \approx \frac{1}{4}\left|\int_{t_i}^{t} dt'\Omega(t')e^{-i[2\phi(t')-\Delta t'-\int^{t'} S(u)du]}\right|^2, \tag{2.5}$$

where the error is of order $O(\epsilon^3)$ with respect to half of the partial area of the Rabi frequency: $\epsilon(t) \equiv \int_{t_i}^{t} dt'\Omega(t')/2$. Here, t_i indicates the initial time of the interaction. The phase matching condition (2.4) is however valid beyond the perturbation theory as long as the validity of two-state model (2.2) is preserved.

It is of interest to determine general analytic pulse shaping programming to satisfy this phase matching condition [21]. Below we derive and test approximate conditions with simple pulse shapes, compensating the dynamical Stark shifts, in order to produce more efficient population transfer at moderate field intensities.

Optimal phase matching condition near the peak value of the Stark shift. We make a series expansion of the dynamical Stark shift and of the phase in the time domain to satisfy the phase matching condition near its maximum in absolute value, i.e. around $t = 0$.

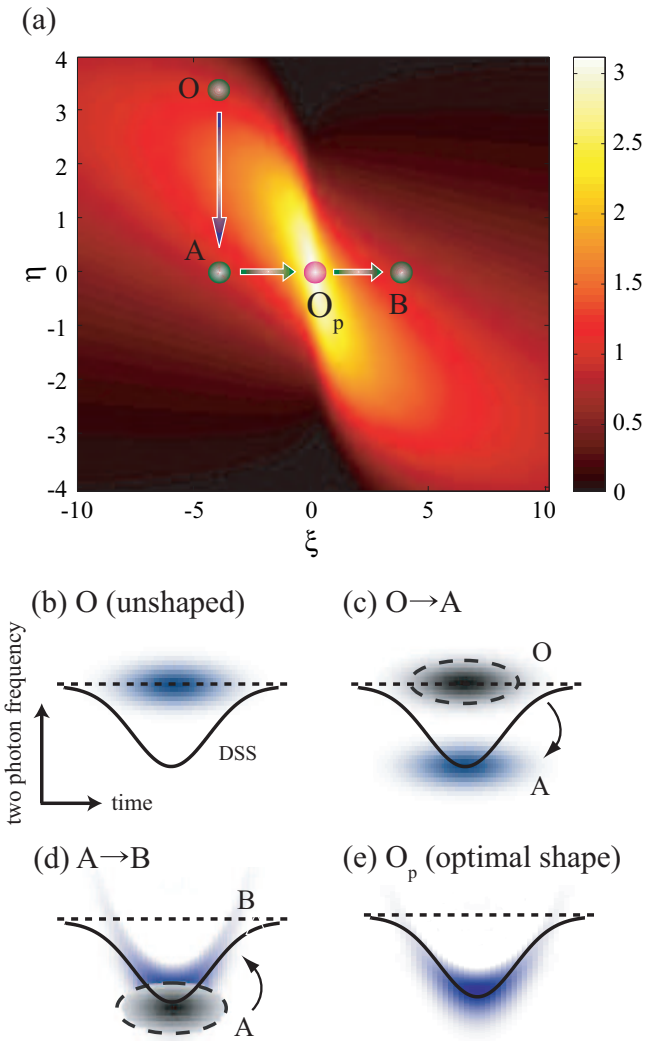

FIG. 2.1 - *(a) Strong-field two-photon excitation probability, $P_e(\eta, \xi)$ (arbitrary units), calculated as a function of dimensionless parameters: the frequency detuning η and the spectral curvature ξ. (b) Two-photon spectrogram (as shaded contour plot, see the definition in section 1.7) of the unshaped pulse at the point $O(S_0\tau/3, -\Delta\tau - S_0\tau)$, where Δ and δ_0 denote the static and peak dynamic level shifts, respectively. The (negative) dynamic level shift is drawn as a full line. (c) Control of the detuning along $\overline{OA}$. (d) Spectral curvature control along $\overline{AB}$. (e) Two-photon spectrogram of the optimally shaped pulse at the point $O_p(0,0)$.*

Truncating the series keeping the cubic terms, we get a transfer probability proportional to the peak intensity of the field:

$$P_e(\eta,\theta,\xi) \propto \left| \int_{-\infty}^{\infty} e^{-X^2+i\eta X+i\theta X^2+i\xi X^3} dX \right|^2, \tag{2.6}$$

where the dimensionless control parameters are defined as $\eta = 2\dot{\phi}(0)\tau - (S_0+\Delta)\tau$, $\theta = \ddot{\phi}(0)\tau^2$, and $\xi = [\dddot{\phi}(0)\tau^3 + S_0\tau]/3$. We determine the optimal pulse shape from the maximum value of (2.6), which corresponds to $\eta = \theta = \xi = 0$. This leads to nonzero linear and cubic phase terms and a zero quadratic phase:

$$2\phi(t) = (\Delta + S_0)t - \frac{1}{3}\frac{S_0}{\tau^2}t^3. \tag{2.7}$$

Figure 2.1(a) shows the probability of strong-field two-photon excitation from Eq. (2.6). The point O in Fig. 2.1(a) corresponds to the unshaped transform-limited pulse, and O_p the optimal pulse shape ($\eta = \xi = 0$). The spectro-temporal shape at O_p is illustrated as in Fig. 2.1(e). The control parameters $\dot{\phi}(0)$ in η and $\dddot{\phi}(0)$ in ξ denote the frequency offset (detuning) and the frequency curvature in a spectrogram, respectively. Therefore, the change of η along the path $\overline{\mathrm{OA}}$ in Fig. 2.1(a) is the frequency detuning as illustrated in Fig. 2.1(c). Also, the change of ξ along $\overline{\mathrm{AB}}$ is the frequency curvature control as shown in Fig. 2.1(d).

2.2 Description of the experiments

For the experiment performed by S. Lee *et al.*, sub-picosecond infrared pulses were used [71] with a pulse energy of up to 100 μJ produced from a Ti:Sapphire laser amplifier system operating at a repetition rate of 1 kHz. The pulses were shaped by an acousto-optic programmable dispersive filter (DAZZLER) and illuminated on Cesium atoms (^{133}Cs) of a gas density of 2.2×10^{16} m^{-3} in an optical cell at room temperature. The laser frequency was tuned to make the two-photon resonant condition for the $6S_{1/2}-8S_{1/2}$ transition at the low laser intensity limit implying $S \approx 0$, i.e. $\Delta = 0$. The laser peak intensity (at the focus) was varied in the range of 0 .. $0.2I_0$ ($I_0 = 10^{11}$ W/cm^2). We remark that intensities above this range start producing a significant ionization from the upper state (see Appendix A for details of the model including the ionization rate from the upper state). Then, the atoms in the excited $8S_{1/2}$ state decay first to the $7P_{1/2}$ state and then down to the $6S_{1/2}$ ground state. The $7P_{1/2}-6S_{1/2}$ fluorescence signal collected by a photo-multiplier tube (PMT) was used to estimate the excitation probability of the $6S_{1/2} - 8S_{1/2}$ transition. The collision coherent time and the transit time (average escape time of atoms passing the beam diameter) are 66 ns and 390 ns, and the lifetime of $8S_{1/2}$ is 90 ns [34].

The field before its spectral shaping is of Gaussian shape with mean frequency ω_0: $\mathcal{E}_{\mathrm{in}}(t) = \mathcal{E}_{0\mathrm{in}} e^{-(t/\tau_{\mathrm{in}})^2} e^{i\omega_0 t}$. The programming target pulse $\mathcal{E}(t)$ is chosen to be also of Gaussian shape:

$$\mathcal{E}(t) = \mathcal{E}_0 e^{-(t/\tau)^2} e^{i(\omega_0 t+\phi(t))}. \tag{2.8}$$

The shaping in the frequency domain is such that

$$\widetilde{\mathcal{E}}(\omega) = \mathcal{T}(\omega)e^{i\widetilde{\phi}(\omega)}\widetilde{\mathcal{E}}_{\text{in}}(\omega), \tag{2.9}$$

where $0 \leq \mathcal{T}(\omega) \leq 1$ is the transparency coefficient of the shaping device, $\widetilde{\phi}(\omega)$ is the spectral phase, and $\widetilde{F}(\omega) = \frac{1}{2\sqrt{\pi}} \int_{-\infty}^{+\infty} F(t)e^{-i\omega t}dt$ denotes the Fourier transform.

The laser beam focused on to the atoms has a spatial intensity profile

$$I(r,z) = I_0 \frac{w_0^2}{w^2(z)} e^{-r^2/w^2(z)}, \tag{2.10}$$

where $w(z)$ is the beam waist. As a result, we have determined numerically that the averaged field intensity and consequently the averaged dynamic Stark shift is approximately reduced by a factor 2 with respect to an uniform intensity profile. The calculated averaged dynamic of Stark shift is roughly -10×10^{12} rad/s (or -10 Trad/s) at 20 GW/cm^2 (see Appendix A for a more detailed discussion about the modelling of the driven Cesium atoms).

2.3 Results and Discussion

2.3.1 Verification of the optimal pulse shaping.

The verification of the optimal pulse shaping scheme discussed in Section II is carried out by measuring the $7P_{1/2} - 6S_{1/2}$ fluorescence as a function of the phase $\phi(t)$ defined in Eq. (2.8). The result is shown in Fig. 2.4, where $\phi(t)$ is programmed as a function of the coefficient a_1 and a_2 defining the variations of the cubic phase:

$$\phi(t) = a_1 t + a_2 t^3. \tag{2.11}$$

In the experiment peak intensities were used such that $I_{\text{peak}} \lesssim 0.2I_0$ and fields of duration $\tau = 90$ fs (corresponding to an intensity time-profile of full width at half maximum 150 fs). A field of peak intensity $I_{\text{peak}} = 0.47I_0 = 47$ GW/cm^2 leads to a complete population transfer (at the focus). We have checked from numerics that one can use Eq. (2.5) to determine the line shapes (and contour lines) in a rather good approximation. Moreover, the use of Eq. (2.6) instead of Eq. (2.5) to fit our experiments does not show a significant difference. The experiment does not allow us to determine very accurately the optimal value of a_2.

Along the vertical lines in Fig. 2.1(a), the frequency detuning experiments are shown in Fig. 2.3, compared with the numerical calculations. Figure 2.3(a) shows the line shapes of the signal, measured at the three different laser peak intensities, as functions of the frequency offset a_1 at zero cubic phase, i.e. $a_2 = 0$. The maximum of the signal is found at a larger frequency offset for a larger I_{peak}. A more careful analysis shows that a_1 is proportional to I_{peak} as predicted in Section 2.1 [see Eq. (2.7)].

Also, the signal is measured as a function of the frequency curvature $a_2\tau^2$ at zero linear phase, i.e. $a_1 = 0$. As shown in Fig. 2.3(b), the signal is measured with zero detuning, i.e.

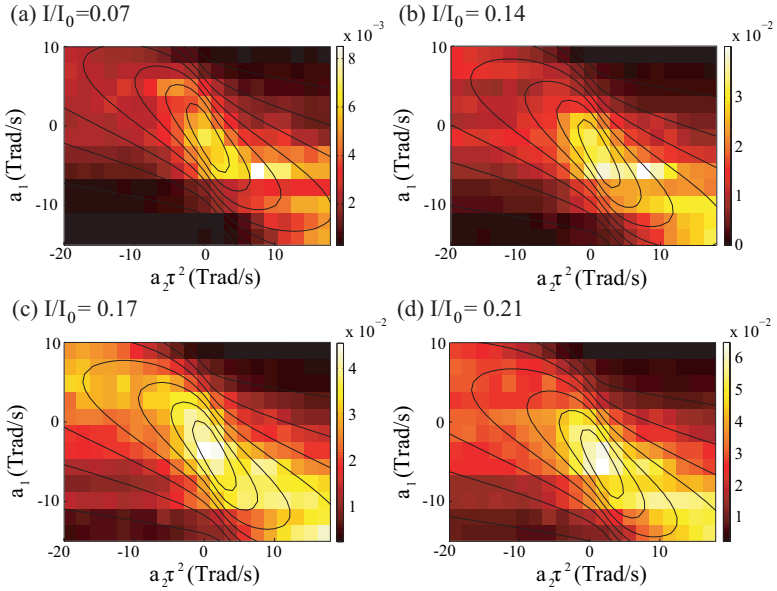

FIG. 2.2 - *Fluorescence 2D maps measured at laser peak intensities,* $I_{\mathrm{peak}}/I_0 = 0.06,\ 0.14,\ 0.17$ *and* 0.21*, as a function of* a_1 *and* $a_2\tau^2$ *parameters. Contour lines are calculated using Eq.* (2.6).

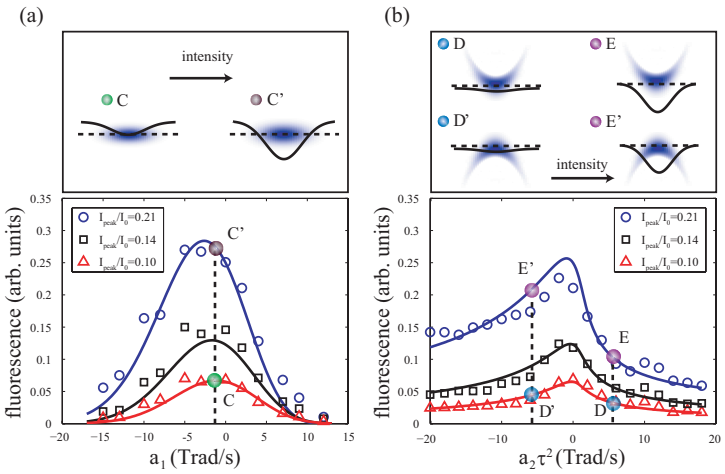

FIG. 2.3 - *Strong-field two-photon excitation of Cesium studied at three different laser intensities,* $I_{\mathrm{peak}}/I_0 = 0.21,\ 0.14,\ 0.10$*. The theoretical lines from Eq.* (2.6) *are compared with the* $7P_{1/2} - 6S_{1/2}$ *fluorescence signal measured (a) as a function of the frequency offset* a_1*, defined in Eq.* (2.11)*, at zero frequency curvature* $a_2 = 0$*; and (b) as a function of the frequency curvature* $a_2\tau^2$ *at zero frequency offset* $a_1 = 0$*. The upper inserts show the two-photon spectrograms (shaded contour plots) overlapped with the corresponding dynamically shifted energy levels (solid lines). The dotted lines represent the center frequency* ω_0 *of the shaped pulse.*

$a_1 = 0$, as a function of the frequency curvature $a_2\tau^2$. The line shape is symmetric at a low intensity (the lowest red line) but becomes gradually asymmetric at higher intensities (the upper black and blue lines). As the peak intensity increases, the overlap between the shifted energy level and the laser spectral distribution gradually decreases. As a result, the two-photon excitation in Cesium at zero frequency offset is better achieved by a negative cubic phase term. This seems counterintuitive because the curvature of the laser spectral distribution is opposite to that of the shifted energy level. However, as illustrated in the top panel of Fig. 2.3(b), the pulse at E' with a negative cubic phase makes a better overlap with the detuned energy level than the pulse at E with a positive cubic phase. Therefore, the two-photon excitation rate in Cesium at zero frequency offset is higher with a negative quadratic frequency chirp.

Figure 2.4 shows the pulse-shape dependence of the two-photon excitation in Cesium. For a simple detuning experiment (a_2=0), shown in the black line in Fig. 2.4(a), the excitation maximum is found at a negative a_1 since $S_0 < 0$. We note that the optimal point for the intensity $I_{\rm peak} = 1.7 \times 10^{10}$ W/cm^2 is located at $a_1 = -4.25$ Trad/s and $a_2\tau^2 = 1.4$ Trad/s from the analysis of Section II. The curvature control experiments shown in Fig. 2.4(b) are along the horizontal lines in Fig. 2.1(a). The measured signals are of more complex line shapes: Near the optimal detuning at $a_1 = 0$ (black line), as the curvature a_2 increases, the signal gradually grows and rapidly increases near $a_2 = 0$ (near O_p). For a more (less) detuned case with the positive (negative) a_1 in the blue (red) line, the signal rapidly decreases (increases) near $a_2 = 0$.

Finally, from Eq. (2.6), the intensity invariant forms of excitation probability can be calculated as a function of each single parameter η and ξ, respectively:

$$P_e(\eta, 0, 0) = \sqrt{\pi} e^{-\eta^2/2}, \tag{2.12}$$

$$P_e(0, 0, \xi) = \sum_{k=0}^{\infty} (-1)^k \xi^{2k} \frac{\Gamma(3k + 1/2)}{(2k)!}. \tag{2.13}$$

They are drawn in Fig. 2.5 overlaid with the measured data points from Fig. 2.2. We note that the overall probabilities of strong-field two-photon transition, $P_e/I^2\tau^2$, follow the theoretically obtained intensity invariant forms from Eq. (2.6).

2.3.2 Further optimization of the phase matching condition

One can further improve the approximate condition (2.7) by determining conditions that allow one to recover the population transfer that would be obtained without Stark shifts beyond the perturbative regime. To that end, we determine the population transfer to the excited state at the end of the process, from the numerical integration of the Schrödinger equation, for various (strong or not) peak field amplitudes and Stark shifts using a phase of the form (2.11). We do not consider here the spatial averaging. We first make the analysis using the two-state model (2.2). This is extended in the next subsection to a more accurate model of Cesium for strong fields. Figure 2.6 shows two typical contour plots of the deviation from the population

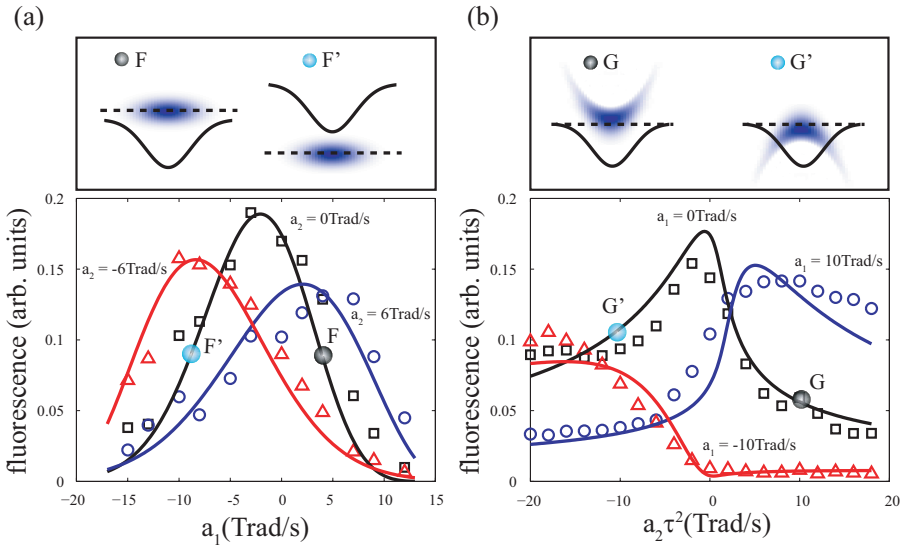

FIG. 2.4 - *Pulse-shape dependence of two-photon excitation in Cesium: The excitation is measured (a) as a function of frequency offset a_1 at fixed frequency curvatures $a_2 = 0$, 6, and -6 Trad/s, respectively; and (b) as a function of frequency curvature $a_2\tau^2$ at fixed frequency offsets $a_1 = 0$, 10, and -10 Trad/s, respectively. The peak intensity of the laser pulse is maintained at $I_{\text{peak}} = 1.7 \times 10^{10}$ W/cm^2. Upper inserts: as in Fig. 2.3*

.

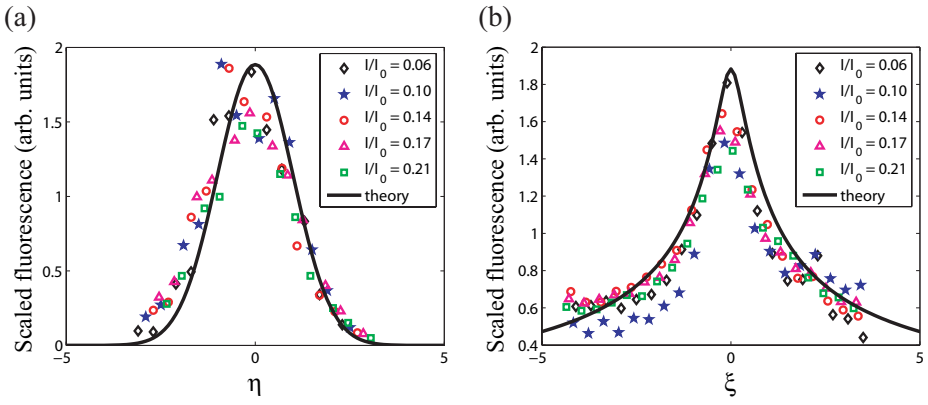

FIG. 2.5 - *Scaled strong-field two-photon absorption profile $P_e/I^2\tau^2$ in Eq. (2.6) is plotted as a function of (a) $\eta = (2a_1 - S_0)\tau$ and (b) $\xi = 2a_2\tau^3 + S_0\tau/3$.*

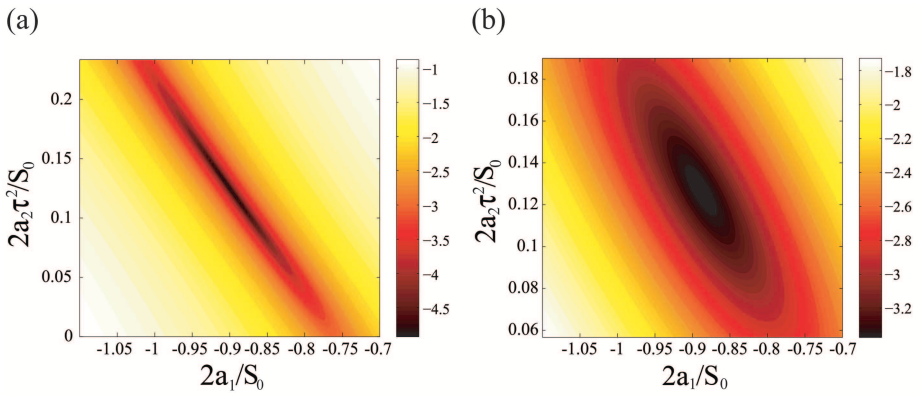

FIG. 2.6 - *Contour plot (in logarithmic scale to the base 10) at the end of the pulse of the deviation from the population transfer in absence of Stark shifts as a function of the dimensionless quantities* $2a_1/S_0$ *and* $2a_2\tau^2/S_0$ *for* $\Delta = 0$, $S_0 = \Omega_0$, *and (a)* $\tau\Omega_0 = \sqrt{\pi}$ *and (b)* $\tau\Omega_0 = \sqrt{\pi}/2$. *They correspond respectively to complete and half population transfers in absence of Stark shifts.*

transfer to the excited state achieved without Stark shifts, with a pulse area of (a) π and (b) $\pi/2$, corresponding to a population transfer without Stark shifts respectively of 1 and 0.5. We obtain (taking $\Delta = 0$) the approximate optimal function that allows one to recover accurately the population transfer without Stark shifts:

$$2\phi(t) = S_0 \left(0.89t - 0.12\frac{t^3}{\tau^2} \right). \tag{2.14}$$

This has been obtained for a field intensity not larger than the one leading to a complete population transfer in absence of Stark shifts.

The demonstration of the exact optimal values of the linear and cubic terms in Eq. (2.14) is found to be beyond the scope of the accuracy of the experiments described previously. However, it is remarkable that this optimized function is a simple linear function of the peak Stark shift and thus of the peak field amplitude, as anticipated in the preceding analysis. The value obtained for the linear term is close to the one determined with the truncated expansion (2.7). We have checked that the perturbation theory (2.5) gives a good approximation for the population transfer until transfer of approximately 0.15 (error of 5%), that corresponds to a pulse area approximately of 0.25π (consistent with the estimated error of the perturbative expansion). Despite this limitation, we have obtained the interesting result that the line shapes can be approximately well described, up to a scaling factor (which depends on the intensity and the Stark shifts and that has to be determined with the numerical simulation), by the perturbation theory even for stronger field intensities.

2.3.3 Optimized phase matching beyond the two-state model for Cesium

For the population transfer in Cesium atoms between the states $6S_{1/2} - 8S_{1/2}$, a two-state approximation is in principle valid for intensities not larger than approximately 10 GW/cm^2 (see Appendix A for a precise statement). Using the four-state Hamiltonian (7.3) derived in Appendix A, we numerically derive conditions of cubic phase matching to get the best population transfer at the lowest possible field intensity. The lowest field intensity has been found to be $I = 47$ GW/cm^2 with the cubic phase

$$2\phi(t) = S_0 \left(0.75t - 0.10\frac{t^3}{\tau^2} \right). \tag{2.15}$$

We get a population transfer of 99%, and the rest is ionized. We remark that the use of only a linear phase allows already a good transfer (98%). We notice that, for increasing intensities, deviating from the two-state model, the optimal cubic phase moves to smallest values in absolute values for the linear and cubic terms. We have obtained numerically that the coefficients after the spatial averaging saturates to $a_1 \approx -4.5$ Trad/s and $a_2\tau^2 \approx 0.5$ Trad/s for fields intensities beyond 20 GW/cm^2 in consistency with the experimental results.

2.3.4 Strong-field two-photon excitation in other alkali atoms

The two-photon excitation (TPE) in Cesium is characterized as non-resonant for a sufficiently low field intensity, meaning that no-intermediate states are directly involved (see Appendix A for the precise conditions of this statement). The dynamic Stark shifts of the $6S_{1/2}$ state is mainly determined by its coupling with the $6P_{1/2}$ and $6P_{3/2}$ states. The other couplings lead to a much smaller shift [35]. The $6S_{1/2}$ state is up-shifted by the dynamic Stark effect due to its repulsion with the two dressed states $|6P_{1/2}, -1\rangle$ and $|6P_{3/2}, -1\rangle$. The shift of the $8S_{1/2}$ is due to its coupling mainly with the P states and weakly with the continuum. The net dynamic shift between $6S_{1/2} - 8S_{1/2}$ is negative (see Appendix A).

On the other hand, TPE in Rubidium or in Sodium features an additional single-photon resonance. A typical femtosecond laser pulse of the center wavelength at 778 nm, that allows in principle TPE in Rubidium between the states $5S_{1/2}$ and $5D_{3/2,5/2}$, indeed strongly induces population into the intermediate nearly resonant state $5P_{3/2}$ [58]. Thus, the TPE in Rubidium should be described by a three-level model $5S_{1/2} - 5P_{3/2} - 5D_{3/2,5/2}$ even for moderate field intensities. Note that the $5P_{1/2}$ can also be populated for strong fields. In Sodium, a laser pulse of center wavelength 777 nm induces the $3S_{1/2} - 4S_{1/2}$ TPE process, but also a $4S_{1/2} - 7P_{1/2}$ single-photon process [33]. Therefore, TPE in Sodium should be modelled by a three-level system, similar to the case of Rubidium. In both cases, the detuning corresponding to the one-photon resonance is one order of magnitude smaller than the one in Cesium from $6S_{1/2}$ and $6P_{3/2}$.

Second part

Optimizing adiabatic passage in multi-level systems

Chapter 3

High fidelity and robust adiabatic passage in two-state systems

The time evolution of non-dissipative quantum systems is governed by the Schrödinger equation that depends on the charachteristic time T, e.g. the duration of a pulse. When T is large the analysis of the dynamics can be simplified using the adiabatic approximation.
In a two-state system, the fastest process to achieve a complete population transfer corresponds to a pulse with area π for the Rabi frequency for any time dependence of the (diagonal) detuning [32]. This process is however non-robust with respect to variations of the area that are often difficult to avoid in practice. In nuclear magnetic resonance (NMR), a series a π-pulses with well-defined static phases, known as composites pulses, have been proposed to compensate unknown errors in the parameters [43]. This technique is being investigated in quantum optics [44].

On the other hand, adiabatic passage and its variations [20, 46] allow robustness of the transfer as one increases the pulse area. But it leads in principle to an incomplete transfer reaching one only asymptotically in the adiabatic limit, i.e. $T \to \infty$. One can estimate the efficiency of the transfer for a concrete model using a complex time method leading to the Davis-Dykhne-Pechukas (DDP) formula [47–50].

Modern technologies allow the shaping of the field amplitude and phase even in the ultrafast femtosecond regime. In this case, the field is shaped in the frequency domain through the spatial separation and manipulation of the spectral components [1,51]. Finding an optimal shape that offers the best compromise between the fastness of the process, i.e. featuring an area as close as possible to π, and its robustness is thus important for applications.

Such an optimization has been proposed on the basis of the DDP formula resulting in the parallel adiabatic passage (PLAP) technique in which the fields produce eigenenergies which are parallel to each other [26–28]. The use of an additional field that cancels the nonadiabatic coupling has also been proposed [54, 55]. We remark however that this technique is expected to have in practice a limited advantage regarding robustness since it requires to have explicit knowledge of the (small) non-adiabatic coupling. In particular, in the present work use of this technique does not give better results than the PLAP with respect to an imperfect knowledge

of the field area (section VI). This chapter is organized as follows: We first recall the adiabatic theorem, adiabatic passage and the Davis-Dykne-Pechkas formula. Next we define the parallel adiabatic passage PLAP and the adiabatic passage complemented by destructive interference DIAP techniques on a concrete example with a Gaussian pulse which allows one to deduce two types of optimal shaping. Their implementation in the frequency domain is shown in Section 3.2.3. Their respective robustness is analyzed in Section 3.2.4. We conclude in Section 3.2.5.

3.1 Generalities on adiabatic passage

3.1.1 Adiabatic theorem

Let's consider a quantum system with Hamiltonian $H = \hat{H}(t/T)$ wich evolves slowly and continously in time. The evolution is adiabatic when T goes to infinity. Let's denote by $E_1(t), E_2(t), ..., E_n(t), ...$ the eigenvalues of the instantaneous Hamiltonian, by $|\Psi_n^\alpha(t)\rangle_{\alpha=0,...d_n}$ the associated eigenvectors, with respective degeneracies $d_1, d_2, ..., d_n, ...,$ and by $P_1(t), P_2(t), ...P_n(t)...$ the projectors on its subspaces:

$$H|\Psi_n^\alpha(t)\rangle = E_n(t)|\Psi_n^\alpha(t)\rangle, \tag{3.1}$$

$$\langle\Psi_m^\alpha(t)|\Psi_n^\beta(t)\rangle \ = \delta_{mn}\delta_{\alpha\beta} \tag{3.2}$$

$$P_n(t) = \sum_{\alpha=0}^{d_n} |\Psi_n^\alpha(t)\rangle\langle\Psi_n^\alpha(t)|. \tag{3.3}$$

The evolution operator or propagator, of the system $U(t, t_i)$ connects the state of the system $|\Psi(t)\rangle$ at time t with the initial one $|\Psi(t_i)\rangle$ by the relation

$$|\Psi(t)\rangle = U(t, t_i)|\Psi(t_i)\rangle. \tag{3.4}$$

The adiabatic theorem can be stated in the following way [45]: If the instantaneous eigenvalues do not cross each other, i.e. $|E_n(t) - E_m(t)| > \delta_0 \quad \forall t$, in the limit $T \to 0$, the evolution within the instantaneous eigenspaces of the system is independent from each other:

$$\lim_{T\to\infty} P_n(t)U(t, t_i) = \lim_{T\to\infty} U(t, t_i)P_n(t, t_i). \tag{3.5}$$

3.1.2 Adiabatic basis and adiabatic approximation for driven two-level systems

The theoretical discussion of time-dependent quantum systems is greatly facilitated by introducing instantaneous eigenstates of the time-dependent Hamiltonian

$$H(t)|\varphi_\pm(t)\rangle = \varepsilon_\pm|\varphi_\pm(t)\rangle \tag{3.6}$$

For the Hamiltonian of the form (in the basis $|\psi_1\rangle, |\psi_2\rangle$)

$$\mathsf{H}(t) = \frac{1}{2}\begin{bmatrix} 0 & \Omega \\ \Omega & 2\Delta \end{bmatrix}, \quad \Omega \geq 0 \tag{3.7}$$

the eigenvalues are

$$\varepsilon_{\pm}(t) = \frac{\Delta}{2} \pm \frac{1}{2}\sqrt{\Omega^2 + \Delta^2} \tag{3.8}$$

and their difference

$$\varepsilon(t) = \varepsilon_{+}(t) - \varepsilon_{-}(t) = \sqrt{\Omega^2 + \Delta^2}, \quad \epsilon > 0, \tag{3.9}$$

which defines the energy splitting. We can write the instantaneous eigenvectors expressed as superpositions of the bare states $|\psi_1\rangle$ and $|\psi_2\rangle$:

$$|\varphi_{+}(t)\rangle = \cos\theta(t)|\psi_1\rangle + \sin\theta(t)|\psi_2\rangle, \tag{3.10}$$

$$|\varphi_{-}(t)\rangle = -\sin\theta(t)|\psi_1\rangle + \cos\theta(t)|\psi_2\rangle \tag{3.11}$$

leading to transformation

$$R(\theta(t)) = \begin{bmatrix} \cos\theta(t) & -\sin\theta(t) \\ \sin\theta(t) & \cos\theta(t) \end{bmatrix} \tag{3.12}$$

corresponding to

$$\begin{bmatrix} \varphi_{+}(t) \\ \varphi_{-}(t) \end{bmatrix} = R^{-1}(\theta(t)) \begin{bmatrix} |\psi_1\rangle \\ |\psi_2\rangle \end{bmatrix} \tag{3.13}$$

with

$$R^{-1} \equiv R^{\dagger} = R^{T} \tag{3.14}$$

and to

$$R^{-1}(\theta(t))H(t)R(\theta(t)) = \begin{bmatrix} \varepsilon_{+} & 0 \\ 0 & \varepsilon_{-} \end{bmatrix}, \tag{3.15}$$

where the mixing angle $\theta(t)$ is defined as follows

$$\tan 2\theta(t) = -\frac{\Omega(t)}{\Delta(t)}, \quad 0 \leq \theta \leq \pi/2. \tag{3.16}$$

We express the state vector $|\Psi(t)\rangle$ as a superposition of the adiabatic states

$$|\Psi(t)\rangle = a_{-}(t)|\varphi_{-}(t)\rangle + a_{+}(t)|\varphi_{+}(t)\rangle \tag{3.17}$$

with coefficients $a_{-}(t)$ and $a_{+}(t)$. The connection between the superposition coefficients for the diabatic basis $(C_1(t), C_2(t))$ and the adiabatic basis $(a_{-}(t), a_{+}(t))$ is expressed in terms of $R(\theta(t))$:

$$\begin{bmatrix} C_1(t) \\ C_2(t) \end{bmatrix} = \begin{bmatrix} \cos\theta(t) & -\sin\theta(t) \\ \sin\theta(t) & \cos\theta(t) \end{bmatrix} \begin{bmatrix} a_{+}(t) \\ a_{-}(t) \end{bmatrix} \tag{3.18}$$

The Schrödinger equation in the adiabatic basis is:

$$i\frac{d}{dt}[R(\theta(t)a(t)] = H(t)[R(\theta(t)a(t)] \tag{3.19}$$

After taking the time derivative, the result for the Schrodinger equation is

$$i\frac{d}{dt}a(t) = \underbrace{[R^{-1}(\theta(t))H(t)R(\theta(t))}_{\text{diagonal part}} - \underbrace{iR^{-1}(\theta(t))\dot{R}(\theta(t))]a(t)}_{\text{non-diagonal part}}, \tag{3.20}$$

or written in matrix form

$$i\frac{d}{dt}\begin{bmatrix} a_-(t) \\ a_+(t) \end{bmatrix} = \begin{bmatrix} \varepsilon_- & -i\dot{\theta} \\ i\dot{\theta} & \varepsilon_+ \end{bmatrix}\begin{bmatrix} a_-(t) \\ a_+(t) \end{bmatrix}. \tag{3.21}$$

The adiabatic states can serve as a moving coordinate system in which the state vector $|\Psi(t)\rangle$ can be expanded as it changes under the influence of the coherent radiation pulse. Such coordinates are most useful when the elements of the Hamiltonian - the Rabi frequency and the detuning - change sufficiently slowly (i.e. adiabatically); then the state vector remains fixed in the adiabatic coordinate space. Mathematically, adiabatic evolution requires the off-diagonal elements of the Hamiltonian (3.21) to be negligible compared to the diagonal ones, i.e.

$$|\dot{\theta}| \ll \varepsilon(t), \tag{3.22}$$

which expresses the adiabatic condition. According to this condition, adiabatic evolution requires a smooth pulse, long interaction time, and large Rabi frequency and/or large detuning. When the adiabatic condition holds, there are no transitions between the adiabatic states and their populations are conserved. That is, the state vector remains fixed in the time-varying coordinate system of adiabatic states, as the latter move with respect to the fixed basis states $|\psi_1\rangle$ and $|\psi_2\rangle$. In particular, if the state vector $|\Psi(t)\rangle$ coincides with a single adiabatic state at some time t, then it will remain in that adiabatic state as long as the evolution is abiabatic; the state vector $|\Psi(t)\rangle$ will adiabatically follow the state $|\phi(t)\rangle$.

There are two distinct types of adiabatic population changes depending on the behavior of the diabatic energies of the Hamiltonians. The no-crossing case, for which there is no change of sign of the detuning, is depicted in Fig. 3.1 in the particular case of a constant positive detuning (leading to $\pi/4 \leq \theta \leq \pi/2$ with $\theta = \pi/2$ where $\Omega = 0$); the diabatic energies are parallel to each other. In the absence of interaction, the adiabatic energies coincide with the diabatic ones, but the (pulsed) interaction $\Omega(t)$ pushes them away from each other. As (3.10) and (3.11) show, at early and late times each adiabatic state is identified with the same diabatic state:

$$|\varphi_-(t \to \pm\infty)\rangle = -|\psi_1\rangle, \tag{3.23}$$

$$|\varphi_+(t \to \pm\infty)\rangle = |\psi_2\rangle, \tag{3.24}$$

whereas at intermediate times it is a superposition of diabatic states. Consequently, starting from the ground state $|\psi_1\rangle$, the population makes a partial excursion into the excited state $|\psi_2\rangle$ at intermediate times and eventually returns to $|\psi_1\rangle$ in the end (bottom left frame of Fig. 3.1). Hence, in the no-crossing case, adiabatic evolution leads to a complete population return.
A rather different situation occurs when the detuning $\Delta(t)$ changes its signe during time. For instance Fig. 3.1 (top right frame) shows a situation where $\Delta(t)$ sweeps slowly from some large negative value to some large positive value (irrespective of whether the laser frequency or the transition frequency is changed). Thus such an adiabatic change (chirp) of $\Delta(t)$ will produce complete population transfer from the initially populated state $|\psi_1\rangle$ to the initially unpopulated state $|\psi_2\rangle$ as shown in Fig. 3.1 (bottom right frame). The process is known as rapid adiabatic passage (RAP) [22].

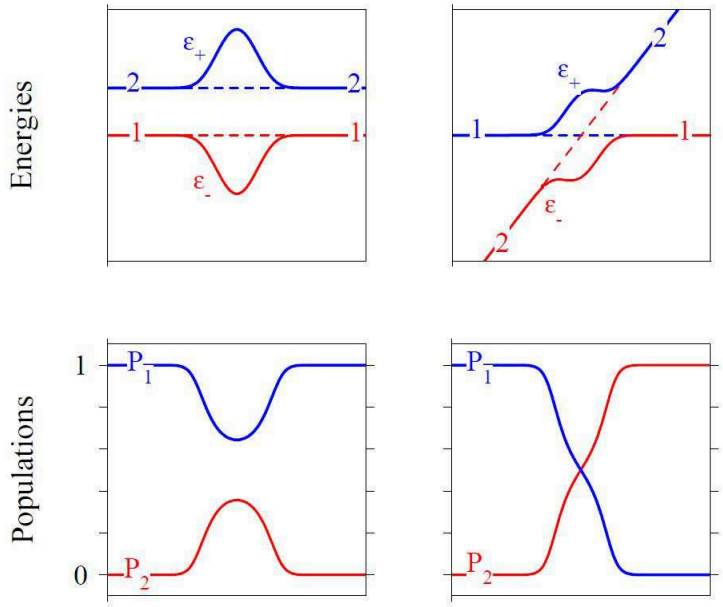

FIG. 3.1 - *Time evolution of the energies (upper frames) and the populations (lower frames) in a two-state system. In the upper plots, the dashed lines show the unperturbed (diabatic) energies, and the solid curves show the adiabatic energies. The left-hand frames are for the no-crossing case, and the right-hand frames are for the level-crossing case.*

3.2 Optimal adiabatic passage by shaped pulses: Efficiency and robustness

3.2.1 The DDP formula

We study the population transfer between an initially populated ground state $|g\rangle$ and an excited state $|e\rangle$ (of respective energies $\hbar\omega_g$ and $\hbar\omega_e$) that can be modeled in the resonant approximation (and up to terms proportional to the identity) by a two-state effective dressed Hamiltonian of the type [22] (in the dressed-state basis $\{|g;1\rangle, |e;0\rangle\}$, where the second label stands for a relative number of photons):

$$\mathsf{H}^{[\Omega,\Delta]} = \frac{\hbar}{2}\begin{bmatrix} 0 & \Omega \\ \Omega & 2\Delta \end{bmatrix} \tag{3.25}$$

with the two time dependent parameters $\Omega \equiv \Omega(t)$ (the effective Rabi frequency) and $\Delta \equiv \Delta(t)$ (the detuning), that can be a priori varied as wished. Here the effective Rabi frequency (assumed real and positive for simplicity) reads $\Omega = -\mu\mathcal{E}/\hbar$ with μ the dipole coupling and $\mathcal{E}(t)$ the field amplitude of instantaneous frequency $\omega(t) = \omega_0 + \dot{\phi}(t)$ (with $\omega_0 t + \phi(t)$ the phase of the field) such that $\Delta(t) = \omega_e - \omega_g - \omega(t)$.

Adiabatic passage means that, in the adiabatic limit, the dynamics projects at all times, up to a phase, on the instantaneous eigenvector of $H(t)$ that is continuously connected to the initial state. It leads to a population transfer when this eigenvector finally connects to the target excited state. This typically occurs in the so-called crossing models, corresponding to pulsed interactions whose instantaneous frequency crosses the resonance,i.e. for a detuning changing its sign during the interaction. For a finite time of interaction (characterized by T), the preceding statement becomes only approximative and deviations from it are generally referred to as non-adiabatic losses that lead to some population being brought back to the initial state at the end of the interaction. The DDP formalism allows one to determine the efficiency of the population transfer at the end of the interaction. For a crossing model, the DDP formula gives more precisely the probability P_g of return to the initial ground state. The population transfer to the excited state is thus $P_e = 1 - P_g$. In the adiabatic limit, the probability of return is given by a coherent sum:

$$P_g = \left| \sum_{k=1}^{N} \Gamma_k e^{i\mathcal{D}(t_k)} \right|^2 \tag{3.26}$$

where Γ_k are phase factors $\Gamma_k = \pm 1$ for a real Ω, and

$$\mathcal{D}(t) = \int_0^t \lambda(z)dz, \qquad \lambda(t) = \sqrt{\Omega^2(t) + \Delta^2(t)}. \tag{3.27}$$

This takes into account all the (complex) N transition points t_k, $k = 0, \cdots, N-1$, defined as the complex zeros of the eigenenergy splitting:

$$\lambda(t_k) = 0, \tag{3.28}$$

lying on the Stokes line γ in the upper complex plane, defined as

$$\Im[\mathcal{D}(\gamma)] = const. = \Im[\mathcal{D}(t_0)] = \cdots = \Im[\mathcal{D}(t_{N-1})], \tag{3.29}$$

and closest to the real axis.

The conditions of validity of the DDP formula are: (i) $\lambda(t) \neq 0$ for all real t (non-degeneracy condition), (ii) $\lambda(z)$ is analytic and single-valued in a complex domain that includes the Stokes line closest to the real axis and the real axis.

The DDP formula had been initially established for the generic case with a single transition point [47–49]. It was then formulated [48] and proved [50] for multiple transition points, which is the situation often encountered in practice, in particular when one considers symmetric (i.e. odd or even) pulses and detunings.

The DDP formula (3.26) shows that the complete population transfer (in the adiabatic limit) occurs when $P_g = 0$, which is in principle exactly satisfied from Eq. (3.26) either when (i) the transition points go to infinity, i.e. when the eigenvalues are parallel at all times [26] (PLAP), or when (ii) the coherent sum interferes destructively (DIAP). The latter situation requires technically two transition points in the complex-time plane. Since it is based on specific conditions of interference, it is expected to have a limited robustness. We will compare in this section the robustness of these two techniques and we show that it is superior for PLAP in a concrete model of interest.

We remark that the Allen-Eberly model [52] with $\Omega = \Omega_0 \operatorname{sech}(t/T)$ and $\Delta = \Delta_0 \tanh(t/T)$ possesses singularities in the complex plane which prevent the transition points to go to infinity when we force the eigenvalues to be parallel: the first transition points merge instead to the first singularity in this case [26]. Thus, this model is not expected to show a better efficiency for the situation of parallel eigenvalues.

Below we briefly recall the technique of parallel adiabatic passage. We next show that the single-parameter linear chirp allows the complete population transfer by DIAP. The robustness of the two techniques are compared in the Section 3.2.3.

3.2.2 Parallel adiabatic passage

Definition. PLAP is satisfied when the dynamics follows a trajectory in the parameter space (Ω, Δ) given by

$$\Omega^2 + \Delta^2 = \Omega_0^2. \tag{3.30}$$

Assuming a given pulse shape $0 \leq \Lambda_T(t) \leq 1$ for the coupling

$$\Omega(t) = \Omega_0 \Lambda_T(t), \tag{3.31}$$

one can easily extract Δ for PLAP as a function of this shape:

$$\Delta_\pm(t) = \pm\Omega_0 \sqrt{1 - \Lambda_T^2(t)}. \tag{3.32}$$

Assuming that the field is maximum at $t = 0$, i.e. $\Lambda_T(0) = 1$, we can choose for convenience $\Delta(t) = \Delta_+(t)$ for $t > 0$ and $\Delta(t) = \Delta_-(t)$ for $t < 0$, which leads to

$$\Delta(t) = \Omega_0 g(t), \qquad g(t) = \mathrm{sign}(t)\sqrt{1 - \Lambda_T^2(t)}. \tag{3.33}$$

We consider here a Gaussian shape $\Lambda_T(t) = e^{-(t/T)^2}$. The upper frame of Fig. 3.2 shows the transfer efficiency after the interaction, by numerical solution of the Schrödinger equation, as functions of $\Omega_0 T$ and $\Delta_0 T$ with such a Gaussian shape and a detuning of the form $\Delta(t) = \Delta_0 g(t)$. The transfer efficiency is better for a darker zone.

The left frame of Fig. 3.2 shows for $\Delta_0 = 0$ the Rabi oscillations where the transfer is complete when the Rabi frequency has an area equal to an odd multiple of π. They extend as roughly vertical lines of highly efficient transfer which merge approximately (and better for larger area) to a zone surrounding the PLAP line ($\Delta_0 = \Omega_0$). An important feature is that the width of the region of efficient population transfer around the PLAP line becomes larger for larger pulse areas. On the other hand, the widths of the vertical lines located below the PLAP line are much smaller. From these observations, one can anticipate the high robustness with respect to the pulse area of the PLAP technique. This is analyzed in Section 3.2.4.

The efficiency of the PLAP technique is already very good from $\Omega_0 T = 2.15$, which corresponds to an area of $3.8 \approx 1.2\pi$ (to be compared to the area π that is the minimal one that leads to a complete population transfer). For this value, the error is less than 1%. One can get an ultrahigh efficiency, with an error less than 10^{-4}, from $\Omega_0 T = 2.53$, which corresponds to an area of $4.5 \approx 1.45\pi$.

Transitionless parallel adiabatic passage. As confirmed in the upper frame of Fig. 3.2, despite the remarkably large region of efficient transfer surrounding the PLAP line, the transfer is in general not strictly complete *on* the PLAP line (but is close to it). One can improve it by suppressing the non-adiabatic losses as originally suggested in [54] for three-state systems and reformulated in [55] as a transitionless quantum driving technique. We thus construct the transitionless parallel adiabatic passage (T-PLAP) which transforms the PLAP line to a line of strictly complete population transfer.

One proposed version of the technique is based on adding to the original Hamiltonian a corrector driving Hamiltonian $H_c(t)$ in order to compensate at each time the non-adiabatic coupling which would induce unwanted transitions. This leads to the new Hamiltonian

$$\hat{H}(t) = \mathsf{H}^{[\Omega,\Delta]} + H_c(t) \tag{3.34}$$

with the corrector Hamiltonian

$$H_c(t) = \frac{\hbar}{2}\begin{pmatrix} 0 & -i\Omega_c(t) \\ i\Omega_c(t) & 0 \end{pmatrix}, \quad \Omega_c(t) = \frac{\Omega\dot{\Delta} - \dot{\Omega}\Delta}{\Omega^2 + \Delta^2}. \tag{3.35}$$

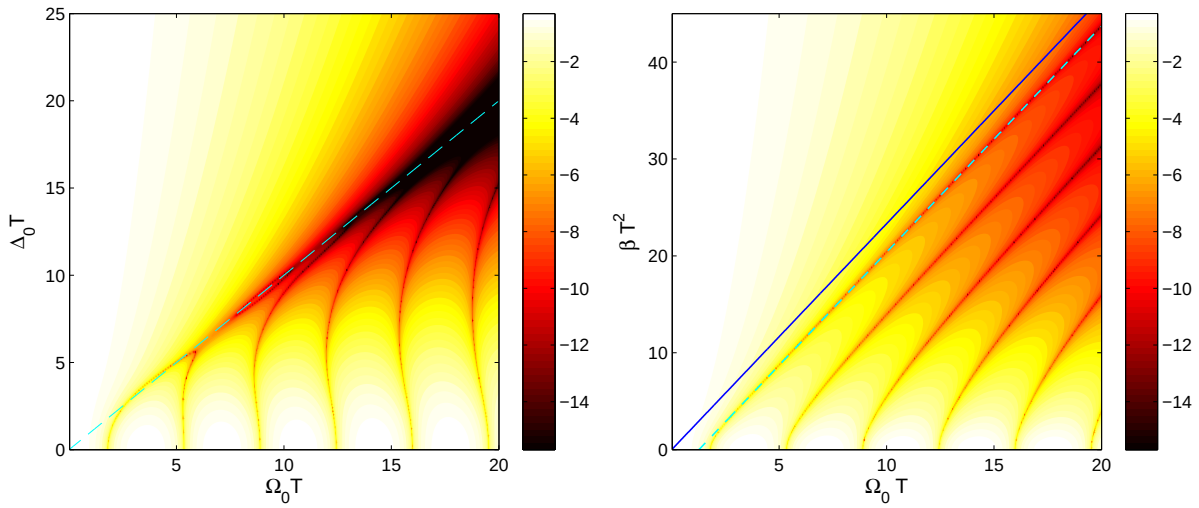

FIG. 3.2 - *Contour plot (in decimal logarithmic scale) of the probability of return to the ground state at the end of the interaction for a coupling of Gaussian shape* $\Omega(t) = \Omega_0 \Lambda_T(t)$, $\Lambda_T(t) = e^{-(t/T)^2}$, *as a function of* $\Omega_0 T$ *and (i)* $\Delta_0 T$ *with* $\Delta(t) = \Delta_0 g(t)$ *(left frame), (ii)* βT^2 *with a linear chirp* $\Delta(t) = \beta t$ *(right frame). The dashed blue line* $\Delta_0 = \Omega_0$ *[(3.46)] of the left (right) frame corresponds to PLAP (DIAP with the minimum Rabi frequency area). The full line (right frame) is the transition line* (3.39) *between the zones of single and double transition points.*

The initially real Rabi frequency becomes complex: $\Omega(t) \to \Omega(t) - i\Omega_c(t)$. This corresponds to a field decomposed into two parts of equal polarization but with one part in quadrature phase with respect to the other one. We can apply the technique on the PLAP in order to force it to lead to an exact population transfer for any pulse area of the original Rabi frequency. This leads to a correcting Rabi frequency independent of Ω_0:

$$\Omega_c(t) = -\text{sign}(t)\frac{\dot{\Lambda}_T(t)}{\sqrt{1-\Lambda_T^2(t)}}. \tag{3.36}$$

One remarks that the area of this correcting Rabi frequency is, as expected, π, such that when $\Omega_0 = \Delta_0 = 0$, it ensures the complete transfer.

We will show more precisely in Section 3.2.4 on a concrete example with an average over various pulse areas that the transitionless parallel adiabatic passage does not improve PLAP.

3.2.3 Adiabatic passage complemented by destructive interference: The case of Gaussian pulse with linear chirping

The simplest field shaping that features DIAP is the one that leads to a linearly time dependent detuning, a so-called linear chirping:

$$\Delta(t) = \beta t. \tag{3.37}$$

This model and its DDP analysis have been studied in detail in Ref. [41]. Following this reference, we determine below the value of β that leads to the DIAP as a function of the peak Rabi frequency Ω_0 considering its smallest value (since for a given β there are several values of Ω_0 producing the DIAP).

We introduce the variable $s = t/T$. The transition points s_k, solutions of Eq. (3.28), read

$$s_k = \sqrt{\frac{1}{2}W(-\alpha)}, \quad \alpha = \frac{2\Omega_0^2}{(\beta T)^2}, \tag{3.38}$$

where $W(x)$ is known as the Lambert W-function, defined as the inverse function of $f(W) = We^W$. $W(x)$ is real for $x \geq -1/e$, and $W(x) \leq 0$ for $-1/e < x \leq 0$. We have $W(-1/e) = -1$. One can identify a single transition point s_0 lying on the Stokes line closest to the real axis, and of smallest imaginary part, when its real part is zero, which arises when $W(-\alpha)$ in (3.38) is real and negative, i.e. for $\alpha < 1/e$. There are two transition points (on the Stokes line closest to the real axis), denoted $s_\pm$, when $W(-\alpha)$ in (3.38) is not real, i.e. for $\alpha > 1/e$. Thus, the branch

$$\beta T = \sqrt{2e}\Omega_0 \tag{3.39}$$

corresponding to $\alpha = 1/e$, for which we denote the transition point as $s_{0,0} = i/\sqrt{2}$, separates in the plane $(\Omega_0, \beta T)$ the zones of single and double transition points. The two transition points have opposite real parts: $\Re(s_-) = -\Re(s_+)$ and identical imaginary parts: $\Im(s_-) = \Im(s_+)$. This implies $\Im[\widetilde{\mathcal{D}}(s_-)] = \Im[\widetilde{\mathcal{D}}(s_+)]$ and $\Re[\widetilde{\mathcal{D}}(s_-)] = -\Re[\widetilde{\mathcal{D}}(s_+)]$, where we have denoted $\widetilde{\mathcal{D}}(s) = \mathcal{D}(t)$. The probability of population return reads in the case of two transition points (in the adiabatic limit)

$$P_g = 4e^{-2\Im[\mathcal{D}(t_+)]}\cos^2\Re[\mathcal{D}(t_+)] \tag{3.40}$$

where we have also used $\Gamma_- = \Gamma_+ = 1$ (since we consider an even coupling and an odd detuning).

The smallest peak coupling Ω_0, for a given β, that leads to DIAP is thus solution of

$$\Re[\widetilde{\mathcal{D}}(s_+)] = \frac{\pi}{2}. \tag{3.41}$$

One cannot solve this equation exactly but only approximately. We achieve this remarking that the corresponding transition point $s_+ = t_+/T$ is located close to $s_{0,0} = i/\sqrt{2}$ corresponding to the branch (3.39). Using a series expansion of $W(x)$, for $x := -\alpha \lesssim -1/e$, denoting $\epsilon = -1/e - x > 0$, we obtain with a very good accuracy (with an error less than 2 % as checked numerically)

$$s_+ \simeq s_{0,0} + \frac{1}{2}\sqrt{e\epsilon}\left(1 - \frac{5}{36}e\epsilon\right) - i\frac{1}{\sqrt{2}}\frac{e}{12}\epsilon. \tag{3.42}$$

Next we decompose the integral (3.27) as follows:

$$\widetilde{\mathcal{D}}(s_+) = \beta T^2\left(\int_0^{s_{0,0}} + \int_{s_{0,0}}^{s_+}\right)\sqrt{z^2 + \frac{\alpha}{2}e^{-2z^2}}\, dz. \tag{3.43}$$

The first integral leads to an imaginary value, hence:

$$\Re[\widetilde{\mathcal{D}}(s_+)] = \beta T^2 \int_{s_{0,0}}^{s_+} \sqrt{z^2 + \frac{\alpha}{2} e^{-2z^2}}\, dz \tag{3.44}$$

At the lowest order of ϵ, for large β and Ω_0, we find for the solution of (3.41):

$$\beta T \sim \sqrt{2e}\Omega_0, \quad \beta \to \infty, \tag{3.45}$$

which gives a line parallel to (and below) the branch (3.39) separating the zones of single and double transition points.

A numerical analysis of the integral (3.44) allows one to determine an approximate equation of this line for finite values of β:

$$\beta T \approx \sqrt{2e}\,(\Omega_0 - 1.25/T). \tag{3.46}$$

This line is shown in the right frame of Fig. 3.2, where the error of the transfer probability to the excited state is numerically determined as a function of $\Omega_0 T$ and βT^2. It fits very well the zone of efficient population transfer of smallest area (for a given β), and is parallel to the transition line (3.39) between the zones of single and double transition points.

For respectively $\Delta_0 = 0$ and $\beta = 0$, the two frames of Fig. 3.2 show the same Rabi oscillations. A salient feature is that the zones of complete transfer can be extended for both frames: They all merge to the PLAP line in the left frame, while only the one of smallest Ω_0 (i.e of smallest pulse area) approximately coincides (and better for larger $\Omega_0 T$) to the DIAP line. The extensions of the other zones of complete transfer are approximately parallel to the DIAP line. One notices that, in both cases, these extensions are surrounded by larger zones of efficient transfer for larger $\Omega_0 T$, which clearly indicates an expected better robustness for larger $\Omega_0 T$. However the size of this zone of efficient transfer is shown to be much larger around the PLAP line. We thus anticipate a better robustness of the PLAP technique with respect to the DIAP technique. This is analyzed in detail in Section 3.2.4.

3.2.4 Implementations by spectral shaping

The implementation of adiabatic techniques with chirped fields can be achieved in the femtosecond regime by a spectral shaping [1, 51].

The DIAP with a Gaussian pulse and a linear chirping (3.37) analyzed in the preceding section can be simply implemented in practice since, when the mean frequency of the initial field matches the transition frequency, it requires a device which shapes only the spectral phase, which can be achieved using a grating [58] or a single spatial light modulator [59](see section 1.6.2). On the other hand, the PLAP requires a shaping of both the spectral phase and amplitude as shown below. This can be produced for instance with a double-layer liquid-crystal spatial light modulator such as the one used in [42].

The output pulse $E(t)$ that subsequently interacts with the system is chosen to be of Gaussian shape:

$$E(t) = \mathcal{E}_0 \Lambda_T(t) e^{i(\omega_0 t + \phi(t) - \theta)}, \quad \Lambda_{T_{\rm in}}(t) = e^{-(t/T)^2} \tag{3.47}$$

with a phase θ to be defined and the instantaneous frequency $\omega(t) = \omega_0 + \dot{\phi}(t)$ giving the relation between the phase $\phi(t)$ and the one-photon detuning of our initial problem:

$$\phi(t) = (\omega_e - \omega_g - \omega_0)\, t - \int^t \Delta(s) ds. \tag{3.48}$$

This choice for the output pulse to be Gaussian is arbitrary; it is here chosen for its simplicity. The spectral shaping allows the transformation in the frequency domain of the input field into the output field through a transparency coefficient $0 \leq \mathcal{T}(\omega) \leq 1$ and a phase $\varphi(\omega)$ as follows:

$$\widetilde{E}(\omega) = \mathcal{T}(\omega) e^{i\varphi(\omega)} \widetilde{E}_{\rm in}(\omega) \tag{3.49}$$

with $\widetilde{E}(\omega)$ denoting the Fourier transform of $E(t)$ and $E_{\rm in}(t) = E_{0{\rm in}} \Lambda_{T_{\rm in}}(t) e^{i\omega_0 t}$, $\Lambda_{T_{\rm in}}(t) = e^{-(t/T_{\rm in})^2}$. Two masks are generally used: one operates on the transparency while the other one on the phase. The duration T of the output Gaussian pulse has to be carefully chosen such that there exists a solution for the transparency $\mathcal{T}(\omega)$ and the phase $\varphi(\omega)$ of (4.8) that leads to the desired output field (4.6), and, more precisely, that this solution works well within the input Gaussian spectrum. A smooth solution that is easily implementable is also be desirable.

From Eqs. (1.87) and (1.89) we can determine a relation between the slope β of the chirp (3.37) and the coefficient γ of the quadratic phase (1.85) as:

$$\beta T^2 = 8 \frac{\gamma}{T_{\rm in}^2}, \tag{3.50a}$$

$$\simeq 2 \frac{T}{T_{\rm in}}, \text{ for } \gamma \gtrsim T_{\rm in}^2. \tag{3.50b}$$

This means that any value βT^2 can be obtained by adjusting appropriately γ, which amounts to choosing T [from Eq. (1.89)]. Since one can also produce any value $\Omega_0 T$ by choosing the peak intensity of the field, any region of the lower part of Fig. 3.2 can be in principle obtained from a concrete implementation with a pulse of limited bandwidth. A practical limitation will be a limited field intensity to avoid unwanted destructive effects such a ionization.

PLAP The achievement of PLAP by a spectral shaping necessitates a shaping both in phase and amplitude even when the mean frequency of the input field matches with the transition frequency, $\omega_0 = \omega_e - \omega_g$ (that is the situation we consider here for simplicity). One cannot determine in a closed form the transparency and the phase shaping of (4.8), but they can be obtained numerically by applying the Fourier transform of a given output pulse:

$$\mathcal{T}(\omega) = |\widetilde{E}(\omega)/\widetilde{E}_{\rm in}(\omega)|, \quad \varphi(\omega) = \arg[\widetilde{E}(\omega)/\widetilde{E}_{\rm in}(\omega)]. \tag{3.51}$$

The finite spectrum of the input field imposes for the amplitude of the chirp $\Delta_0 = \Omega_0$:

$$\Omega_0 \lesssim 2/T_{\rm in}, \tag{3.52}$$

such that the maximum of the transparency is well located within the spectrum.

In practice, we choose the amplitude of the chirp $\Delta_0 = \Omega_0$ and the duration $T > T_{\rm in}$ of the output field of the form

$$E(t) = \mathcal{E}_{0\rm in}\, \kappa e^{-(t/T)^2} e^{i(\omega_0 t + \phi(t))} \tag{3.53}$$

with the phase

$$\phi(t) = -\Omega_0 \int^t \mathrm{sign}(s)\sqrt{1 - \Lambda_T^2(s)}\, ds. \tag{3.54}$$

The additional factor κ in the amplitude of the field (3.53) has to be fixed such that $\mathcal{T}(\omega) \leq 1$.

Figure 3.3 shows an example of the resulting shaping. The transparency and the phase of the shaping are shown to be smooth functions that are expected to be easily implemented from a practical point of view.

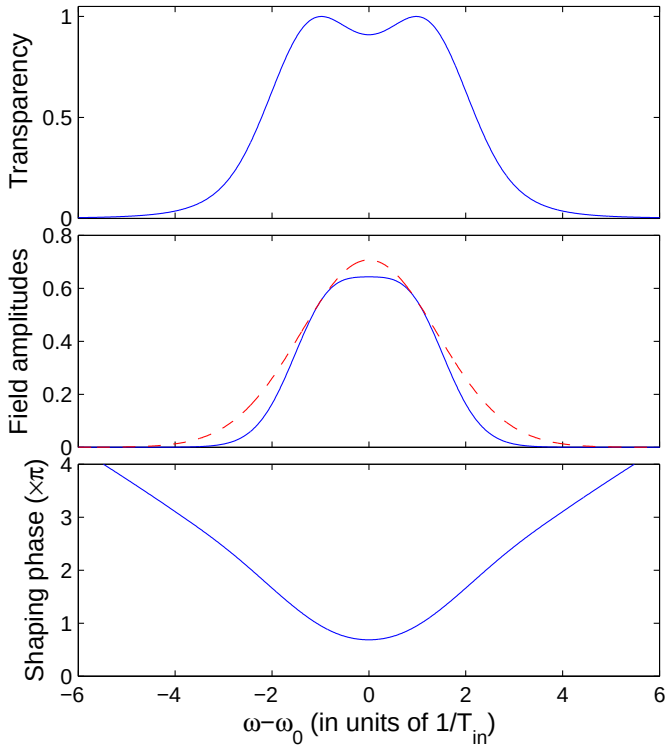

FIG. 3.3 - *Spectral shaping corresponding to a parallel adiabatic passage as a function of the angular frequency (in units of $1/T_{in}$)for Gaussian input* (4.5) *and output* (3.53) *fields with $\Delta_0 = \Omega_0 = 1.5/T_{in}$, and $T = 3T_{in}$. Upper frame: Transparency $\mathcal{T}(\omega)$; middle frame: Fourier transform of the input and output field shapes : $\widetilde{\Lambda}_{T_{in}}(\omega)$ (dashed line) and $\mathcal{T}(\omega)\widetilde{\Lambda}_{T_{in}}(\omega)$ (full line). Lower frame: Phase $\varphi(\omega)$. Here the coefficient κ of* (3.53) *is found to be $\kappa \approx 0.53$.*

3.2.5 Comparative study of robustness

In this section we analyse and compare the robustness of DIAP and PLAP with respect to fluctuations of the instantaneous amplitude and detuning, and also with respect to fluctuations of the pulse area.

The robustness with respect to instantaneous fluctuations of PLAP and DIAP is a priori questionable since these techniques are based on the use of the Davis-Dykhne-Pechukas formula in the time complex plane requiring analytic functions as the pulse parameters.

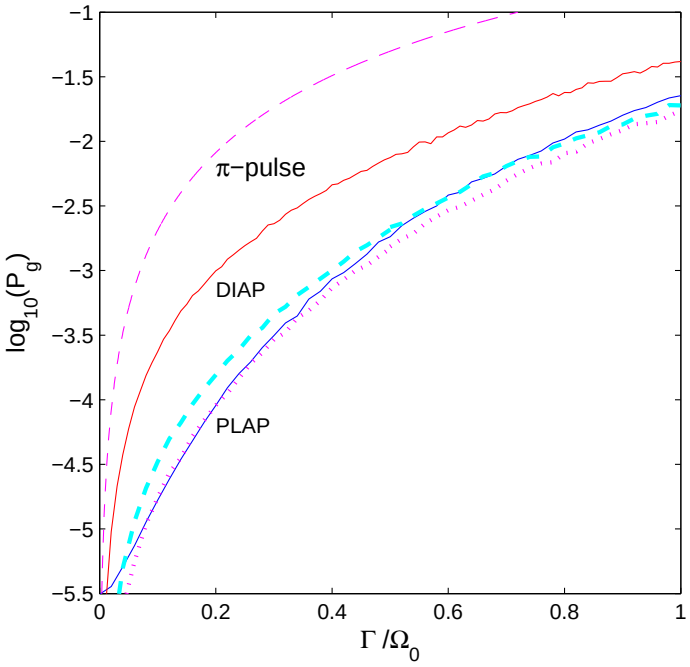

FIG. 3.4 - *Infidelity (in decimal logarithmic scale) for the PLAP (lower full line) and DIAP (upper full line) techniques for* $\Omega_0 T = 5$ *(corresponding to a pulse area* $\int \Omega(t)dt = 5\sqrt{\pi}$*), and for the* π*-pulse (upper dashed line) with respect to an imperfect knowledge of the pulse area. The transitionless PLAP (T-PLAP) technique is shown as dotted and lower dashed lines for* $\int \Omega(t)dt = 5\sqrt{\pi}$ *(larger area for T-PLAP) and* $\int |\Omega(t) - i\Omega_c(t)|dt = 5\sqrt{\pi}$ *(same area for PLAP and T-PLAP), respectively.*

3.2.6 Pulse area fluctuation

The robustness of the process with respect to an imperfect knowledge of the pulse areas is shown in Fig. 3.4 through ensemble averaging. We have determined the final populations by averaging over many realizations of an ensemble of systems with different peak Rabi frequencies uniformly distributed over the range $\Omega_0 \pm \Gamma/2$. Their peak Rabi frequency $\Omega_{0,j}$ is chosen as

$$\Omega_{0,j} = \Omega_0(1 + r_j\Gamma/\Omega_0), \tag{3.55}$$

where $-0.5 \leq r_j < 0.5$ is a uniformly distributed random number, Ω_0 is the average Rabi frequency, and Γ is the width of the probability distribution.

Such an averaging gives for the π-pulse population return:

$$\bar{P}_g^{(\pi)} = \frac{1}{2}\left(1 - \frac{2}{\Gamma\sqrt{\pi}} \sin\frac{\Gamma\sqrt{\pi}}{2}\right). \tag{3.56}$$

Figure 3.4 shows that the robustness of DIAP and PLAP is much improved with respect to the π-pulse technique. It also proves that PLAP is in general much superior (except for very small area fluctuations), despite the fact that DIAP leads, for the considered situation, to a better population transfer in absence of fluctuation. In particular, we can see the remarkable result that the infidelity is smaller or equal to the benchmark 10^{-4} for Γ/Ω_0 as large as 0.2 for PLAP. For this rate, the fidelity of PLAP is better by more than one order of magnitude than the one of DIAP.

We have also tested the transitionless PLAP (T-PLAP), i.e. with the use of an additional field that cancels out the non-adiabatic coupling. The robustness with respect to an imperfect knowledge of the pulse area is displayed in Fig. 3.4 as dotted and lower dashed lines corresponding to a correcting Rabi frequency giving an additional area with respect to the simple PLAP, and to the same total area in absolute value for PLAP and T-PLAP, respectively. This shows that T-PLAP does not improve PLAP overall (even when T-PLAP uses an additional area), but is on the contrary deteriorated on a large range of width Γ when the same area is taken.

3.2.7 Amplitude fluctuations

We model the instantaneous fluctuations of the field envelope with a Gaussian white noise considering a relative deviation $\xi(t)$ as a stochastic variable of average and correlation

$$\langle\xi(t)\rangle = 0, \qquad \langle\xi(t)\xi(t')\rangle = 2\Gamma\delta(t-t'), \tag{3.57}$$

where the brackets $\langle\cdot\rangle$ denote an ensemble average and $\delta(t)$ is the Dirac delta function. Each sequence $\{\xi(t_i)\}$ of the ensemble is generated at discrete times t_i separated by the step Δt according to

$$\xi(t_i) = \sqrt{\frac{2\Gamma}{\Delta t}}\,\mathrm{randn}, \tag{3.58}$$

where randn generates a normally distributed random number. We have determined the instantaneous populations by averaging over many realizations of time histories.

For a sequence j of the ensemble, the Rabi frequency is more precisely defined at a discrete time t_i as

$$\Omega_j(t_i) = \Omega_0\Lambda(t_i)(1+\xi(t_i)) \tag{3.59}$$

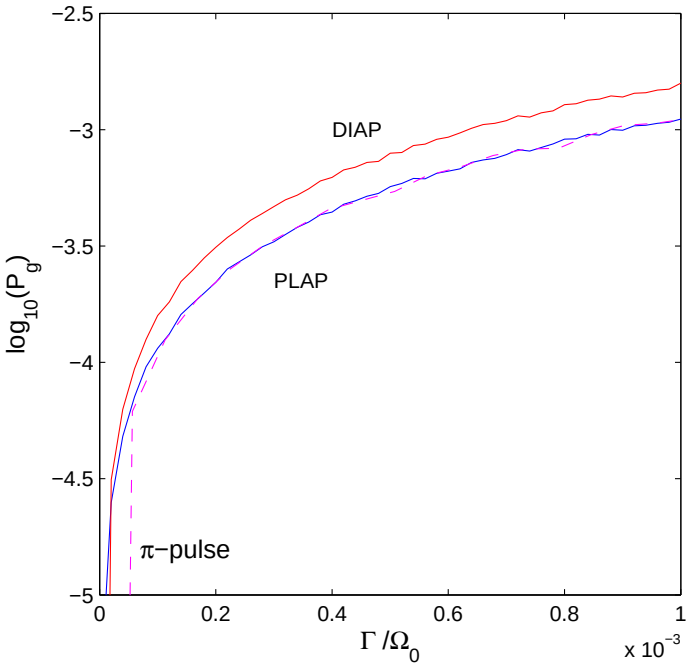

FIG. 3.5 - *Infidelity (in decimal logarithmic scale) for the PLAP (lower full line) and DIAP (upper full line) techniques for* $\Omega_0 T = 5$*, and for the* π*-pulse technique (corresponding to* $\Omega_0 T = \sqrt{\pi}$ *and* $\Delta = 0$*) (dashed line) for an ensemble average over a white noise fluctuating field amplitude of rate* Γ *versus* Γ/Ω_0 *(with* Ω_0 *taken as the respective one).*

with $\Omega_0 \Lambda(t_i)$ the ensemble average of the Rabi frequency at time t_i (that is without fluctuations).

Figure 3.5 shows the infidelity of the transfer as a function of Γ normalized by Ω_0: The PLAP technique is slightly better. The infidelity is smaller than 10^{-4} for $\Gamma \lesssim 10^{-4}\Omega_0$. We make the remarkable observation that the infidelity is nearly the same for PLAP and the π-pulse technique (except for very low noise rate).

Figure 3.6 displays a dynamics of PLAP for a single realization of the fluctuating Rabi frequency (3.59). Despite the relative smallness of Γ/Ω_0, one can notice the relatively large fluctuations of the Rabi frequency due to the small time step.

3.2.8 Phase fluctuations

Gaussian white noise

We can model the instantaneous fluctuations of the detunings as above with a Gaussian white noise but considering now an instantaneous frequency offset for the stochastic variable $\xi(t)$ (3.57). This corresponds to a Wiener-Levy process for the corresponding phase [60]. This

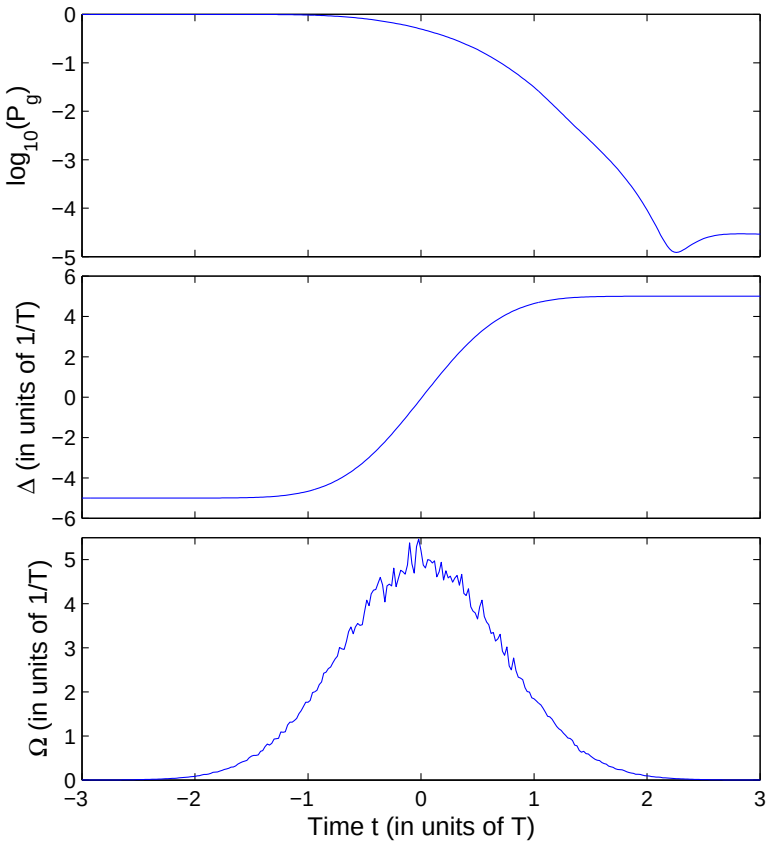

FIG. 3.6 - *Dynamical infidelity (upper frame) for a realization of a PLAP dynamics for* $\Omega_0 T = 5$ *and a white noise fluctuating field amplitude (corresponding to the instantaneous Rabi frequency shown in the lower frame) of rate* $\Gamma = 10^{-4}\Omega_0$. *The detuning (shown in the middle frame) is assumed without fluctuation.*

procedure is known to be equivalent to the use of the density matrix equation for the time evolution with the stochastic variables replaced by the constant dephasing rate Γ [61].

Figure 3.7 displays the infidelity for such a case. One can make the following observations: The three techniques rapidly fail even for relatively small dephasing rate (with respect to Ω_0) and the π-pulse technique is better than DIAP and PLAP techniques. This latter result can be easily interpreted in terms of the dephasing rate: The dephasing corresponds to a destruction of the coherence of the superposition of state necessarily occurring during the dynamics leading to the population inversion. Its effect is thus smaller for a shorter duration of interaction which is the case for the π-pulse (for the same given Ω_0). We can conclude that a dephasing process is more detrimental for adiabatic passage of longer duration.

If the dephasing rate is known, one can improve the efficiency of PLAP by modifying the dynamics such that it alternatively follows an ellipse in the parameter space (Ω, Δ) to accelerate it when the superposition is created, as shown in [62]. However, (i) this improvement is significant only for relatively large dephasing rates, and (ii) it does not allow to reach the benchmark 10^{-4} for the infidelity even for moderate dephasing. For small dephasing rates as

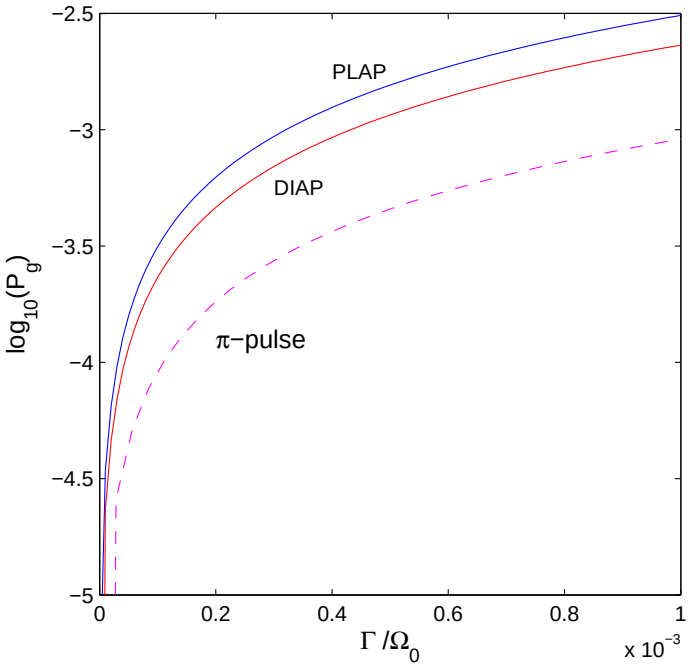

FIG. 3.7 - *Same as Fig. 3.5 but for an ensemble average over a white noise fluctuating detuning of rate* Γ.

the one considered in Fig. 3.7, the improvement is not significant.

A transfer of high efficiency even for appreciable dephasing rates can be recovered with the use of optimal control theory as analyzed in Ref. [63]. Its adiabatic counterpart is an open question.

Gaussian exponentially correlated noise

The preceding Gaussian white noise is less destructive for adiabatic passage if one considers correlations. A typical model is the Ornstein-Uhlenbeck process with a zero-mean and exponentially correlated noise for the stochastic variable (see for instance [64]):

$$\langle \xi(t) \rangle = 0, \qquad \langle \xi(t)\xi(t') \rangle = D\Gamma \exp(-\Gamma|t-t'|). \tag{3.60}$$

For large values of $\Gamma \gg D$, one recovers the Gaussian white noise (3.57). The opposite extreme case $\Gamma \ll D$ corresponds to an ensemble of fields with constant frequencies that obey Gaussian statistics with variance $D\Gamma$.

Figure 3.8 shows that, when the correlation is of larger width, i.e. for a smaller ΓT and a given product $D\Gamma T^2$, the DIAP technique is more efficient than the π-pulse technique, and that the PLAP technique becomes well superior to the two other techniques.

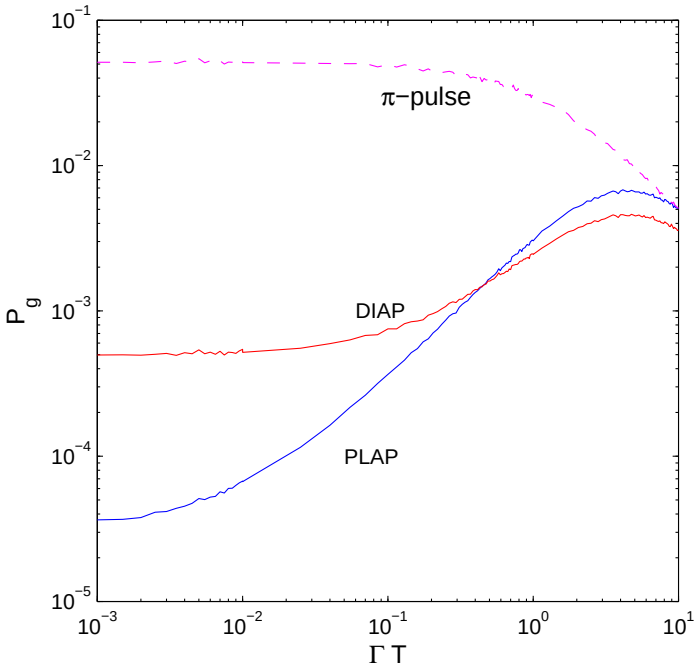

FIG. 3.8 - *Infidelity (in decimal log-log scale) for the PLAP and DIAP techniques for* $\Omega_0 T = 5$ *(full lines), and for the* π*-pulse technique (dashed line), for an ensemble average over a Ornstein-Uhlenbeck fluctuating field detuning as a function of* ΓT *for* $D\Gamma T^2 = 0.1$.

Chapter 4

Multiphoton parallel adiabatic passage by shaped pulses

In this chapter we apply the technique of adiabatic passage in the case of multiphoton transitions, in the strong-field ultrafast regime, for dynamically Stark shifted quantum systems. The requirement for a direct application is that the effective Hamiltonian should be a two-state system. This is tested in particular for a two-photon transition. We show the advantage of this technique with respect to simple linear chirping.
We propose a way to compensate the dynamical Stark shift and to obtain a complete population transfer by using linear chirping which is shifted towards the two-photon resonance. We then compare the robustness of these techniques with respect to the fluctuations of the pulse parameters.
We theoretically demonstrate the possibility of high efficiency population transfer on atomic Cesium by these techniques. We present the shapes of amplitude and phase in the frequency domain of the required fields.
The chapter is organized as follows: In Sec. 4.1, we describe the general technique with the model and the pulse-shaping scheme. Section 4.2 is devoted to the two-photon process and we present the static compensation of the Stark shift. In Sec. 4.3, we apply the technique for a concrete model of the Cs atom. In Sec. 5 we present some conclusions.

4.1 Optimal adiabatic passage for a Stark-shifted two-state system

4.1.1 The model

We study a multiphoton process between an initially populated ground state $|g\rangle$ and an excited state $|e\rangle$ (of respective energies $\hbar\omega_g$ and $\hbar\omega_e$). Considering a n-photon process, one can construct an effective Hamiltonian (the dressed Hamiltonian) in the dressed basis $\{|g;0\rangle, |e;-n\rangle\}$, where the second label stands for the relative number of photons. This means that the excited

state dressed with $-n$ photons is nearly degenerate with the ground state. In the resonant approximation (and up to terms proportional to the identity) the two-state effective Hamiltonian reads [22]:

$$\mathsf{H}^{[\Omega,\delta]} = \frac{\hbar}{2}\begin{bmatrix} 0 & \Omega \\ \Omega & 2\delta + 2S \end{bmatrix} \tag{4.1}$$

with the two time dependent parameters $\Omega \equiv \Omega(t)$ (the effective Rabi frequency) and $\delta \equiv \delta(t)$ (the n-photon detuning), that can be a priori varied as wished, and the dynamical Stark shift $S \equiv S(t)$. Here the effective Rabi frequency $\Omega(t)$, assumed real and positive for simplicity, is proportional to $\mathcal{E}^n(t)$ with $\mathcal{E}(t)$ the field amplitude of instantaneous frequency $\omega(t) = \omega_0 + \dot{\phi}(t)$ (with $\omega_0 t + \phi(t)$ the phase of the laser) and n the number of photons needed to reach the resonance: $\omega_g + n\omega(t) + \delta(t) = \omega_e$. The relative Stark shift between state $|g\rangle$, of Stark shift $S_g(t)$, and state $|e\rangle$, of Stark shift $S_e(t)$, is denoted $S(t) = S_e(t) - S_g(t)$. In general the Stark shift is order $\mathcal{E}^2$. It is a priori a function of Ω and δ. Since, in practice, δ varies only slightly with respect to the mean frequency of the field, it is in general a good approximation to neglect the variation of S upon δ. We have here assumed for simplicity stable states.

4.1.2 Parallel adiabatic passage

The strategy to optimally populate the excited state from the initial ground state by adiabatic passage is to follow a level line in the diagram of the difference of the instantaneous eigenenergies as studied in the preceding chapter and refered to as parallel adiabatic passage (PLAP).

Applying the result stated in the preceding chapter to this model (4.1) leads to PLAP for the dynamics satisfying in the parameter space (Ω, δ) the trajectory given by

$$\Omega^2 + (\delta + S)^2 = \Omega_0^2. \tag{4.2}$$

Since S is a priori a function of Ω and δ, this leads to a complicated trajectory. As remarked previously, it is often a good approximation to consider S independent of δ. In this case, one can easily extract δ as a function of Ω and S:

$$\delta_\pm(t) = \pm\Omega_0\sqrt{1 - \Lambda_T^2(t)} - S(t), \quad \Omega(t) = \Omega_0\Lambda_T(t), \tag{4.3}$$

where $0 \leq \Lambda_T(t) \leq 1$ is the pulse shape. Assuming that the field is maximum at $t = 0$, i.e. $\Lambda_T(0) = 1$, we can choose $\delta(t) = \delta_+(t)$ for $t > 0$ and $\delta(t) = \delta_-(t)$ for $t < 0$, which leads to

$$\delta(t) = \mathrm{sign}(t)\Omega_0\sqrt{1 - \Lambda_T^2(t)} - S(t). \tag{4.4}$$

Note that this choice of sign is arbitrary. The opposite sign (ie. $\delta(t) = \delta_+(t)$ for $t < 0$ and $\delta(t) = \delta_-(t)$ for $t > 0$,) gives exactly the same final result.

4.1.3 Shaping the spectral phase and amplitude

The implementation of adiabatic techniques with chirped fields can be achieved in the femtosecond regime by a spectral shaping as presented in the preceding chapters [1,51]. PLAP requires a shaping of both the spectral phase and the amplitude. We assume an input field of Gaussian shape with mean frequency ω_0 and the width at half maximum (for the corresponding intensity) $T_{\text{in,FWHM}} = T_{\text{in}}\sqrt{2\ln 2}$:

$$E_{\text{in}}(t) = \mathcal{E}_{0\text{in}}\Lambda_{T_{\text{in}}}(t)e^{i\omega_0 t}, \quad \Lambda_{T_{\text{in}}}(t) = e^{-(t/T_{\text{in}})^2}. \tag{4.5}$$

The output pulse $E(t)$ that is designed to interact with the system is chosen to be also of Gaussian shape:

$$E(t) = \mathcal{E}_0 e^{-(t/T)^2} e^{i(\omega_0 t + \phi(t))} \tag{4.6}$$

with the instantaneous frequency $\omega(t) = \omega_0 + \dot{\phi}(t)$ giving for a n-photon resonance

$$\phi(t) = \left(\frac{\omega_e - \omega_g}{n} - \omega_0\right) t - \frac{1}{n}\int^t \delta(s)ds. \tag{4.7}$$

The spectral shaping is defined as

$$\widetilde{E}(\omega) = \mathcal{T}(\omega)e^{i\varphi(\omega)}\widetilde{E}_{\text{in}}(\omega) \tag{4.8}$$

with $\widetilde{E}(\omega)$ denoting the Fourier transform of $E(t)$. Here $0 \leq \mathcal{T}(\omega) \leq 1$ is the transparency coefficient of the shaping device, and $\varphi(\omega)$ is the spectral phase. Two masks are generally used: one operates on the transparency while the other one on the phase. The duration T of the output Gaussian pulse has to be carefully chosen such that there exists a solution for the transparency $\mathcal{T}(\omega)$ and the phase $\varphi(\omega)$ of (4.8) that leads to the desired output field (4.6), and, more precisely, that this solution works well within the input Gaussian spectrum. A smooth solution that is easily implementable is also be desirable.

4.2 The two-photon process

4.2.1 PLAP

We study as the simplest example with a non negligible Stark shift the two-photon process. The procedure described below can be easily generalized to multiphoton processes of higher order.

For the two-photon process, the Rabi frequency and the Stark shift read respectively [22]

$$\Omega(t) = \alpha_{ge}\mathcal{E}^2(t), \quad S(t) = (\alpha_{ee} - \alpha_{gg})\mathcal{E}^2(t) \tag{4.9}$$

with α_{ij} the component i,j of the polarizability tensor (see chapter I).

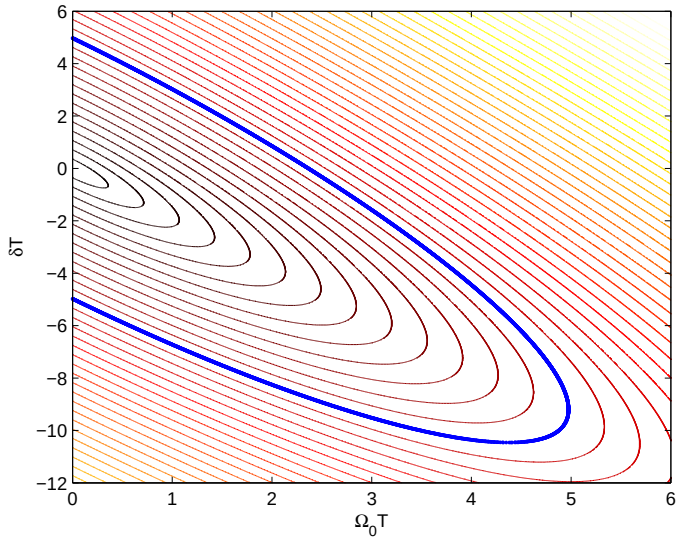

FIG. 4.1 - *Contour plot corresponding to the difference of the eigenenergies for the two level model* (4.1) *with* $r = 1.85$. *The thick line corresponds to a specific path* (4.4) *with* $\Omega_0 T = 5$.

Condition (4.4) reads in this case

$$\delta(t) = \text{sign(t)}\Omega_0\sqrt{1-\Lambda^2(t)} - r\Omega_0\Lambda(t), \quad \Omega(t) = \Omega_0\Lambda(t), \tag{4.10}$$

where r is the coefficient of proportionality between the relative Stark shift and the Rabi frequency: $S(t) = r\Omega(t)$.

Figures 4.1, 4.2, 4.3, 4.4 show an example with $r = 1.85$ (corresponding to the two-photon process in Cesium as studied in section 4.3, but in a two-state approximation). Figure 4.1 shows the contour plot of the level lines corresponding to the differences of the eigenenergies for a two-state approximation. In Fig. 4.2 we show the dynamics corresponding to the specific path taken from Fig. 4.1. The pulse shapes correponding to this dynamics is presented in Figs. 4.3 and 4.4. In Fig. 4.3 we show the shaped amplitude and phase in the frequency domain. Figure 4.4 shows the unshaped amplitude in the frequency domain and the shaped (modulated) amplitude required for the dynamics. A more realistic model for Cs is tested in section 4.3.

4.2.2 Chirped and static compensation of the Stark shift: The shifted linear chirp.

Here we present an alternative way to get a high efficiency transfer of population by linear chirp defined as

$$\dot{\phi} = at + b, \tag{4.11}$$

where b is a static parameter that shifts the chirp: we refer this technique to as the shifted linear chirp. The parameters a and b are numerically adjusted to increase the efficiency. In Fig.

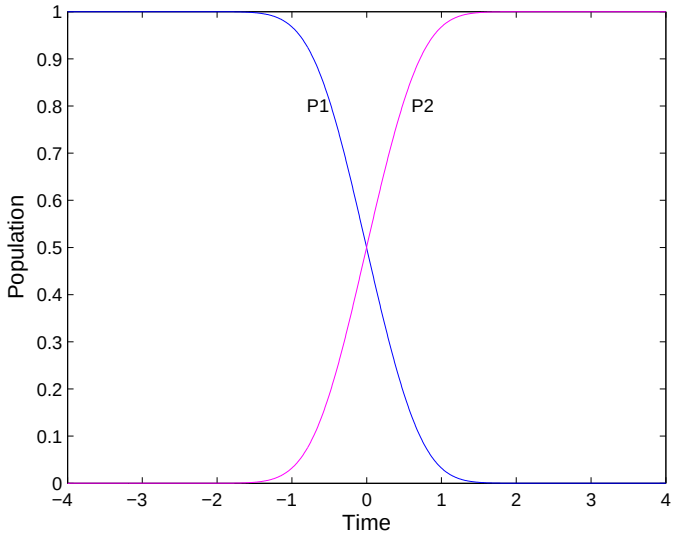

FIG. 4.2 - *Dynamics of the population* $P_j, j = 1, 2$ *corresponding to the path* (4.4) *shown in Fig. 4.1 with the initial condition* $P_1 = 1$.

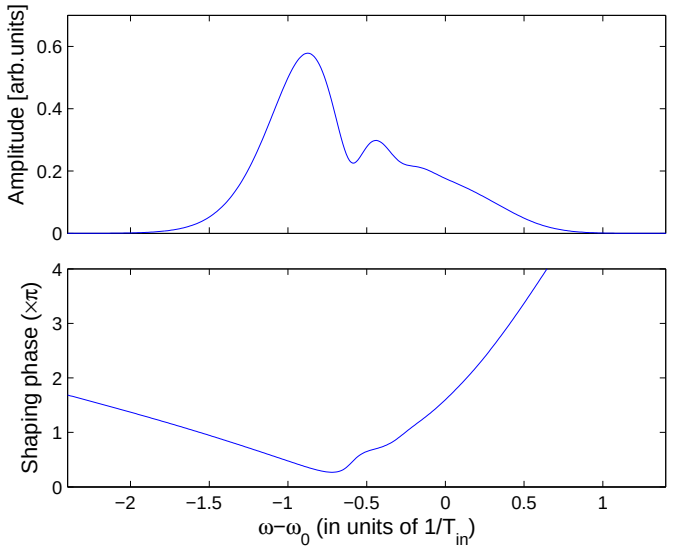

FIG. 4.3 - *Upper frame: Shaped spectral amplitude as a function of the angular frequency; Lower frame: Shaped spectral phase corresponding to the two-level model* (4.1) *by parallel adiabatic passage with* $r = 1.85$ *and* $\Omega_0 T = 5$.

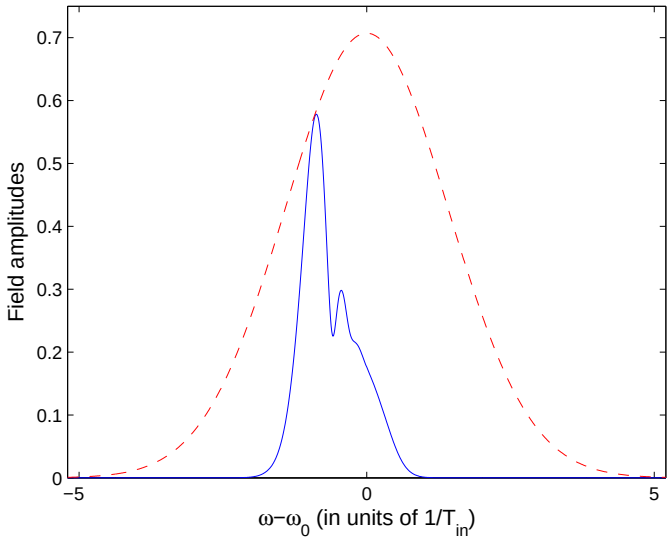

FIG. 4.4 - *Unshaped spectral amplitude (dashed line) and shaped spectral amplitude (blue line) as a function of the angular frequency corresponding to the two-level model* (4.1) *by parallel adiabatic passage with* $r = 1.85$ *and* $\Omega_0 T = 5$.

4.5 we show the two-photon transfer of population for two level model depending on the two chirp parameters. One can see that the coefficient b shifts the spectrum towards the resonance, compensating the Stark effect on the system. Without the static part b the maximum transfer of the population for the two level model (4.1) with parameters $r = 1.85$ and $\Omega_0 T = 5$ is only 65%. The dynamics of the energy levels as a function of time corresponding to the black point in the contour plot Fig. 4.5 is shown in Fig. 4.6. Figures 4.7 and 4.8 show the spectral shaping according to (4.8) for the two-level dynamics shown in Fig. 4.6. We can notice for Fig. 4.5 that the result is symmetrically identical with respect to the sign of the chirp as it is for PLAP. The main observation that can be made when comparing the shaping resulting from PLAP (Fig. 4.4) and the one from numerical tests with a static compensation (Fig. 4.7) is that the main peak in amplitude of the two techniques is located approximately at the same frequency. The additional structures obtained from PLAP (Fig. 4.4) allow the finer dynamics required for the parallel passage. In both cases, the frequencies corresponding to a negative detuning are prefered, in consistency with the sign of the Stark shift. The other frequencies are removed, as they are detrimental for the full achievement of the transfer. We also remark that the curvature of the parabolic shaping of the phase in Fig. 4.8 is opposite to the global curvature of the shaping phase in Fig. 4.3. This is due to the choice for the phase shown in Fig. 4.5 with a positive a. The symmetrically opposite choice with a negative a would give an opposite curveture for the shaping phase in Fig. 4.8.

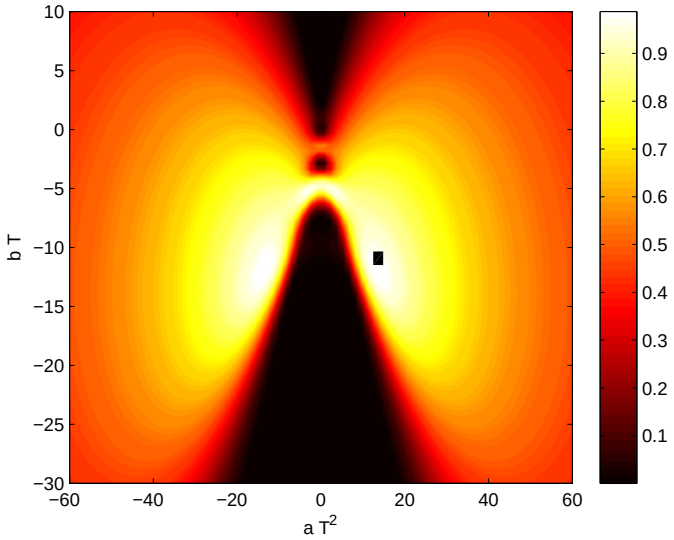

FIG. 4.5 - *Contour plot corresponding to the transfer of population depending on the two dimensionless chirp parameters aT^2 and bT for the two-level model* (4.1) *with* $r = 1.85$ *and* $\Omega_0 T = 5$. *The black square corresponds to 99% of population.*

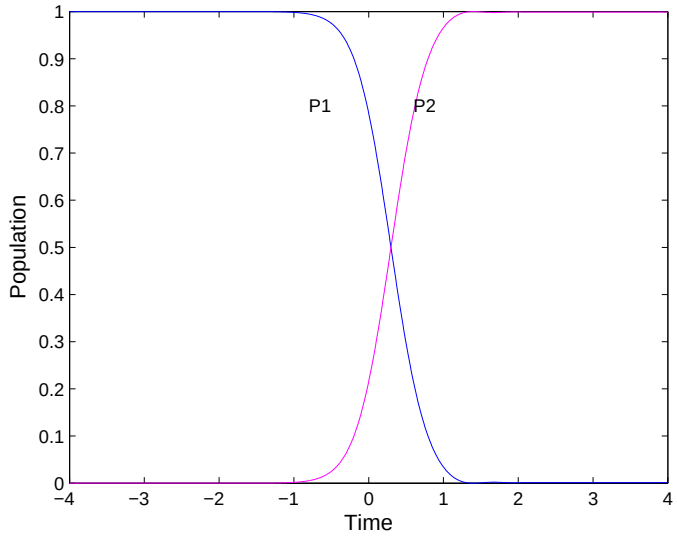

FIG. 4.6 - *Dynamics of the population* $P_j, j = 1, 2$ *corresponding to the contour plot shown in Fig. 4.5 with the initial condition* $P_1 = 1$.

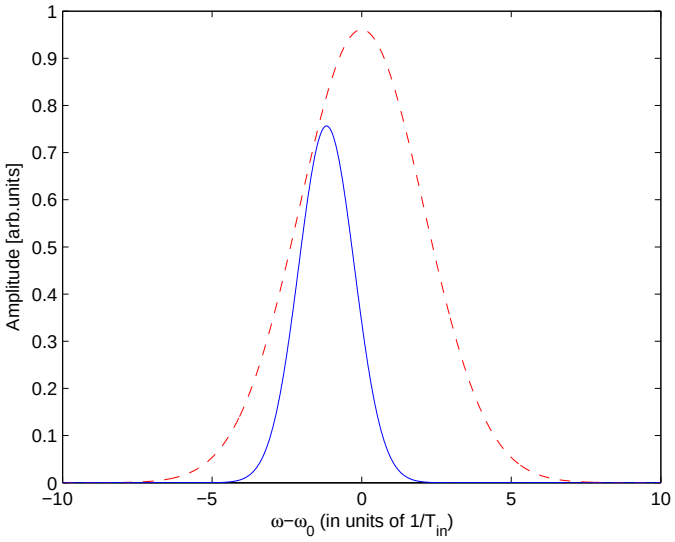

FIG. 4.7 - *Unshaped spectral amplitude (dashed line) and shaped spectral ampltude (blue line) as a function of the angular frequency corresponding to the two-level dynamics by the linear chirp shown in Fig. 4.6 with* $r = 1.85$ *and* $\Omega_0 T = 5$.

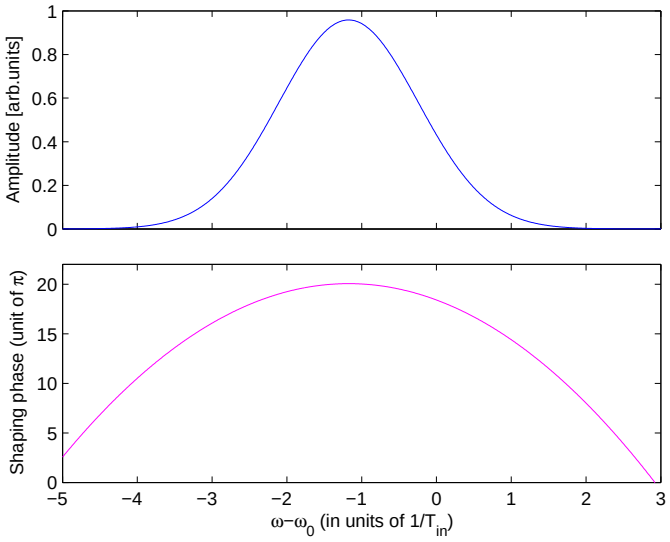

FIG. 4.8 - *Upper frame: Shaped spectral amplitude as a function of the angular frequency. Lower frame: Shaped spectral phase corresponding to the two-level dynamics by linear chirp shown in Fig. 4.6 with* $r = 1.85$ *and* $\Omega_0 T = 5$.

4.3 Application to Cesium

The two-photon $6S_{1/2}$-$8S_{1/2}$ transition in Cesium by parallel adiabatic passage

We here consider the two-photon transition in Cesium between the state $g \equiv 6S_{1/2}$ and $e \equiv 8S_{1/2}$ taking into account a more realistic model at the considered intensities than the simple two-state approximation. The mean frequency ω_0 of the laser (corresponding to the laser frequency of the Fourier transform limited pulse, i.e. before its shaping) is exactly two-photon resonant: $\omega_0 = (\omega_g - \omega_e)/2$. The relevant parameters for the considered transition are given in Table 7.1 of Appendix A. We have determined the parameters involving the dipole moment couplings with Eqs. (7.4), (7.4) and (7.4) using Ref. [37] for the bound-bound couplings and the Fues model potential [38, 39] for the bound-free couplings (see also [40] for a general discussion of model potential methods).

Figure 4.9 shows the level lines corresponding to the four-state approximation of Cs. The specific path depicted by a solid line is taken to produce the dynamics in Fig. 4.10. As one can see the intermediate state $6P_{3/2}$ is populated during the dynamics, because it has an energy close to one photon resonance. The field shapes corresponding to this dynamics are given in Fig. 4.11 and 4.12. Figure 4.11 displays the shaped spectral amplitude and phase in the frequency domain. The field is taken with 70 fs at FWHM corresponding to facilities in the group of J.Ahn from KAIST (Korea) with whom we have an ongoing collaboration. Figure 4.12 shows the comparison of the spectral unshaped and shaped amplitudes. The frequency $2\dot{\phi}$ is represented in Fig. 4.9 instead of detuning δ in Fig. 4.1. One notices an overall change of sign in the frequency compensation comparing Fig. 4.1 and Fig. 4.9. This is due to the fact that Ω_0, as defined in section 4.1, is negative for the Cesium atom, and a positive Ω_0 has been considered in Fig. 4.1.

The two-photon $6S_{1/2}$-$8S_{1/2}$ transition in Cesium by shifted linear chirp

Figure 4.13 shows the contour plot of the population of the $8S_{1/2}$ level of the Cs atom depending on the two chirp parameters defined by

$$\dot{\phi} = at + b. \tag{4.12}$$

The parameter b is a constant part of the phase which stands for the shift of the spectrum. Figure 4.14 displays the dynamics of the population and the time dependence of the parameters of the field. Here one can also see that the intermediate level $6P_{3/2}$ is populated during the dynamics. The respective spectral shaping determined from Eq. (4.8) corresponding to this dynamics are presented in Fig. 4.15 and Fig. 4.16. Figure 4.15 shows the shaped amplitude and phase in the frequency domain. Here again, the amplitude has a Gaussian form, but it is shifted and includes only some frequency components of the initial one similarly to the spectrum obtained from the two-state system (Fig. 4.8). However, one can remark that the sign of the chirp is here crucial, unlike for the two-state model where the transfer was symmetrically

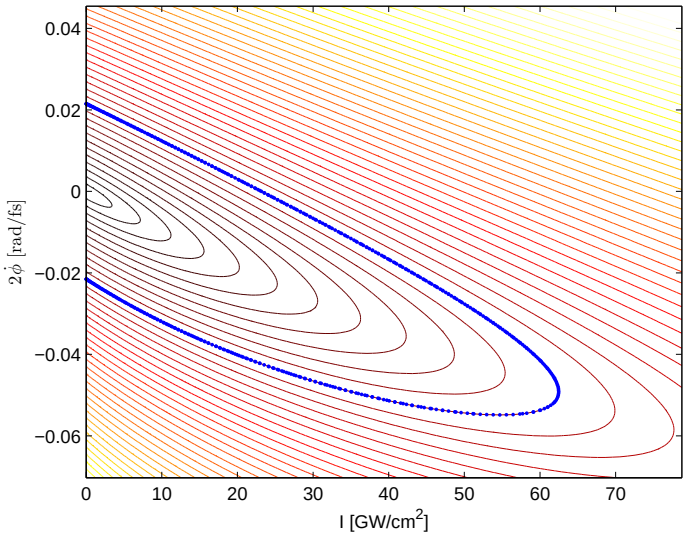

FIG. 4.9 - *Contour plot in the space of laser pulse parameters I (intensity) and $2\dot{\phi}$ (derivative of the phase) corresponding to the $6S_{1/2}$-$8S_{1/2}$ transition of the Cs atom. The thick line corresponds to a specific path corresponding to the dynamics shown in Fig. 4.10.*

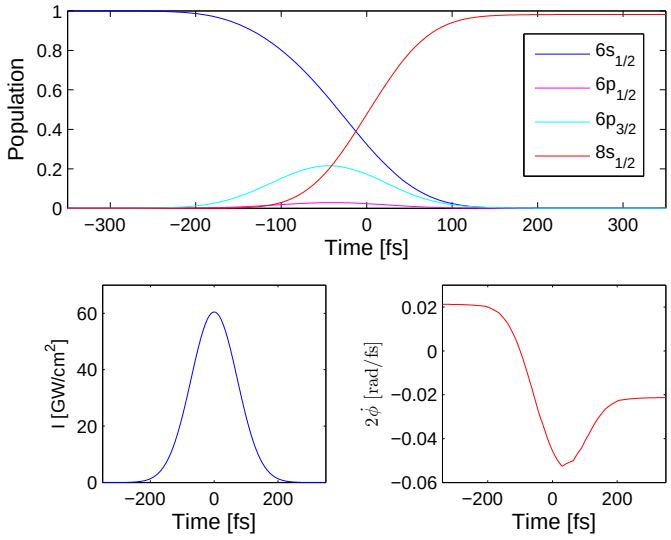

FIG. 4.10 - *Upper frame: Dynamics of the population of the energy levels of Cs as a function of time. Lower frame: Laser pulse parameters: intensity (left) and derivative of the phase as a function of time.*

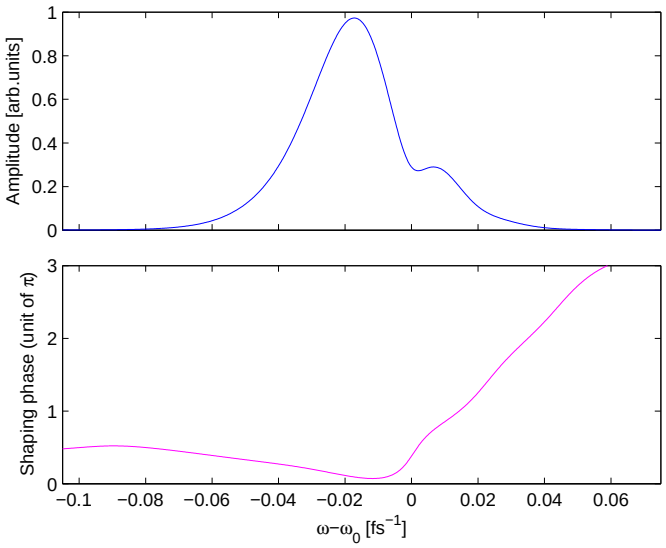

FIG. 4.11 - *Upper frame: Shaped spectral amplitude as a function of the angular frequency. Lower frame: Shaped spectral phase as a function of the angular frequency corresponding to* $6S_{1/2}$-$8S_{1/2}$ *transition of the Cs atom by PLAP techniques.*

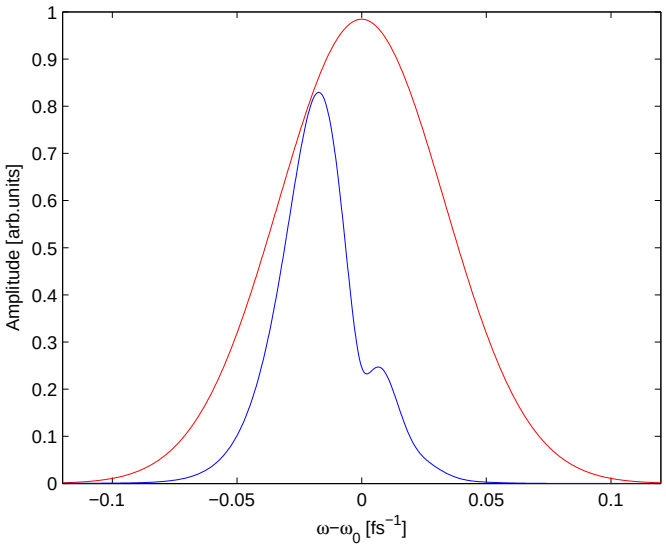

FIG. 4.12 - *Unshaped spectral amplitude (dashed line) and shaped spectral amplitude (blue line) as a function of the angular frequency corresponding to the* $6S_{1/2}$-$8S_{1/2}$ *transition of the Cs atom by PLAP techniques.*

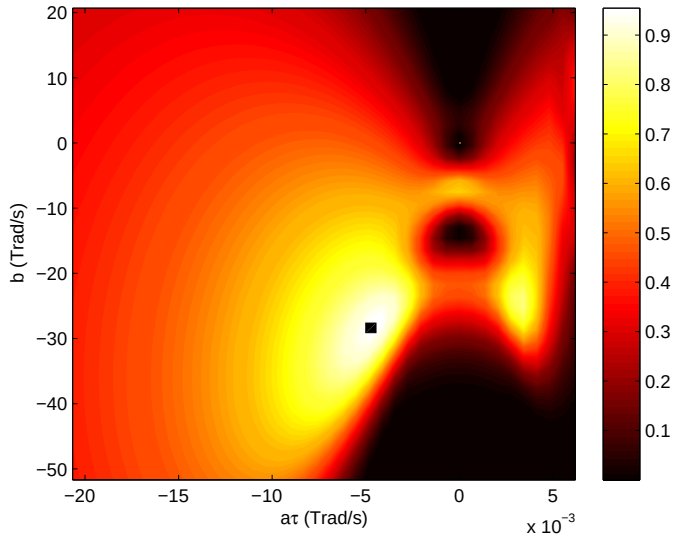

FIG. 4.13 - *Contour plot of the population of the $8S_{1/2}$ level of the Cs atom depending on the two chirp parameters. The black square corresponds to 98% of population.*

identical with respect to this sign. One can explain this result by the presence of the intermediate states which breaks more the validity of the two-state approximation when the detuning from the resonance with them is smaller.

4.4 Comparative study of robustness

In this section we analyse and compare the robustness of the linear chirping, shifted linear chirping and PAP techniques with respect to fluctuations of the pulse area for the two-state problem in the (4.1) in the case of a two photon transition with $\Omega_0 T = 5$ and $r = 1.85$.

We have determined the final populations by averaging over many realizations of an ensemble of systems with different peak Rabi frequencies uniformly distributed over the range $\Omega_0 \pm \beta/2$. Their peak Rabi frequency $\Omega_{0,j}$ is chosen as

$$\Omega_{0,j} = \Omega_0(1 + r_j\beta/\Omega_0), \tag{4.13}$$

where $-0.5 \leq r_j < 0.5$ is a uniformly distributed random number, Ω_0 is the average Rabi frequency, and β is the width of the probability distribution.

In Fig. 4.17 and 4.18 we compare the robustness of the three techniques, linear chirp, shifted linear chirp and parallel adiabatic passage, with respect to the pulse area fluctuations. One can see that the PLAP technique gives the most efficient and robust solutions with respect to pulse area fluctuations. The efficiency of the linear chirping even without fluctuations is only 65%, while the shifted linear chirping allows a complete population transfer also in a quite robust way.

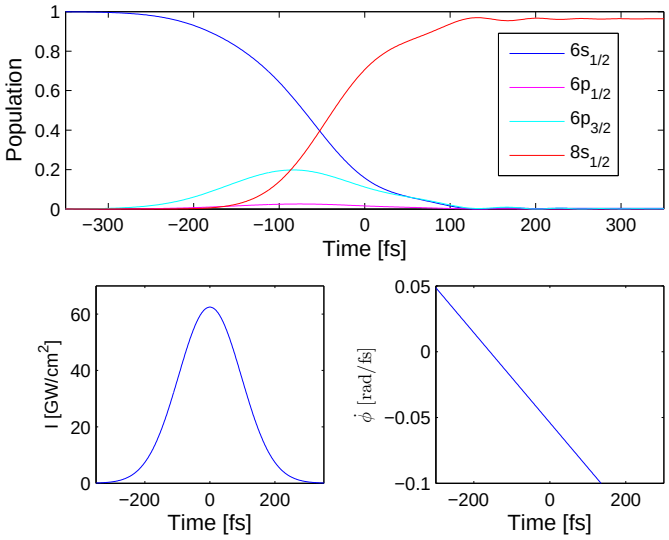

FIG. 4.14 - *Upper frame: Dynamics of the population of the energy levels of Cs as a function of time. Lower frame: Laser pulse parameters: the intensity (left) and the derivative of the phase (right).*

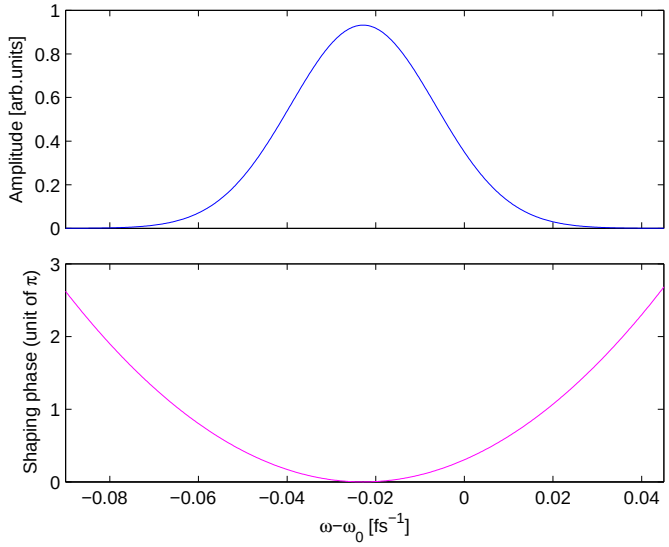

FIG. 4.15 - *Upper frame: Shaped spectral amplitude as a function of the angular frequency. Lower frame: Shaped spectral phase as a function of the angular frequency corresponding to the $6S_{1/2}$-$8S_{1/2}$ transition of the Cs atom by linear chirp techniques.*

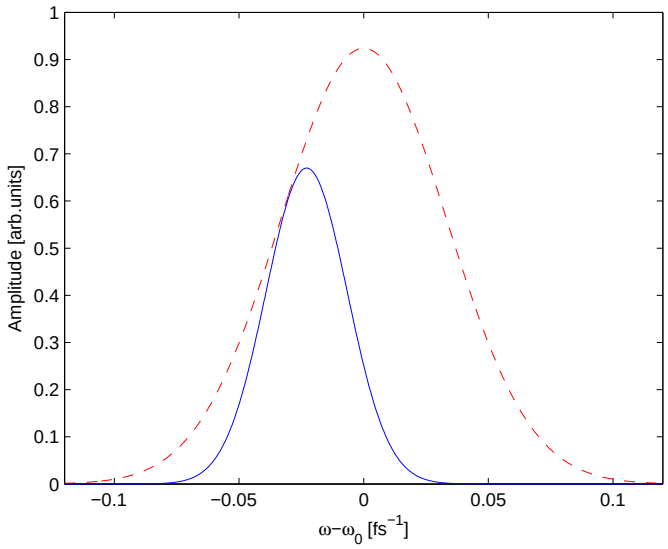

FIG. 4.16 - *Unshaped spectral amplitude (dashed line) and shaped spectral amplitude (full line) as a function of the angular frequency corresponding to the $6S_{1/2}$-$8S_{1/2}$ transition of the Cs atom by linear chirp techniques.*

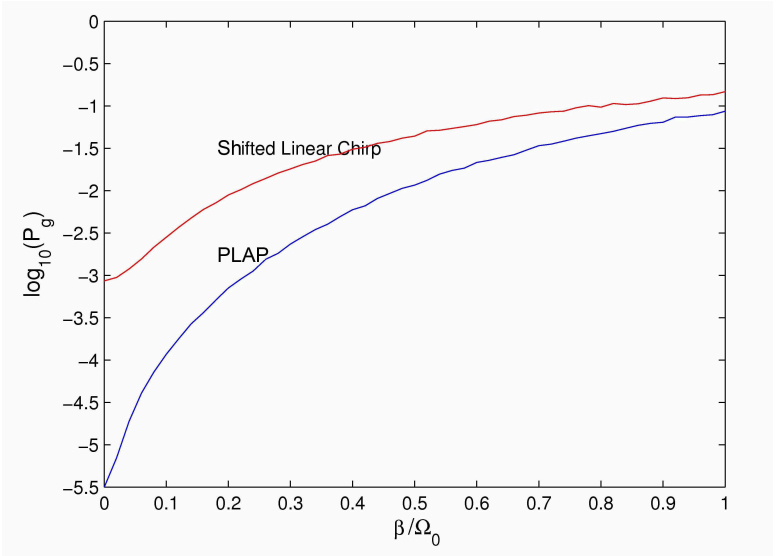

FIG. 4.17 - *Infidelity (in decimal logarithmic scale) of the PLAP (lower line) and shifted linear chirp (upper line) techniques with respect to variations of the pulse area for two-level system* (4.1) *on a two-photon transition with $\Omega_0 T = 5$ and $r = 1.85$.*

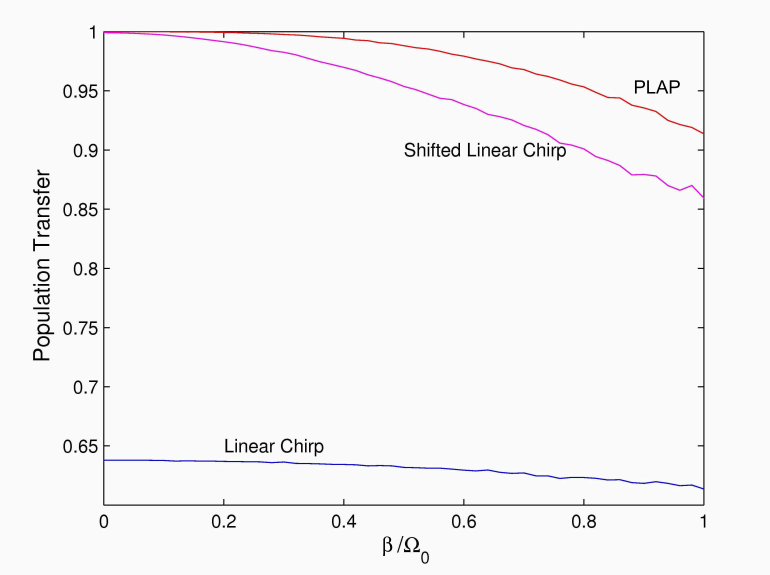

FIG. 4.18 - *Infidelity of the PLAP (upper line), shifted linear chirp (middle line) and linear chirp (lower line) techniques in the same conditions as Fig. 4.17 (but with a linear scale).*

Chapter 5

Selective population transfer in multi-level system by parallel adiabatic passage

In this chapter we show the selective population transfer of atomic states by making the dynamics follow parallel eigenvalues at all time, driven by appropriately shaped fields. We remark that with two parameters for the field (the amplitude and the phase) one can not force the system to feature all the parallel eigenvalues since the system here is too complicated. We have however shown that it is possible for Λ-system with two fields that can be chirped and delayed [27]. We thus use a weaker condition forcing the eigenvalue which is populated in dynamics to be parallel to the closest one. This is refered to as local parallel adiabatic passage. We perform calculations on the qualitative five level model of the sodium atom including 3s, 4s, 5p, 6p, 7p states in a process featuring $2+1$ photon and 3 photon resonance ($2+1$ photon resonance means a 3 photon process with an intermediate state which is two photon nearly resonant). We choose an adiabatic path (this is achieved from a geometric picture showing the difference of eigenenergies as functions of the field parameters) to selectively populate the 6p and 7p states. We also analyse the dynamics on a model of the sodium atom including more levels that are relevant for the considered dynamics: $3s_{1/2}, 3p_{1/2}, 3p_{3/2}, 4s_{1/2}, 5p_{1/2}$, $5p_{3/2}, 6p_{1/2}, 6p_{3/2}, 7p_{1/2}, 7p_{3/2}, 3d_{3/2}, 3d_{5/2}, 5f_{5/2}, 5f_{7/2}, 6f_{5/2}, 6f_{7/2}$.
We also show the possibility of high efficiency transfer of population by linear chirp including a static detuning from exact resonance. The field shapes in the frequency domain for both techniques are determined.

5.1 The Model

Figure 5.1 shows the excitation scheme of the sodium atom by intense 795nm, 30fs FWHM (Full Width at Half Maximum) laser pulses corresponding to the laser facilities in the Institute of Physics of University of Kassel (Germany), where experiments on this system have been carried out. The predominant pathways are indicated by red arrows. For the theoretical model we consider that excitation arises through the channel wich involves the five states 3s, 4s, 5p, 6p,

7p. The energy levels and transition dipole couplings are taken from the NIST database [70]. The state 3p here is adiabatically eliminated, but it has strong influence on the population dynamics as it induces dynamical Stark shift on the energy levels of the 3s and the 4s states. The quantum dynamics is governed by the time-dependent Schrödinger equation (TDSE)

$$i\hbar\frac{d}{dt}\Psi(t) = H(t)\Psi(t), \tag{5.1}$$

where the effective Hamiltonian of the system in the RWA is given by [46]

$$H(t) = \hbar\begin{bmatrix} \Delta_1 + S_1 & \frac{1}{2}\Omega_{12} & 0 & 0 & 0 \\ \frac{1}{2}\Omega_{12} & \Delta_2 + S_2 & \frac{1}{2}\Omega_{23} & \frac{1}{2}\Omega_{24} & \frac{1}{2}\Omega_{25} \\ 0 & \frac{1}{2}\Omega_{23} & \Delta_3 & 0 & 0 \\ 0 & \frac{1}{2}\Omega_{24} & 0 & \Delta_4 & 0 \\ 0 & \frac{1}{2}\Omega_{25} & 0 & 0 & \Delta_5 \end{bmatrix}. \tag{5.2}$$

Here $\Delta_n = \omega_n - k_n\omega_L(t)$ are the atom-laser detunings, where ω_n are the atomic state energies with $n = 1, 2, 3, 4, 5$ respectively for the states 3s, 4s, 5p, 6p, 7p, k_n is the order of the transition and $\omega_L(t) = \omega_0 + \dot{\phi}$ is the instantaneous laser frequency composed by the central laser frequency ω_0 and the derivative of the instantaneous relative phase $\dot{\phi}$. We consider $\omega_1 = 0$ (reference energy). We have $k_1 = 0$ (i.e. $\Delta_1 = 0$), $k_2 = 2$, $k_3 = 3$, $k_4 = 4$, $k_5 = 5$. The Stark shifts S_1 and S_2, respectively of the 3s and 4s states, are due to their coupling to the intermidiate state 3p:

$$S_1 = -\frac{\Omega_{3s3p}^2}{4\Delta_{3p}}, \quad S_2 = -\frac{\Omega_{3p4s}^2}{4\Delta_{3p}}, \tag{5.3}$$

where $\Delta_{3p} = \omega_{3p} - \omega_L$. The two-photon Rabi frequency Ω_{12} between the states 3s and 4s is

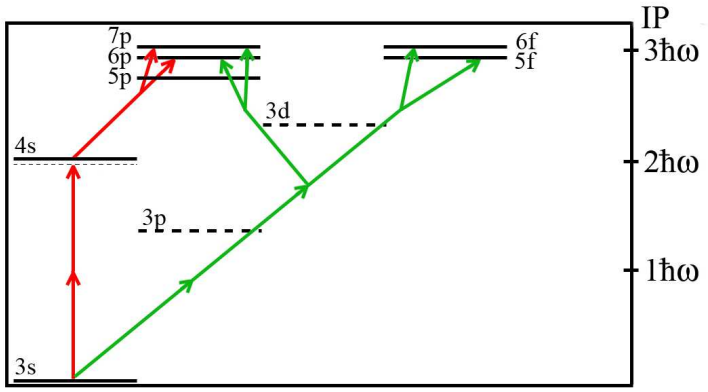

FIG. 5.1 - *Energy level structure of the Na atom. The red and green arrows show the two possible channels.*

given by

$$\Omega_{12}(t) = -\frac{\mathcal{E}^2(t)}{2\hbar^2}\sum_{m\neq 1,2}\frac{\mu_{1m}\mu_{m2}}{\omega_m - \omega_1 - \omega_L(t)}, \tag{5.4}$$

with μ_{1m}, μ_{2m} the transition dipole moments respectively between the states 3s-3p and 3p-4s and the field envelope $\mathcal{E}(t) = \mathcal{E}_0 e^{-(t/T)^2}$ taken as a Gaussian . The one-photon couplings are defined as $\Omega_{2n} = -\mathcal{E}\mu_{2n}/\hbar$, where μ_{2n} are the transition dipole moments between states 2 and n ($n = 3, 4, 5$).

5.1.1 Adiabatic passage by following parallel eigenvalues: the local parallel adiabatic passage

The strategy of optimal population transfer by adiabatic passage is based on the idea of following a level line in the diagram of the difference of the instantaneous eigenenergies [26] corresponding to the eigenstate which is populated in the adiabatic limit and the closest one. This is refered to as a local parallel adiabatic passage. The three-photon transition between the states 3s→ 6p and 3s→ 7p for the five level model can be efficient by following the level lines in parameter space (I, Δ). Figures 5.2 and 5.3 show level lines of constant differences between the eigenvalues involving these two transitions respectively. Figures 5.4 and 5.5 present the population of the energy levels following the parameters taken from the level lines for the five level model. Here the population $6p$ corresponds to the sum of the populations of $6p_{1/2}$ and $6p_{3/2}$, and $7p$ is the sum of $7p_{1/2}$ and $7p_{3/2}$. One can see that there are intermediate states that can be populated during the dynamics. Figures 5.6 and 5.7 show the resulting dynamics with the previous parameters applied on the complete model with 16 levels, which includs levels which have very close energies with the target states. As one can see, the five level model describes the system well and the specific path taken from Figs. 5.2 and 5.3 allows to be selective even between very close energies. Figures 5.8 and 5.9 show the shapes of the fields used respectively for Figs. 5.6 and 5.7. Figures 5.8 and 5.9 show the shaped amplitudes in the frequency domain. They display some oscillations that occur when there is a large Stark shift in the system. In Figs. 5.10 and 5.11 the Stark shift is smaller and thus the oscillations in amplitude are reduced. In Figs. 5.8 and 5.10 we show the comparison of the unshaped and shaped pulse amplitudes. There are spectral components that have to be removed in order to achieve efficiently the complete population transfer.

5.1.2 Static compensation of the Stark shift

In this section we present a way to get a high efficiency population transfer by a linear chirp defined as

$$\dot{\phi} = at + b, \tag{5.5}$$

where b is a static shift, which can be adjusted numerically, as well as a, to increase the efficiency. In Figs. 5.12 and 5.14 we show the three photon population transfer between the levels 3s→ 6p and 3s→ 7p respectively, depending on the two chirp parameters. One can see that in the case of zero shift (b=0) the population of the excited levels are not very high. The calculations

are done with the complete model (with 16 levels) and a peak intensity 1.5×10^{12} W/cm^2. The dynamics corresponding to these contour plots are shown in Figs. 5.13 and 5.15. There are many levels that are populated during the dynamics, but this technique also allows one to be selective and efficient between very close energy levels. It permits as well to be very fast. Figures 5.16 and 5.17 present the pulse shaping corresponding to Figs. 5.13 and 5.15 respectively: The shaped amplitudes have Gaussian forms, but they include only some part of the initial spectrum. The other components are removed from the initial spectrum. One can interpret this by the fact that they can produce additional Stark shifts leading to incomplete population transfer. The shapes of the spectral phases are parabolas, corresponding to a linear chirping.

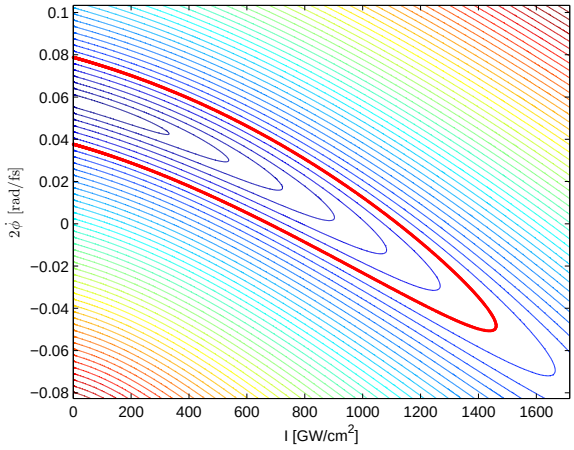

FIG. 5.2 - *Contour plot of the difference of eigenenergies as a function of the laser parameters corresponding to the* $3s_{1/2} \rightarrow 6p$ *three photon transition of the Na atom. The thick red line correponds to a specific path chosen for the dynamics shown in Fig. 5.4 and Fig. 5.6.*

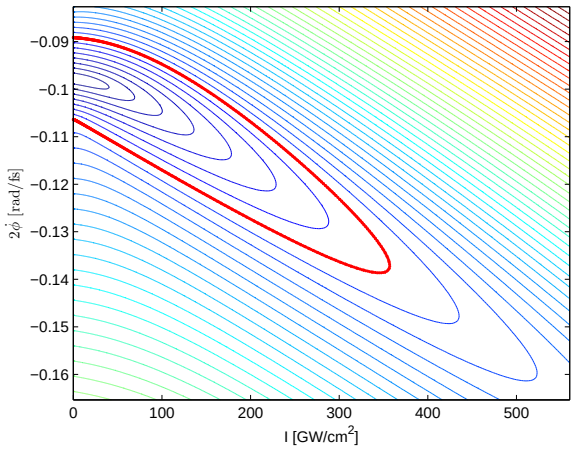

FIG. 5.3 - *Same as Fig.5.2 but for the* $3s_{1/2} \rightarrow 7p$ *three photon transition. The thick line correponds to a specific path chosen for the dynamics shown in Fig. 5.5 and Fig. 5.7.*

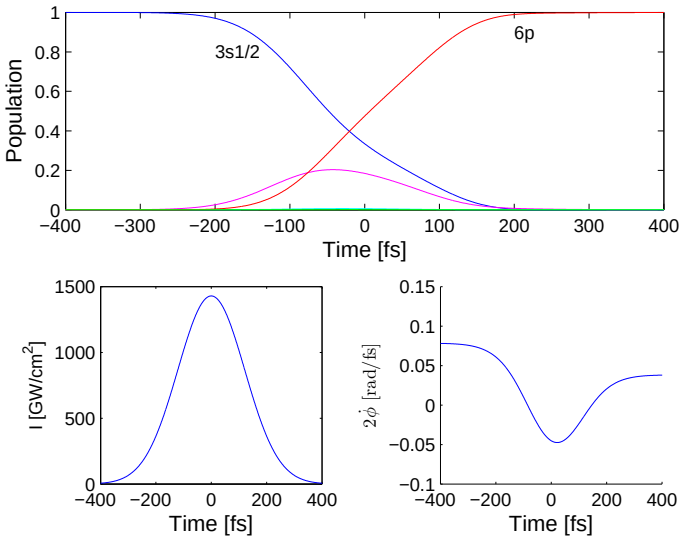

FIG. 5.4 - *Population transfer from* $3s_{1/2}$ *to* $6p$*. Upper frame: Dynamics of the populations corresponding to the five-level model* (5.2) *for the time dependent parameters determined from Fig. 5.2 (where the field amplitude is taken as Gaussian); Lower frames: Laser pulse parameters: intensity (left) and the derivative of the phase (right).*

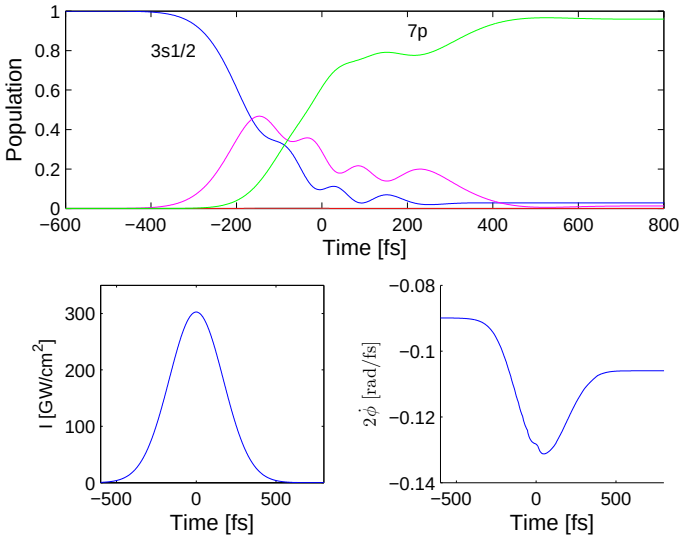

FIG. 5.5 - *Same as Fig. 5.4, but for the population transfer to 7p, and the parameters determined from Fig. 5.3.*

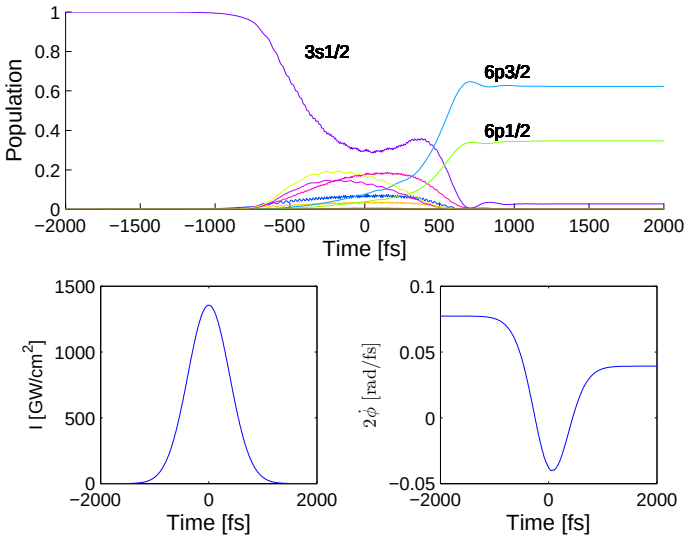

FIG. 5.6 - *Same as Fig. 5.4, but for the 16-level model.*

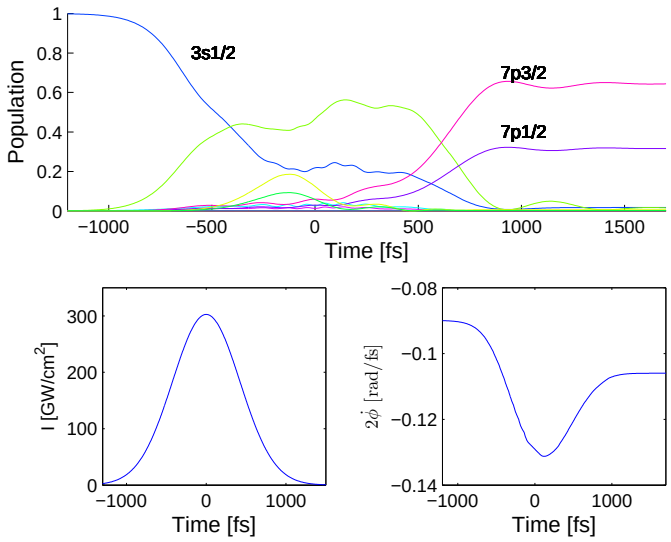

FIG. 5.7 - *Same as Fig. 5.5, but for the 16-level model.*

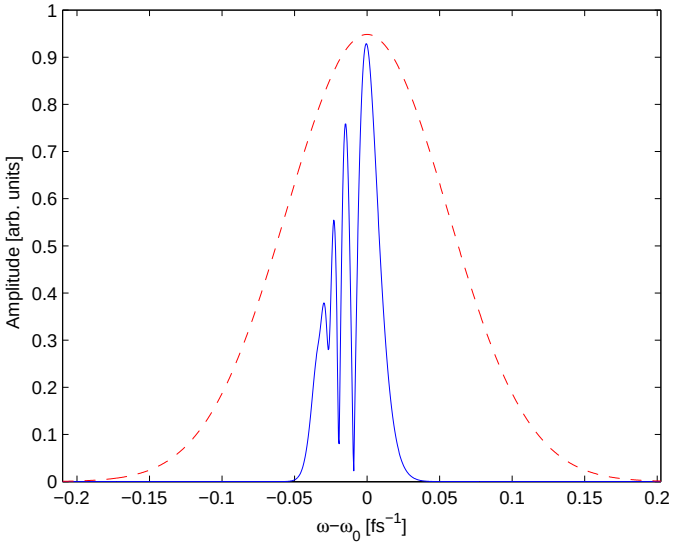

FIG. 5.8 - *Unshaped spectral amplitude (dashed line) and shaped spectral amplitude (full line) as a function of the angular frequency corresponding to the* $3s_{1/2} \rightarrow 6p$ *three photon transition corresponding to the path shown in Fig. 5.2 and leading to the dynamics of Figs 5.4. 5.6.*

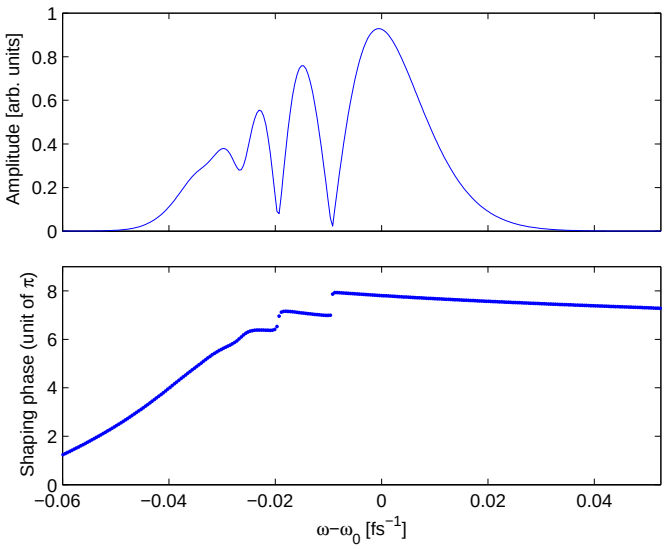

FIG. 5.9 - *Shaped spectral amplitude (upper frame) and shaped spectral phase (lower frame) in the same conditions as in Fig. 5.8.*

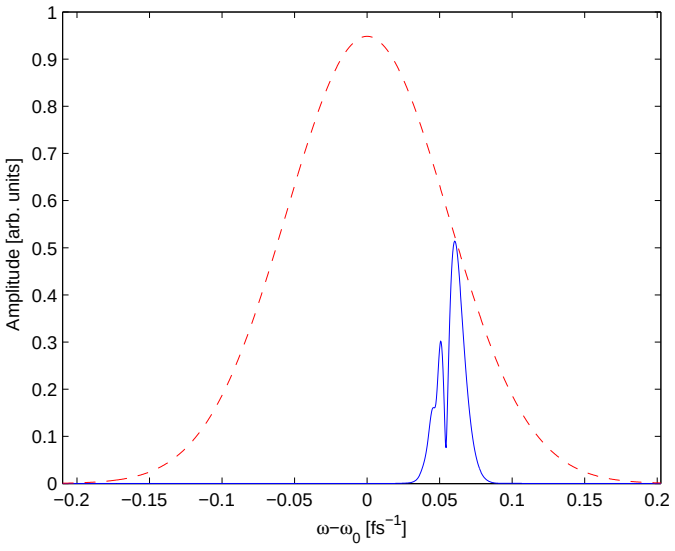

FIG. 5.10 - *Same as Fig. 5.8 but for the transition to 7p (path shown in Fig. 5.3 and dynamics in Figs. 5.5 and 5.7).*

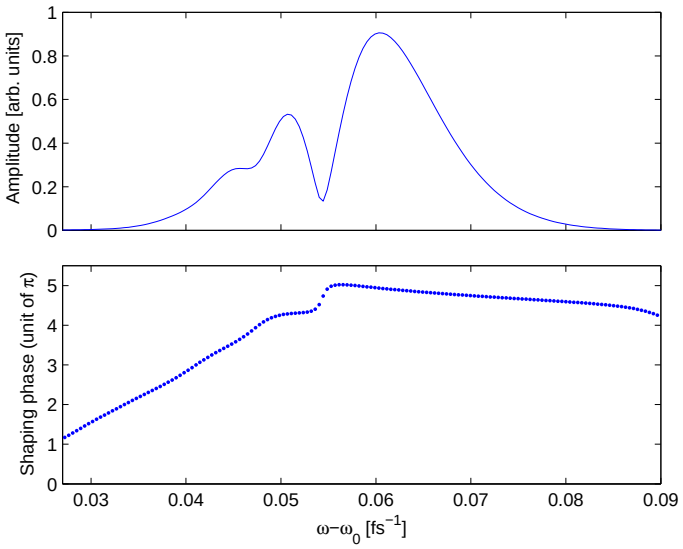

FIG. 5.11 - *Same as Fig. 5.9 but for the transition 7p*

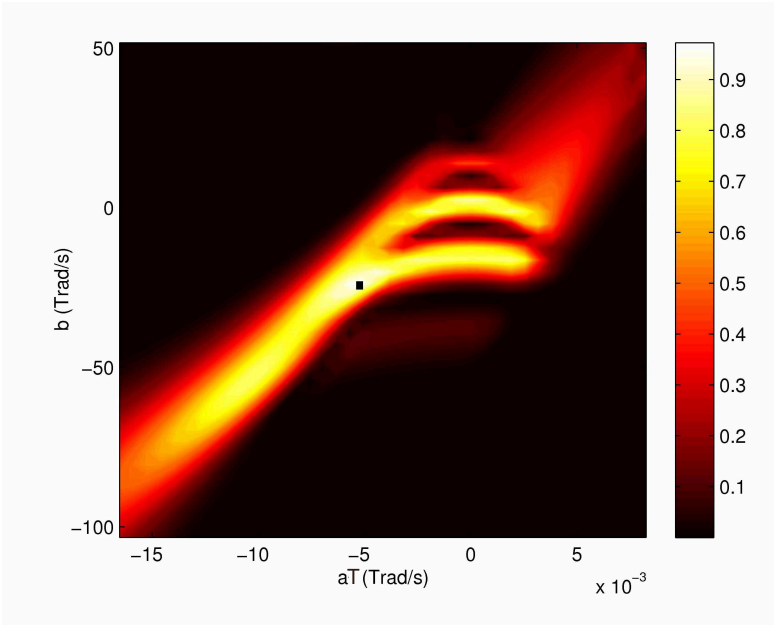

FIG. 5.12 - *Contour plot of the population of the 6p level of the 16-level model of the Na atom depending on the two chirp parameters. The black square corresponds to 99.9% of population transfer.*

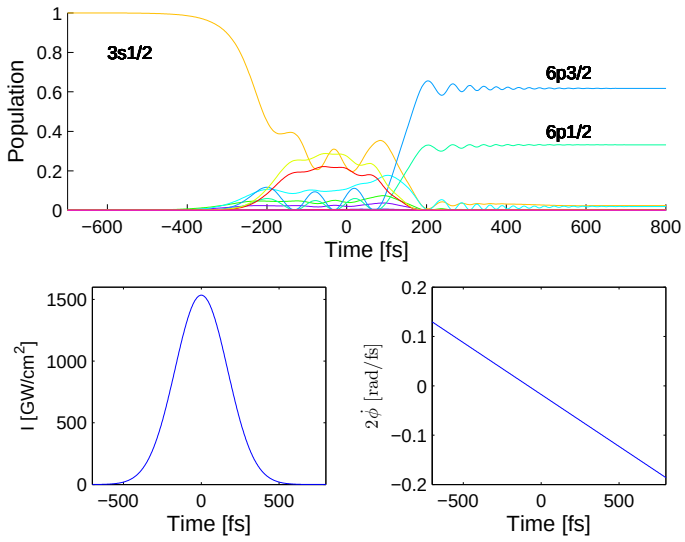

FIG. 5.13 - *Upper frame: Dynamics of the population of the energy levels of the Na atom as a function of time corresponding to the black square in Fig. 5.12. Lower frames: Laser pulse parameters: intensity (left) and the derivative of the phase (right).*

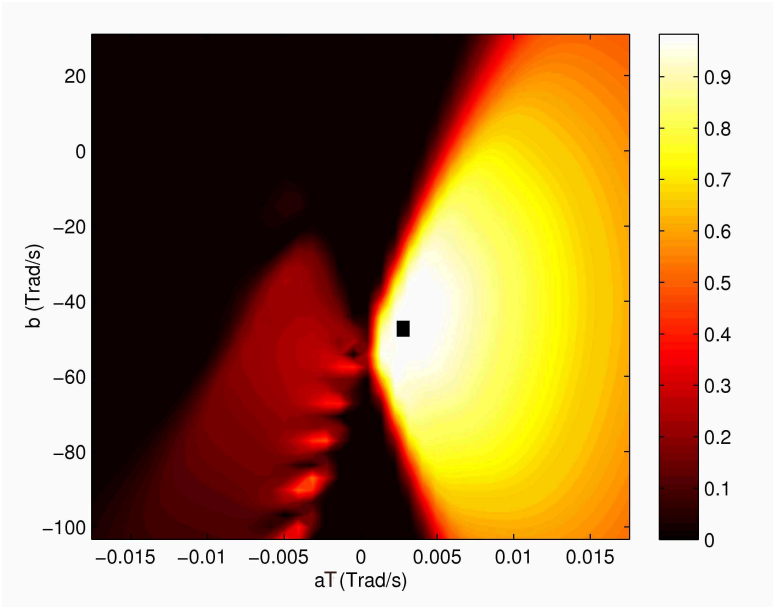

FIG. 5.14 - *Contour plot of the population of the 7p level of the 16 level model of the Na atom depending on the two chirp parameters. The black square corresponds to 99.9% of population transfer.*

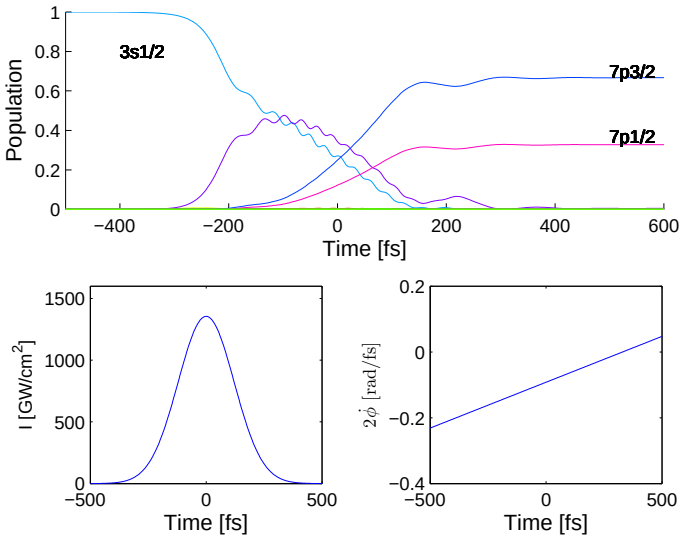

FIG. 5.15 - *Upper frame: Dynamics of the energy levels of the Na atom as a function of time corresponding to the black point in Fig .5.14. Lower frames: laser pulse parameters: intensity (left) and the derivative of the phase (right).*

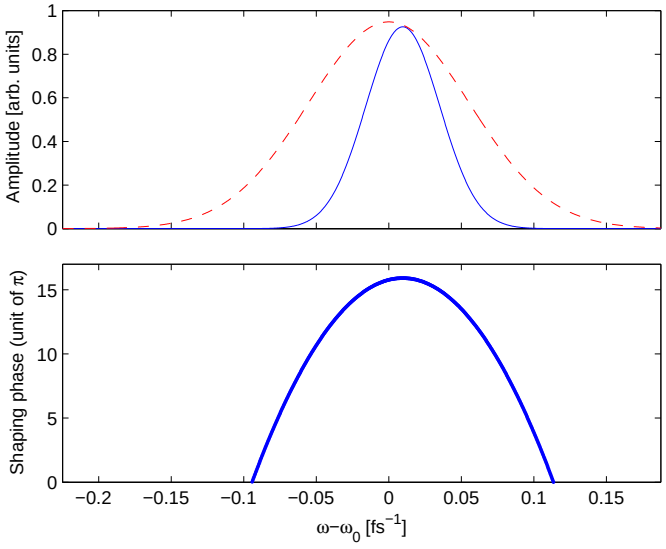

FIG. 5.16 - *Upper frame: Unshaped spectral amplitude (red line) and shaped spectral amplitude (blue line) as a function of the angular frequency. Lower frame: Shaped spectral phase as a function of the angular frequency corresponding to the dynamics shown in Fig. 5.13.*

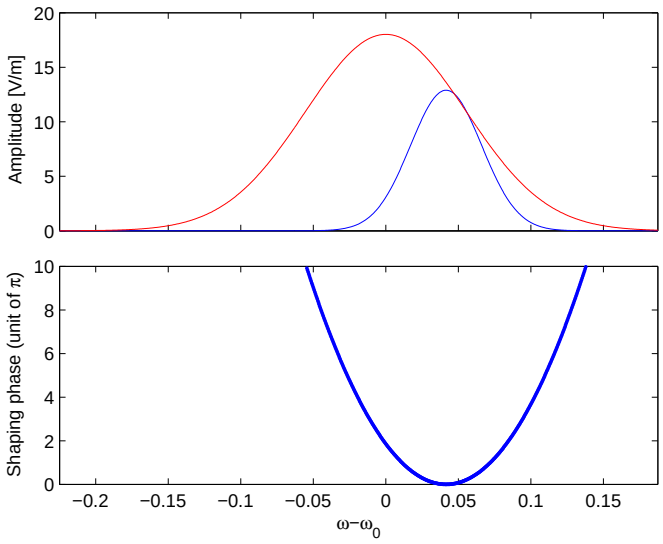

FIG. 5.17 - *Upper frame: Unshaped spectral amplitude (red line) and shaped spectral amplitude (blue line) as a function of the angular frequency. Lower frame: Shaped spectral phase as a function of the angular frequency corresponding to the dynamics shown in Fig. 5.15.*

Chapter 6

Superposition of states by controlled Stark shift adiabatic passage in a Potassium atom

In this chapter we extend the preceding technique to achieve a transfer of population from a single quantum state into a coherent superposition of excited states, by bichromatic adiabatic passage on a K atom. The transfer is executed with spectrally shaped femtosecond laser pulses. The excited states are dynamically shifted in energy due to the presence of nonresonant components of the two different channels of the K atom. This results in an incomplete population transfer to the target superposition. We show that a third field can compensate this Stark shift and that it allows a robust and complete population transfer for appropriately shaped fields.

6.1 The model

We consider a three-state system where the two upper states are near degenerate and do not couple each other by dipole interaction. Our aim is to transfer by adiabatic passage the population from the ground state $|0\rangle$ to a superposition of the two upper states $|1\rangle$ and $|2\rangle$ (of respective energy ω_1 and $\omega_2 = \omega_1 + \delta$, in units such that $\hbar = 1$) which reads, up to an uncontrolled global phase

$$|\psi\rangle = c_1 e^{-i\omega_1 t}|1\rangle + c_2 e^{i\varphi} e^{-i\omega_2 t}|2\rangle, \tag{6.1}$$

with c_1 and c_2 real and positive (without loss of generality). We require a robust control of the amplitudes c_1 and c_2 and the relative phase of the superposition φ. Denoting by μ_j the dipole moment of the transition $|0\rangle \leftrightarrow |j\rangle$, which we assume real and positive, we label the state following the convention $\mu_2 > \mu_1$. We have then $\delta > 0$ ($\delta < 0$) if the upper (lower) state corresponds a larger dipole moment.

For that purpose, we use a chirped polychromatic pulse of the form

$$E(t) = \mathcal{E}_1 \cos(\omega_1 t + \phi_1) + \mathcal{E}_S \cos(\omega_S t + \phi_S) + \mathcal{E}_2 \cos(\omega_2 t + \phi_2) \tag{6.2}$$

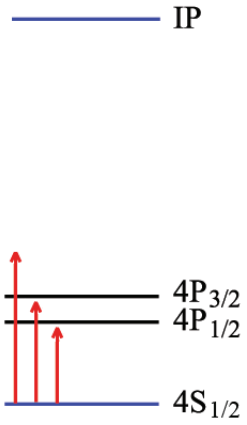

FIG. 6.1 - *The energy levels diagram of K atom.*

with $\mathcal{E}_j \equiv \mathcal{E}_j(t)$, and $\phi_j \equiv \phi_j(t)$, $j = 1, 2, S$. One chooses this field following the intuition that the field labeled 1 (labeled 2) controls the transition $|0\rangle \leftrightarrow |1\rangle$ ($|0\rangle \leftrightarrow |2\rangle$) through the chirp $\dot{\phi}_1$ ($\dot{\phi}_2$). However, these two interaction channels cannot be treated strictly independently in practice when the field is strong and dynamic cross-talks between simultaneously driven transitions have to be taken into account through dynamical Stark shifts. The Stark shift causes (i) a shift of the resonance, which is expected to be overcome by the adiabatic process and (ii) a relative detrimental dynamical phase in the superposition. The role of the third field labeled S, while also producing itself a Stark shift, is to give an additional control over the total Stark shift and to cancel its detrimental effects.

In the resonant approximation (RWA), in the basis

$$\{|0\rangle,\ e^{-i\omega_1 t}|1\rangle,\ e^{-i\omega_2 t}|2\rangle\}, \tag{6.3}$$

the Hamiltonian is of the form

$$\hat{H}(t) = \frac{1}{2} \tag{6.4}$$
$$\times \begin{bmatrix} 0 & \Omega_1 e^{i\phi_1} + \Omega_2 \frac{\mu_1}{\mu_2} e^{i(\delta t + \phi_2)} + \Omega_S e^{i[(\omega_S - \omega_1)t + \phi_S]} & \Omega_2 e^{i\phi_2} + \Omega_1 \frac{\mu_2}{\mu_1} e^{-i(\delta t - \phi_1)} + \frac{\mu_2}{\mu_1}\Omega_S e^{i[(\omega_S - \omega_2)t + \phi_S]} \\ * & 0 & 0 \\ * & 0 & 0 \end{bmatrix},$$

where the symbols $*$ ensure that the Hamiltonian is self-adjoint. We assume without loss of generality that the Rabi frequencies are defined as

$$\Omega_j = \mu_j \mathcal{E}_j, \quad j = 1, 2, \qquad \Omega_S = \mu_1 \mathcal{E}_S. \tag{6.5}$$

The RWA Hamiltonian (6.4) is valid for $\Omega_j, |\delta| \ll \omega_j$.

We can apply the phase transformation

$$T = \begin{bmatrix} 1 & 0 & 0 \\ 0 & e^{-i\phi_1} & 0 \\ 0 & 0 & e^{-i\phi_2} \end{bmatrix} \tag{6.6}$$

to get

$$T^\dagger \hat{H}(t) T - i T^\dagger \frac{dT}{dt} = \tag{6.7}$$
$$\frac{1}{2}\begin{bmatrix} 0 & \Omega_1 + \Omega_2 \frac{\mu_1}{\mu_2} e^{i(\delta t + \phi_{2,1})} + \Omega_S e^{i[(\Delta+\delta)t + \phi_{S,1}]} & \Omega_2 + \Omega_1 \frac{\mu_2}{\mu_1} e^{-i(\delta t + \phi_{2,1})} + \frac{\mu_2}{\mu_1}\Omega_S e^{i(\Delta t + \phi_{S,2})} \\ * & -\dot{\phi}_1 & 0 \\ * & 0 & -\dot{\phi}_2 \end{bmatrix}$$

with

$$\phi_{i,j} = \phi_i - \phi_j, \quad \Delta = \omega_S - \omega_2, \tag{6.8}$$

in the basis

$$\{|0\rangle,\ e^{-i(\omega_1 t - \phi_1)}|1\rangle,\ e^{-i(\omega_2 t - \phi_2)}|2\rangle\}. \tag{6.9}$$

We next treat the non-resonant channels as Stark shifts under the conditions

$$\Omega_1, \Omega_2 \ll |\delta|, \quad \Omega_S \ll |\Delta|, |\delta| \tag{6.10}$$

leading to the effective Hamiltonian

$$H(t) = \frac{1}{2}\begin{bmatrix} 0 & \Omega_1 & \Omega_2 \\ \Omega_1 & 2(S_1 - \dot{\phi}_1) & S_{12} \\ \Omega_2 & S_{12}^* & 2(S_2 - \dot{\phi}_2) \end{bmatrix}. \tag{6.11}$$

The (diagonal) Stark shifts read

$$S_1 = S_{1,2} + S_{1,S} + \frac{1}{2}\left(S_{2,1} + S_{2,S}\right), \tag{6.12a}$$
$$S_2 = S_{2,1} + S_{2,S} + \frac{1}{2}\left(S_{1,2} + S_{1,S}\right) \tag{6.12b}$$

with the dominant terms

$$S_{1,2} = -\frac{1}{2}\left(\frac{\mu_1}{\mu_2}\right)^2 \frac{\Omega_2^2}{\dot{\phi}_2 + \delta}, \tag{6.13a}$$
$$S_{2,1} = -\frac{1}{2}\left(\frac{\mu_2}{\mu_1}\right)^2 \frac{\Omega_1^2}{\dot{\phi}_1 - \delta}, \tag{6.13b}$$
$$S_{1,S} = -\frac{1}{2}\frac{\Omega_S^2}{\dot{\phi}_S + \Delta + \delta}, \tag{6.13c}$$
$$S_{2,S} = -\frac{1}{2}\left(\frac{\mu_2}{\mu_1}\right)^2 \frac{\Omega_S^2}{\dot{\phi}_S + \Delta}. \tag{6.13d}$$

We have also kept the non-diagonal term

$$S_{12} = -\frac{\Omega_2\Omega_S}{4}\left(\frac{1}{\dot\phi_S+\Delta}+\frac{1}{\dot\phi+\delta}\right)e^{i[(\Delta-\delta)t+\phi_S-\phi]} - \frac{\mu_2}{\mu_1}\frac{\Omega_1\Omega_S}{4}\left(\frac{1}{\dot\phi_S+\Delta+\delta}+\frac{1}{\dot\phi-\delta}\right)e^{-i[(\Delta+2\delta)t+\phi_S-\phi]}, \tag{6.14}$$

which is relevant when $S_1-\dot\phi_1 = S_2-\dot\phi_2$ corresponding to a dynamical degenerate subspace spanned by the upper states [if one takes into account only the dominant terms (6.13)], as it will be considered in the next section. This term S_{12}, which is in general oscillatory, cancels out by averaging when

$$\left|\frac{\Omega_2\Omega_S}{4}\left(\frac{1}{\dot\phi_S+\Delta}+\frac{1}{\dot\phi+\delta}\right)\right| \ll |\Delta-\delta|, \tag{6.15a}$$

$$\left|\frac{\mu_2}{\mu_1}\frac{\Omega_1\Omega_S}{4}\left(\frac{1}{\dot\phi_S+\Delta+\delta}+\frac{1}{\dot\phi-\delta}\right)\right| \ll |\Delta+2\delta|. \tag{6.15b}$$

The first (second) term of S_{12} is real and non-oscillatory, and thus preserved, for $\Delta=\delta$ ($\Delta=-2\delta$) and $\phi_S=\phi$.

6.2 Strategy

The wished relative phase φ is obtained when one chooses at all times

$$\phi_2(t) = \phi_1(t)+\varphi, \tag{6.16}$$

leading to

$$\dot\phi_2 = \dot\phi_1 \equiv \dot\phi. \tag{6.17}$$

The coefficients of the superposition

$$c_1 = \cos\theta = \frac{\Omega_1}{\Omega_0},\ c_2 = \sin\theta = \frac{\Omega_2}{\Omega_0},\ \Omega_0 \equiv \sqrt{\Omega_1^2+\Omega_2^2} \tag{6.18}$$

are revealed by the time-independent Morris-Shore transformation:

$$M = \begin{bmatrix} 1 & 0 & 0 \\ 0 & \cos\theta & -\sin\theta \\ 0 & \sin\theta & \cos\theta \end{bmatrix}, \quad \tan\theta = \frac{\Omega_2}{\Omega_1} \tag{6.19}$$

It requires the respective amplitudes of the two fields 1 and 2 to have a common shape. It gives indeed

$$M^\dagger H M = \tag{6.20}$$

$$\begin{bmatrix} 0 & \Omega_0/2 & 0 \\ \Omega_0/2 & S_1\cos^2\theta+S_2\sin^2\theta+(S_{12}+S_{12}^*)\cos\theta\sin\theta-\dot\phi & (S_2-S_1)\cos\theta\sin\theta+S_{12}\cos^2\theta-S_{12}^*\sin^2\theta \\ 0 & (S_2-S_1)\cos\theta\sin\theta+S_{12}^*\cos^2\theta-S_{12}\sin^2\theta & S_2\cos^2\theta+S_1\sin^2\theta-(S_{12}+S_{12}^*)\cos\theta\sin\theta-\dot\phi \end{bmatrix}$$

which corresponds to an effective two-state system connected to the initial ground state

$$H_2 = \frac{1}{2}\begin{bmatrix} 0 & \Omega_0 \\ \Omega_0 & 2(S-\dot{\phi}) \end{bmatrix} \tag{6.21}$$

in the basis

$$\{|0\rangle,\ e^{i\phi_1}|\psi\rangle\} \tag{6.22}$$

if (i) the Stark shifts are equal

$$S_2 = S_1 \equiv S, \tag{6.23}$$

which is satisfied for

$$\Omega_S = \Omega_1 \sqrt{\frac{\left(\frac{\mu_1}{\mu_2}\right)^2 \frac{\tan^2\theta}{\dot{\phi}+\delta} - \left(\frac{\mu_2}{\mu_1}\right)^2 \frac{1}{\dot{\phi}-\delta}}{\left(\frac{\mu_2}{\mu_1}\right)^2 \frac{1}{\dot{\phi}_S+\Delta} - \frac{1}{\dot{\phi}_S+\Delta+\delta}}}. \tag{6.24}$$

and (ii)

$$S_{12}\cos^2\theta - S_{12}^*\sin^2\theta = 0. \tag{6.25}$$

The latter is satisfied either (a) when the term S_{12} cancels out by averaging requiring Δ efficiently different from δ and from -2δ, or (b) when $\Delta = \delta$ (or $\Delta = -2\delta$), $\phi_S = \phi$ and $\theta = \pi/4$ (equal superposition). Equation (6.24) shows that the Stark shift compensation is possible in general under the conditions

$$\text{for } \delta > 0: \qquad \Delta > 0 \text{ or } \frac{\delta}{q^2-1} < \Delta < -\delta \tag{6.26a}$$

$$\text{for } \delta < 0: \qquad \Delta < 0 \text{ or } -\delta < \Delta < \frac{\delta}{q^2-1}. \tag{6.26b}$$

The compensation is more efficient, i.e. it requires a smaller Stark pulse amplitude, for Δ closer to 0 or Δ closer to $-\delta$. However the latter situation is inefficient in practice if q^2, which satisfies by definition $q^2 \leq 1$, is well different from 1, since then Δ is not so different from the value $\frac{\delta}{q^2-1}$ which corresponds to a Stark field of infinite amplitude. Situation (a) is anticipated to be efficient for the choice $\Delta = 0.5\delta$ (or $\Delta = -1.5\delta$ only if q^2 is close to 1) as it gives a compromise of an efficient Stark compensation and of satisfying condition (6.15) for the averaging of the off-diagonal elements. Equation (6.24) should give a Stark Rabi frequency Ω_S that has to be furthermore not too large, that is not much larger than Ω_0: $\Omega_S \lesssim \Omega_0$. This is roughly satisfied for

$$|\Delta| \lesssim |\delta| \text{ for } \delta \text{ and } \Delta \text{ of the same sign,} \tag{6.27a}$$

$$|\Delta| \lesssim 2|\delta| \text{ for } \delta \text{ and } \Delta \text{ of opposite sign and } q \sim 1. \tag{6.27b}$$

In brief, the coefficients c_1 and c_2 of the superposition are chosen through the ratio of Ω_2 and Ω_1 [see Eqs. (6.18) and (6.19)]. Its relative phase φ is fixed by the relative phase of the fields 1 and 2 [see Eq. (6.16)]. We can choose Δ and ϕ_S as follows:

(i) If $\tan\theta = 1$,
  (a) $\Delta = \delta$ and $\phi_S = \phi$, or
  (b) if $q^2 \sim 1$, $\Delta = -2\delta$ and $\phi_S = \phi$;
(ii) in general,
  (a) $\Delta = 0.5\delta$ and $\phi_S \sim 0$, or
  (b) if $q^2 \sim 1$, $\Delta = -1.5\delta$ and $\phi_S \sim 0$.

The superposition is reached in a robust way through the complete population transfer by adiabatic passage from the ground state to the upper effective state of Hamiltonian (6.21). This can be achieved by a simple linear chirp or more efficiently by a parallel adiabatic passage which allows in principle the dynamical compensation of the Stark shift of Hamiltonian (6.21). The first strategy allows one to set Ω_0 and $\dot{\phi}$ (the choice must satisfy adiabatic passage and is not unique.) The compensating field Rabi frequency Ω_S is then uniquely determined by (6.24).

The strategy of parallel adiabatic passage is more complicated. For a given pulse shape $\Omega_0 \equiv \Omega_0(t)$, it imposes for the phase

$$\dot{\phi} = S + \mathrm{sign}(t)\sqrt{\Delta_0^2 - \Omega_0^2}, \tag{6.28}$$

where $\Delta_0 = \max_t \Omega_0(t)$, with the Stark shift $S = S_1 = S_2$ given by (6.12) and Ω_S by (6.24). This gives a complicated equation in $\dot{\phi}$ that has to be solved numerically at each time.

For the example of the 50% superposition, i.e. $\theta = \pi/4$ and $\Omega_1 = \Omega_2$, with $\varphi = 0$, and assuming for simplicity $\mu_1 = \mu_2$, we have

$$\Omega_S = \Omega_1\sqrt{\frac{-2(\dot{\phi}_S + \Delta)(\dot{\phi}_S + \Delta + \delta)}{\dot{\phi}^2 - \delta^2}}. \tag{6.29}$$

If one chooses for instance

$$\Delta = \delta, \quad \phi_S = \phi, \tag{6.30}$$

we obtain

$$\Omega_S = \Omega_1\sqrt{\frac{-2(\dot{\phi} + \delta)(\dot{\phi} + 2\delta)}{\dot{\phi}^2 - \delta^2}}. \tag{6.31}$$

If one considers $\dot{\phi} \ll \delta$, this simplifies to

$$\Omega_S = 2\Omega_1. \tag{6.32}$$

6.3 Numerics and the pulse shaping

Here we show the numerical results on the K atom. Fig. 6.3 displays the dynamics of the energy levels of K atom as a function of time with Ω_S Stark shift compensating field, where for the transition dipole coupling elements are used following values $\mu_1 = 1.67$ a.u. and $\mu_2 = 2.37$ a.u.. The components of the field are linearly chirped in the same manner:

$$\dot{\phi}_1 = \dot{\phi}_2 = \dot{\phi}_S = at. \tag{6.33}$$

In Fig. 6.2 we show a typical dynamics without the compensating field Ω_S. The population is distributed between $4P_{3/2}$ and $4P_{1/2}$ by 60% and 40% respectively. One can see that the Ω_S component brings the system to the complete superposition as shown inFig. 6.3. Figure 6.3 shows the pulse shaping for the K atom by an intense 765 nm, 90 fs FWHM (Full Width at Half Maximum) laser pulse. The pulse shaping is determined as described in chapter I for the intensity corresponding to $10^8 \quad W/cm^2$. The three spectral amplitude components have the same spectral phases.

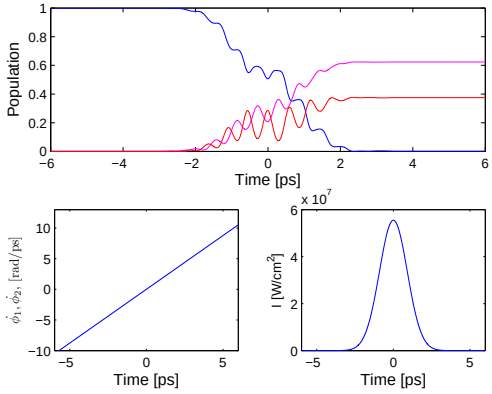

FIG. 6.2 - *Dynamics of the energy levels of the K atom as a function of time without the* Ω_s *field* (6.24)*, with duration of the pulse* $T = 10ps$*, chirp rate* $aT^2 = 4$*,* $\Omega_0 T = 6$ *and area of the pulsed Rabi frequency* $A = 5\pi$*.*

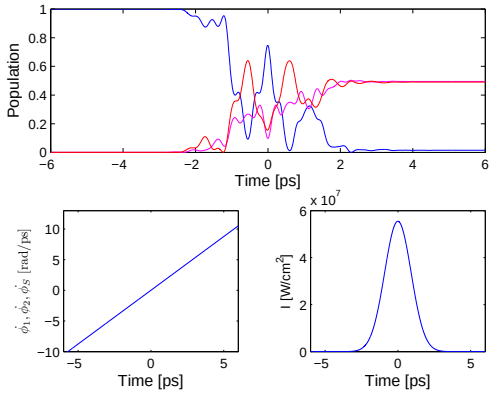

FIG. 6.3 - *Dynamics of the energy levels of the K atom as a function of time in the same conditions as in Fig. 6.2 but with the* Ω_s *field* (6.24)*.*

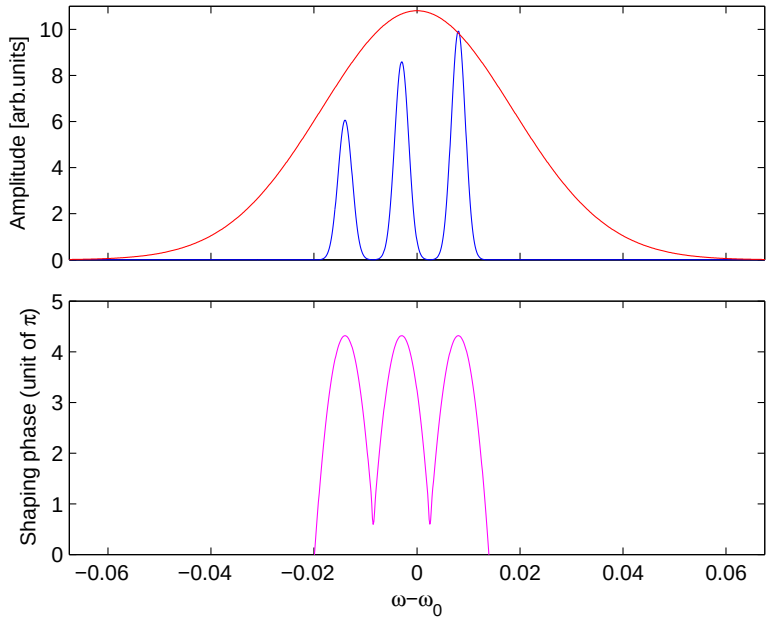

FIG. 6.4 - *The shaping of the field in the frequency domain. Upper frame: The red line is the unshaped field and the blue lines are the shaped fields. Lower frame: Spectral phase corresponding to the outgoing fields.*

Third part

Conclusions

Chapter 7

Conclusions

In the first part of this thesis which constitutes chapter I and chapter II we presented general two-state systems, approximations to solve the time-dependent Schrödinger equation and optimization of two-photon transition by phase shaping. In chapter II we theoretically analyzed the optimization scheme for two-photon two-level systems in moderate and strong field regimes. This scheme was implemented experimentally by analyzing the optimal pulse shaping for the given two-photon excitation using an effective two-state model in a moderate field regime. We have analytically obtained the optimal solution, in maintaining the two-photon resonance condition. This is achieved efficiently by linear and cubic temporal phase terms.

In the second part we introduced the adiabatic passage and parallel adiabatic passage techniques. In chapter III we have investigated and compared two ways to reach population transfer of high fidelity by adiabatic passage, namely the PLAP and DIAP techniques. Both techniques are based on the DDP analysis. The PLAP is such that the eigenvalues are dynamically parallel, while the DIAP corresponds to an adiabatic passage which is complemented by a destructive interference of the non-adiabatic transitions. One can remark that the DIAP can be seen as an extension to a chirped interaction of the Rabi π-pulse transition since the latter can be interpreted as an interference (which is destructive for the probability of population return) of the two components, from the initial state split onto the two eigenstates, having acquired a dynamical phase [65, 66].

In femtosecond regimes, these techniques can be implemented by a spectral shaping. The DIAP with a Gaussian pulse and a linear chirping, when the mean frequency of the initial field matches the transition frequency, requires a device which shapes only the spectral phase. On the other hand, the PLAP is more complicated to produce since it requires in general a shaping of both the spectral phase and the amplitude .

We have analyzed the sensitivity of the techniques to various types of fluctuations. We have considered instantaneous fluctuations of the amplitudes and phases, and also an averaging upon randomly distributed Rabi frequency areas. We expect the latter to be the most critical issue in practical implementation due to an imperfect knowledge of the interaction details (through the area of the pulse itself, the position or the volume of the considered quantum system, ...). We have shown that PLAP is much more robust than DIAP (with a fidelity of more than one

order of magnitude for rates of fluctuation that lead to an infidelity of order 10^{-4}, see Fig. 3) with respect to the lack of knowledge of the Rabi frequency area. We have shown that one cannot improve the robustness of PLAP with respect to pulse areas if one complements it with a field that cancels the non-adiabatic coupling.

On the other hand, uncorrelated instantaneous fluctuations, even if they are expected to be relatively well controlled in practice, have been shown to be in general very detrimental for any coherent techniques. We have shown this for amplitude (Fig. 3.5) and phase (Fig. 3.7) white-noise fluctuations. The phase white-noise fluctuations has been shown to be more detrimental for adiabatic processes that always need more time to operate than the π-pulse technique (for a given field amplitude peak), since this noise corresponds to a dephasing decoherence that destroys the transient superpositions. If we introduce sufficient correlations in the noise, we have shown that we recover the superiority of the PLAP technique (Fig. 3.8).

Extending the results of this chapter to systems with more than two levels necessitates, in principle, the derivation of a DDP formula for multilevel systems. Even for three-state systems, this has been shown to be complicated and not generically solvable due to numerous crossings in the complex plane [48]. Only specific symmetries in the Hamiltonian allow this extension. In the simplest case, the result can be interpreted as a local Landau-Zener analysis of the consecutive avoided crossings between pairs of levels assumed separated and that do not involve interfering paths, such that the final probability is the product of the probabilities corresponding to the consecutive avoided crossings [56,57]. Extending DIAP would thus require a model beyond this simple result.

For an N state with $N > 3$, finding parameters that would allow N parallel eigenstates is expected to be a difficult problem involving the design of many parameters. This could be solvable numerically for specific cases. The quite general choice that has been adopted in this work is a much weaker constraint, supported by a local Landau-Zener analysis, corresponding to the driving the dynamics such that the eigenstate adiabatically transporting the population corresponds to an eigenvalue parallel to the closest one. This idea has been investigated to guide the adiabatic path in a two-parameter space in the context of state selectivity in chapter V.

In chapter IV we theoretically investigated and presented the experimentally realizable two-photon optimal schemes for population transfer in two-level and four-level Stark shifted systems in strong field regime. By using PLAP techniques we have numerically shown that one can achieve efficiently complete population transfer also for four-level quantum system. In chapter V we presented the local PLAP technique, which allows state selectivity for multilevel system. We presented the experimentally realizable three-photon schemes for selective population transfer in multilevel Stark shifted systems in strong field regime. By using PLAP techniques we have numerically shown that one can achieve high selectivity of population transfer for such multilevel quantum systems.

With the advances in producing ultrashort pulses of uv-xuv frequency, one could also con-

sider the extension of such techniques with interacting pulses of a few cycles. In such an interaction, the rotating-wave approximation is itself questionable and PLAP should be investigated within the more general adiabatic Floquet theory [20].

On the other hand in chapters IV and V we demonstrated an efficient way of population transfer by using a linear chirp with additional static detuning. We have compared the robustness of these techniques.

In chapter VI we have developed a method for executing robust and selective transfer of population from a single energy eigenstate to a preselected superposition of energy eigenstates. Viewed in the frequency domain, the method constitutes simultaneous transfer of population to all the energy eigenstates which make up the superposition state by a set of adiabatic passages. We have tested the method numerically by simulating transitions between a single eigenstate and a superposition of energy eigenstates. The method allows complete population transfer and offers control of both the phase and amplitudes of the state composing the target superposition state.

Topics to be investigated further include the transfer dynamics in multilevel systems, such as the ones studied in chapter IV, V and VI, with phase and pulse area fluctuations, in order to test the robustness of the techniques. The effects of propogation in a medium will also be analysed, with a particular study of the robustness of the PLAP technique.

Fourth part

Appendixes

APPENDIX A Effective Hamiltonian for the two-photon $6S_{1/2}$-$8S_{1/2}$ transition in Cesium atoms

We consider the two-photon transition in Cesium between the state $g \equiv 6S_{1/2}$ and $e \equiv 8S_{1/2}$. We decompose the derivative of the phase of the laser as a mean frequency ω_0 (corresponding to the laser frequency of the Fourier transform pulse, i.e. before its shaping and a relative frequency $\phi(t)$). We assume that the mean frequency is exactly two-photon resonant: $\omega_0 = (\omega_e - \omega_g)/2$, i.e. $\Delta = 0$. The relevant parameters for the considered transition are given in Table 7.1. We have determined the parameters involving the dipole moment couplings with Eqs. (7.4), (7.4) and (7.4) using Ref. [37] for the bound-bound couplings and the Fues model potential [38,39] for the bound-free couplings (see also [40] for a general discussion of model potential methods).

A single photon allows the ionization of the atom from the excited state, however, through the small ratio $|\Gamma_e/\Omega| = 6.5 \times 10^{-3}$, where Γ_e is the ionization rate.

TAB. 7.1 - *Parameters for the transition in Cesium $6S_{1/2}$-$8S_{1/2}$*

r	$\omega_e - \omega_g$(rad/s)	ω_0(rad/s)
1.85	4.58×10^{15}	2.29×10^{15}

Two intermediate states ($1 \equiv 6P_{1/2}$ and $2 \equiv 6P_{3/2}$, of respective energies ω_1 and ω_2) are close to a single-photon resonance and lead to strong Stark shifts in the effective two-state model [71]. Here we derive the conditions of validity of this two-state model. The static one-photon detunings are

$$\Delta_{g1} \equiv \omega_1 - \omega_g - \omega_0 = -4.47 \times 10^{-3} \text{ a.u.}, \tag{7.1}$$

$$\Delta_{g2} \equiv \omega_2 - \omega_g - \omega_0 = -1.94 \times 10^{-3} \text{ a.u.} \tag{7.2}$$

For a laser intensity $I = 60$ GW/cm^2, we get for the peak single-photon Rabi frequencies (in a.u.) $\Omega_{g1} = 2.4 \times 10^{-3} \sim |\Delta_{g1}|$ and $\Omega_{g2} = 3.4 \times 10^{-3} > |\Delta_{g2}|$, which prevents the use of a

two-state approximation. In that case, we thus use a four-level approximation:

$$H_4(t) = \hbar \begin{bmatrix} S_g(t) & \frac{1}{2}\Omega_{g1}(t) & \frac{1}{2}\Omega_{g2}(t) & \frac{1}{2}\Omega_{ge}(t) \\ \frac{1}{2}\Omega_{g1}(t) & \Delta_{g1} - \dot{\phi}(t) + S_1(t) & 0 & \frac{1}{2}\Omega_{e1}(t) \\ \frac{1}{2}\Omega_{g2}(t) & 0 & \Delta_{g2} - \dot{\phi}(t) + S_2(t) & \frac{1}{2}\Omega_{e2}(t) \\ \Omega_{ge}(t) & \frac{1}{2}\Omega_{e1}(t) & \frac{1}{2}\Omega_{e2}(t) & -2\dot{\phi}(t) + S_e(t) - i\frac{1}{2}\Gamma_e(t) \end{bmatrix}. \tag{7.3}$$

The Stark shifts $S_g(t)$ and $S_e(t)$ of the ground and excited states respectively, are due to their coupling to the intermediate states m and the continuum channels ℓ:

$$S_j(t) = -\frac{\mathcal{E}^2(t)}{2\hbar^2}\left[\sum_{m\neq j} |\mu_{jm}|^2 \frac{\omega_{mj}}{\omega_{mj}^2 - \omega_L^2(t)} + \mathcal{P}\int \frac{dE}{\hbar}\sum_{\ell} |\mu_{j;E,\ell}|^2 \frac{\omega_{Ej}}{\omega_{Ej}^2 - \omega_L^2(t)}\right]$$

with $j = e, g$, μ_{jm} (resp. $\mu_{j;E,\ell}$) the transition dipole moments between the state j, of energy $\hbar\omega_j$, and the intermediate state (resp. the continuum state of the channel ℓ and of energy E), and $\omega_{mj} = \omega_m - \omega_j$, $\omega_{Ej} = E/\hbar - \omega_j$. $\mathcal{P}$ indicates the principal part of the integral when it is indefinite (if $\omega_j + \omega_L$ reaches the continuum). The effective two-photon Rabi frequency between the ground and the excited state is

$$\Omega(t) = -\frac{\mathcal{E}^2(t)}{2\hbar^2}\left[\sum_{m\neq e,g} \frac{\mu_{gm}\mu_{me}}{\omega_m - \omega_g - \omega_L(t)} + \int \frac{dE}{\hbar}\sum_{\ell} \frac{\mu_{g;E,\ell}\mu_{E,\ell;e}}{E/\hbar - \omega_g - \omega_L(t)}\right].$$

The field intensity $I(t)$ is related to the field amplitude $\mathcal{E}(t)$ through the relation $I[\mathrm{W/cm^2}] \approx 3.51 \times 10^{16}\,(\mathcal{E}[\mathrm{u.a.}])^2$. It is usually a good approximation to consider the mean (or central) frequency of the laser ω_0 instead of the instantaneous one $\omega_L(t)$ to calculate the Stark shifts and the Rabi frequency. This is generally the case when the frequency of the laser is chirped on a very small interval $\Delta\omega_L \equiv \Delta\dot{\phi} \ll \omega_0$ We take into account that the excited state is lossy through ionization by the laser. This is taken into account by summing the partial rates to the continuum channel ℓ:

$$\Gamma_e(t) = \sum_{\ell} \Gamma_e^{(\ell)},\ \Gamma_e^{(\ell)} = \frac{\pi}{2\hbar}\mathcal{E}^2(t)|\mu_{e;E=\hbar\omega_e+\hbar\omega_L,\ell}|^2. \tag{7.4}$$

Here the partial rates have been written for the case of a single photon resonance between the continuum and the excited state.

Bibliography

[1] A. M. Weiner, Rev. Sci. Instrum. **71**, 1929-1960 (2000).

[2] M. Shapiro and P. Brumer, *Principles of the Quantum Control of Molecular Processes*, (Wiley, New York, 2003).

[3] D. J. Tanner and S. A. Rice, J. Chem. Phys. **83**, 5013-5018 (1985).

[4] T. C. Weinacht, J. Ahn, and P. H. Bucksbaum, Nature **397**, 233-235 (1999).

[5] A. Monmayrant, B. Chatel, and B. Girard, Phys. Rev. Lett. **96**, 103002 (2006).

[6] N. Dudovich, D. Oron, and Y. Silberberg, Nature **418**, 512 (2002).

[7] Z. Zheng and A. M. Weiner, Chem. Phys. **267**, 161 (2001).

[8] T. Hournung, R. Meier, D. Zeidler, K.-L. Kompa, D. Proch, M. Motzkus, Appl. Phys. B **71**, 277 (2000).

[9] R. S. Judson, H. Rabitz, Phys. Rev. Lett. **68**, 1500-1503 (1992).

[10] D. Meshulach and Y. Silberberg, Nature **396**, 239-242 (1998).

[11] N. Dudovich, B. Dayan, S. M. Gallagher Faeder, and Y. Silberberg, Phys. Rev. Lett. **86**, 47-50 (2001).

[12] N. Dudovich, D. Oron, and Y. Silberberg, Phys. Rev. Lett. **92**, 103003 (2004).

[13] M. C. Stowe, A. Pe'er, and J. Ye, Phys. Rev. Lett. **100**, 203001 (2008).

[14] N. P. Garayantz, V. S. Grigoryan, S. A. Michaelian, K. B. Petrossian, and K. M. Pokhsrarian, J. Mod. Opt. **38** 591 (1991).

[15] N. Dudovich, T. Polack, A. Pe'er, and Y. Silberberg, Phys. Rev. Lett. **94**, 083002 (2005).

[16] M. Wollenhaupt, A. Präkelt, C. Sarpe-Tudoran, D. Liese, T. Baumert, Appl. Phys. B **82**, 183-188 (2006).

[17] C. Trallero-Herrero, J. L. Cohen, and T. Weinacht, Phys. Rev. Lett. **96**, 063603 (2006).

[18] H. Suchowski, A. Natan, B. D. Bruner, and Y. Silberberg, J. Phys. B:At. Mol. Opt. Phys. **41**, 074008 (2008).

[19] E. A. Shapiro, V. Milner, C. Menzel-Jones, M. Shapiro, Phys. Rev. Lett. **99**, 033002 (2007).

[20] S. Guérin and H.R. Jauslin, Adv. Chem. Phys. **125**, 147 (2003).

[21] S. Lee, J. Lim, and J. Ahn, Opt. Express **17**, 7648 (2009).

[22] B. W. Shore, The Theory of Coherent Atomic Excitation (Wiley, New York, 1990).

[23] P. Král, I. Thanopulos, and M. Shapiro, Rev. Mod. Phys. **79**, 53 (2007).

[24] D. Tannor, *Introduction to Quantum Mechanics: A Time-Dependent Perspective* (University Science Books, Sausalito, CA, 2007).

[25] M.A. Nielson and I.L. Chuang, *Quantum Computation and Quantum Information* (Cambridge University Press, Cambridge, England, 2000).

[26] S. Guérin, S. Thomas and H.R. Jauslin, Phys. Rev. A **65**, 023409 (2002).

[27] G. Dridi, S. Guérin, V. Hakobyan, H. R. Jauslin and H. Eleuch Phys. Rev. A **80**, 043408 (2009).

[28] G.S. Vasilev and N.V. Vitanov, Phys. Rev. A **70**, 053407 (2004).

[29] R. L. Fork, B. I. Greene, C. V. Shank, Appl. Phys. Lett. **38**, 671 (1981).

[30] J. Paye, IEEE J. Quantum Electron. **28**, (1992).

[31] A. Monmayrant, S. Weber, and B. Chatel, J. Phys. B **43**, 103001 (2010).

[32] U. Boscain, G. Charlot, J.-P. Gauthier, S. Guérin, and H. R. Jauslin, J. Math. Phys. **43**, **43**, 2107 (2002).

[33] C. Trallero-Herrero, D. Cardoza, T. C. Weinacht, and J. L. Cohen, Phys. Rev. A **71**, 013423 (2005).

[34] J. Marek, Phys. Lett. **60**, 191-192 (1977).

[35] B. H. Bransden and C. J. Joachin, *Physics of Atoms and Molecules* (Pearson Education, 2003).

[36] B. Broers, H.B. van Linden van den Heuvell, and L.D. Noordam, Phys. Rev. Lett. **69**, 2062 (1992); P. Balling, D.J. Maas, and L.D. Noordam, Phys. Rev. A **50**, 4276 (1994).

[37] A. Sieradzan, M.D. Havey, and M.S. Safranova, Phys. Rev. A **69**, 022502 (2004).

[38] G. Simons, J. Chem. phys. **55**, 756 (1971).

[39] I.L. Glukhov and V.D. Ovsiannikov, J. Phys. B **42**, 075001 (2009).

[40] L.P. Yatsenko, T. Halfmann, B.W. Shore, and K. Bergmann, Phys. Rev. A **59**, 2926 (1999).

[41] G.S. Vasilev and N.V. Vitanov, J. Chem. Phys. **123**, 174106 (2005).

[42] S. Zhdanovich, E. A. Shapiro, J. W. Hepburn, M. Shapiro, and V. Milner, Phys. Rev. A **80**, 063405 (2009).

[43] M.H. Levitt, Prog. NMR Spectrosc. 18, 61 (1986); R. Freeman, Spin Choreography (Spektrum, Oxford, 1997).

[44] S.S. Ivanov, and N.V. Vitanov, Opt. Lett. **36**, 1275 (2011).

[45] A. Messiah, Mécanique Quantique, Dunod, Paris, 1959

[46] N.V. Vitanov, T. Halfmann, B.W. Shore and K. Bergmann, Annu. Rev. Phys. Chem. **52**, 763 (2001).

[47] A.M. Dykhne, Sov. Phys. JETP **14**, 941 (1962).

[48] J.P. Davis and P. Pechukas, J. Chem. Phys. **64**, 3129 (1976); J.-T. Hwang and P. Pechukas, J. Chem. Phys. **67**, 4640 (1977).

[49] A. Joye, H. Kuntz, and Ch-Ed. Pfister, Ann. Phys. **208**, 299 (1991).

[50] A. Joye, G. Mileti, and Ch-Ed. Pfister, Phys. Rev. A **44**, 4280 (1991).

[51] A. Monmayrant and B. Chatel, Rev. Sci. Instrum. **75**, 2668 (2004).

[52] L. Allen and J.H. Eberly, *Optical Resonance and Two-Level Atoms* (Dover, New York, 1987).

[53] G.S. Vasilev, A. Kuhn, N.V. Vitanov, Phys. Rev. A **80**, 013417 (2009).

[54] R.G. Unanyan, L.P. Yatsenko, K. Bergmann, and B.W. Shore, Opt. Commun. 139, 48 (1997).

[55] M.V. Berry, J. Phys. A 42, 365303 (2009); Xi Chen, I. Lizuain, A. Ruschhaupt, D. Guéry-Odelin, and J. G. Muga, Phys. Rev. Lett. **105**, 123003 (2010).

[56] C. E. Caroll and F. T. Hioe, J. Phys. A 19, 1151 (1986).

[57] S. S. Ivanov and N. V. Vitanov, Phys. Rev. A 77, 023406 (2008).

[58] B. Broers, H.B. van Linden van den Heuvell, and L.D. Noordam, Phys. Rev. Lett. 69, 2062 (1992); D.J. Maas, C.W. Rella, P. Antoine, E.S. Toma, and L.D. Noordam, Phys. Rev. A 59, 1374 (1999).

[59] M. Krug, T. Bayer, M. Wollenhaupt, C. Sarpe-Tudoran, T. Baumert, S.S. Ivanov, and N.V. Vitanov, New J. Phys. **11**, 105051 (2009).

[60] N.G. van Kampen, *Stochastic Processes in Physics and Chemistry* (3rd ed, North-Holland, 2007).

[61] G.S. Agarwal, Phys. Rev. A **18**, 1490 (1978).

[62] X. Lacour, S. Guérin, and H.R. Jauslin, Phys. Rev. A **78**, 033417 (2008).

[63] D. Sugny, C. Kontz, and H.R. Jauslin, Phys. Rev. A **76**, 023419 (2007).

[64] L.P. Yatsenko, V.I. Romanenko, B.W. Shore, and K. Bergmann, Phys. Rev. A **65**, 043409 (2002).

[65] M. Holthaus and B. Just, Phys. Rev. A **49**, 1950 (1994).

[66] L.P. Yatsenko, S. Guérin, and H.R. Jauslin, Phys. Rev. A **70**, 043402 (2004).

[67] E. A. Shapiro, A. Peer, J. Ye, and M. Shapiro, Phys. Rev. Lett.101, 023601 (2008).

[68] X. Li et al., J. Chem. Phys. 128, 124314 (2008).

[69] V. S. Malinovsky and J. L. Krause, Phys. Rev. A 63, 043415 (2001).

[70] National Institute of Standards and Technology,http//www.nist.gov

[71] S.Lee, J.Lim, J.Ahn, V.Hakobyan and S. Guérin Rev. Rev. A **82**, 023408 (2010).